OULU 2023
C 912

ACTA UNIVERSITATIS OULUENSIS

Kashif Noor

SPATIOTEMPORAL EVALUATION OF SNOWMELT WATER AND SNOWPACK ISOTOPES (^{18}O AND ^{2}H) AND THEIR APPLICATION IN SUBARCTIC CATCHMENT HYDROLOGY

UNIVERSITY OF OULU GRADUATE SCHOOL;
UNIVERSITY OF OULU,
FACULTY OF TECHNOLOGY

ACTA UNIVERSITATIS OULUENSIS
C Technica 912

KASHIF NOOR

SPATIOTEMPORAL EVALUATION OF SNOWMELT WATER AND SNOWPACK ISOTOPES (^{18}O AND ^{2}H) AND THEIR APPLICATION IN SUBARCTIC CATCHMENT HYDROLOGY

Academic dissertation to be presented with the assent of the Doctoral Programme Committee of Technology and Natural Sciences of the University of Oulu for public defence on Tellus Backstage, Linnanmaa, on 5 December 2023, at 12 noon

UNIVERSITY OF OULU, OULU 2023

Acta Univ. Oul. C 912, 2023

Supervised by
Associate Professor Pertti Ala-aho
Associate Professor Hannu Marttila
Professor Bjørn Kløve

Reviewed by
Professor Tricia Stadnyk
Research Professor Rosemary W. H. Carroll

Opponent
Professor Daniele Penna

ISBN 978-952-62-3905-7 (Paperback)
ISBN 978-952-62-3906-4 (PDF)

ISSN 0355-3213 (Printed)
ISSN 1796-2226 (Online)

Cover Design
Raimo Ahonen

PUNAMUSTA
TAMPERE 2023

Noor, Kashif, Spatiotemporal evaluation of snowmelt water and snowpack isotopes (^{18}O and ^{2}H) and their application in subarctic catchment hydrology.

University of Oulu Graduate School; University of Oulu, Faculty of Technology
Acta Univ. Oul. C 912, 2023
University of Oulu, P.O. Box 8000, FI-90014 University of Oulu, Finland

Abstract

Snow plays a significant role in hydrological studies in cold climates because of its importance for runoff and recharge, provision of water for water supply and energy production, etc. In this thesis, we evaluated snow, with a particular focus on snowmelt processes, from the perspective of stable water isotope ($\delta^{18}O$ and $\delta^{2}H$) hydrology. $\delta^{18}O$ and $\delta^{2}H$ isotopes possess unique fingerprinting properties and are valuable in various snow hydrological applications, including source water identification, quantitative partitioning of water sources and their mixing, and estimating water residence times within catchments. We aimed to answer the following research questions: (i) how do isotope values change vertically across the snow layers in the snowpack? (ii) how do snowmelt isotope values evolve spatiotemporally? and (iii) how do different sampling methods and mathematical approximations of meltwater isotopes influence the extent of potential bias in estimating snowmelt water's contribution to streamflow?

An analysis of the isotope datasets revealed distinct isotopic stratigraphy in the snowpack layers over winter, with an enriched base layer and spatially consistent stratigraphy across the Pallas catchment. Vertical isotope profiles homogenized during the peak melt period, showing an average of 1 to 2‰ higher $\delta^{18}O$ values than before melting. Snowmelt rate influenced liquid-ice fractionation, with pronounced fractionation effects during low melt rates, leading to the depletion of heavy isotopes in initial meltwater samples. Before the peak melt period, meltwater was isotopically heavier and more variable than the depth-integrated snowpack, exhibiting a disparity of approximately 3.1‰ in $\delta^{18}O$, which diminished during the peak melt period. By using $\delta^{18}O$ data from snowfall, snowpack, and meltwater, we quantified the biases and estimated the total contribution of snowmelt water to streamflow during the snowmelt period.

If meltwater samples are unavailable, snowpack isotopes during peak melt period can yield reasonably reliable estimates of meltwater contribution to streamflow, albeit with minor underestimations. Meltwater $\delta^{18}O$ and $\delta^{2}H$ isotopes can better constrain tracer-based ecohydrological models and can enhance our insights into the evolving role of snowmelt. This has profound implications for the hydrological and ecohydrological processes of cold-region catchments.

Keywords: baseflow, depth hoar, isotope fractionation, isotope hydrograph separation, lc-excess, liquid-ice interaction, lysimeter, mixing model, snow hydrology, snow stratigraphy, stream water

Noor, Kashif, Sulamisveden ja lumipatjan isotooppien (^{18}O ja ^{2}H) spatiotemporaalinen vaihtelu ja niiden käyttö subarktisen valuma-alueen hydrologian tutkimuksessa.

Oulun yliopiston tutkijakoulu; Oulun yliopisto, Teknillinen tiedekunta

Acta Univ. Oul. C 912, 2023
Oulun yliopisto, PL 8000, 90014 Oulun yliopisto

Tiivistelmä

Lumi on merkittävässä roolissa kylmien alueiden hydrologiassa. Lumen sulamisvedet ovat tärkeitä vesihuollon, pohjaveden muodostumisen, energiantuotannon, tulvien hallinnan ja maaperän eroosion kannalta. Tässä väitöstyössä arvioimme lunta, erityisesti lumen sulamisprosesseja, veden stabiileja isotooppeja ($\delta^{18}O$ ja $\delta^{2}H$) hyödyntäen. Tutkimuksen tavoitteena oli vastata seuraaviin kysymyksiin: (i) Miten isotooppiarvot vaihtelevat pystysuunnassa lumen eri kerroksissa? (ii) Miten sulavan lumen isotooppiarvot muuttuvat ajallisesti ja alueellisesti? (iii) Miten voimme paremmin arvioida sulavan lumen osuutta purovirtaamassa käyttäen isotooppimenetelmiä ja arvioida analyysin epävarmuuksia?

Lumiprofiilista kerätyt isotooppinäytteet paljastivat selkeän lumipeitteen isotooppisen kerrostuneisuuden. Lumen pohjakerrokset olivat rikastuneet raskailla isotoopeilla, ja lumipatjan kerrosrakenne oli yhtenäinen koko Pallaksen tutkimusalueella. Lumen nopean sulamisen aikana pystysuuntainen isotooppikerrosrakenne muuttui homogeeniseksi, osoittaen keskimäärin 1–2 ‰ korkeampia $\delta^{18}O$ arvoja kuin ennen sulamista. Lumen sulamisvesien alkujakso koostui kevyemmistä isotoopeista, muuttuen loppuvaiheessa raskaampiin isotooppeihin. Lumen sulamisnopeus vaikutti nesteen ja jään väliseen isotooppien fraktioitumiseen etenkin lumen hitaan sulamisen aikana. Erot isotooppiarvoissa sulavan lumen ja lumipeitteen välillä vähenivät sulamisen huippujakson aikana.

Käyttämällä veden isotooppinäytteitä arvioimme lumen sulamisveden kokonaisosuuden purovirtaamassa sulamiskauden aikana. Lisäksi analysoimme systemaattisia virheitä, jotka muodostuvat, jos lumen sulantanäytteiden sijaan analyysissä käytetään veden isotooppinäytteitä lumisateesta tai lumipatjasta. Jos isotooppinäytteitä lumen sulamisvedestä ei ole saatavilla, lumen sulantahuipun aikana kerätyt näytteet lumenpatjan isotooppikoostumuksesta voivat antaa kohtuullisen luotettavia arvioita, vaikkakin hieman aliarvioiden lumen osuutta.

Kaiken kaikkiaan tutkimuksemme korostaa tarvetta tarkempaan lumen sulamisveden $\delta^{18}O$ ja $\delta^{2}H$ arvojen määritykseen ekohydrologisissa tutkimuksissa. Aineistoja lumen sulamisveden isotooppikoostumuksesta voidaan hyödyntää isotooppeja merkkiaineena käyttävissä ekohydrologisissa malleissa, sekä lisäämään tietoa hydrologisista ja ekohydrologisista prosesseista lumivaikutteisilla alueilla.

Asiasanat: hydrografianalyysi, isotooppien fraktioituminen, lc-ylimäärä, lumen kerrosrakenne, lumihydrologia, lysimetri, pohjakuura, pohjavalunta, veden stabiilit isotoopit, vesi-jää-vuorovaikutus, virtavedet

To My Mother

Acknowledgements

I would like to extend my gratitude to the Kvantum Institute at the University of Oulu, Maa-ja vesitekniikan tuki ry (MvTT), and the Sven Hallin Research Foundation for financially supporting my PhD studies. My heartfelt appreciation goes to my principal supervisor, Associate Professor Pertti Ala-aho, as well as co-supervisors Associate Professor Hannu Marttila, and Professor Bjørn Kløve. Their unyielding support, patience, motivation, and insightful and constructive feedback have immensely impacted the quality of my research. Their committed involvement throughout my PhD journey has been invaluable. I am fortunate to have such a dedicated group of supervisors and mentors, whose selfless investment of time and attention has been a pillar of strength for me. I am grateful to Assoc. Prof. Pertti Ala-aho for consistently ensuring I maintain a work-life balance and inquiring about my health – these words meant so much to me. I am also truly thankful to Assoc. Prof. Hannu Marttila for believing in my strengths and supporting me through every challenging phase of my PhD journey.

A special thanks to our trainees and fieldwork assistants, Alexandre, Miika Läpikivi, Aino Erkinaro and Jari-Pekka Nousu, for their assistance in sample collection. My thanks also extend to Päivi Pietikainen, Mirka Hatanpää and Valtteri Hyöky from Metsähallitus for their help with field sampling. I would also like to thank Matthias Sprenger and my friend Filip Muhic for helping to deploy the snowmelt lysimeters. I would like to express my thanks to Associate Professor Ali Torabi Haghighi and Senior Hydrologist Noora Veijalainen for their valuable insights and constructive feedback during my PhD follow-up group meetings. My gratitude also goes to Professor Daniele Penna for accepting the role of opponent, to both pre-examiners, Professor Tricia Stadnyk and Associate Research Professor Rosemary W.H. Carroll, for their encouragement, insightful comments and suggestions on my thesis, and to my co-authors, Professor Jeffrey M. Welker and Kaisa-Riikka Mustonen, for their constructive feedback on the manuscripts which I submitted to journals.

I am thankful to Uzair Akbar Khan for his friendship and shared practical experience, which eased both general and specific issues during my stay. I am also grateful to the senior members and my fellow PhD colleagues for their support. I am grateful to everyone who offered support in any capacity during my PhD journey.

Lastly, my deepest thanks go to my family: my parents, brothers, and sisters, whose consistent support, motivation, and encouragement have been my guiding

light. Their unwavering support, belief and trust in my journey have been the backbone of my academic pursuits, and for that, I will always be indebted to them.

Oulu, October 2023 Kashif Noor

List of abbreviations and symbols

BEMMA	Bayesian Endmember Mixing Model Analysis
DI	Depth-integrated
EHS	Ensemble Hydrograph Separation
EMMA	Endmember Mixing Model Analysis
FMI	Finnish Meteorological Institute
GMWL	Global Meteoric Water Line
IHS	Isotope Hydrograph Separation
LMWL	Local Meteoric Water Line
RCVWSM	time-variant incremental Runoff-Corrected Volume Weighted average SnowMelt
RCVWSP	time-variant incremental Runoff-Corrected Volume Weighted average SnowPack
Roll-RCVWSM	time-variant Rolling Runoff-Corrected Volume Weighted average SnowMelt
Roll-RCVWSP	time-variant Rolling Runoff-Corrected Volume Weighted average SnowPack
S_d	Snow Density
S_h	Snow Depth
SD	Standard Deviation
SE	Standard Error
SM	time-variant SnowMelt
SP	time-variant SnowPack
SWE	Snow Water Equivalent
SYKE	Finnish Environmental Institute
VWSF	time-invariant Volume Weighted average SnowFall
VWSM	time-invariant Volume Weighted average SnowMelt
VWSPB	time-invariant Volume Weighted average SnowPack Before melt period
VWSPD	time-invariant Volume Weighted average SnowPack During melt period

List of original publications

This thesis is based on the following publications, which are referred to throughout the text by their Roman numerals:

I Ala-aho, P., Welker, J. M., Bailey, H., Højlund Pedersen, S., Kopec, B., Klein, E., Mellat, M., Mustonen, K-R., Noor, K., & Marttila, H. (2021). Arctic snow isotope hydrology: a comparative snow-water vapor study. *Atmosphere, 12*(2), 150. https://doi.org/10.3390/atmos12020150

II Noor, K., Marttila, H., Klöve, B., Welker, J. M., & Ala-aho, P. (2023). The spatiotemporal variability of snowpack and snowmelt water ^{18}O and ^{2}H isotopes in a subarctic catchment. *Water Resources Research*, *59*(1), e2022WR033101. https://doi.org/10.1029/2022WR033101

III Noor, K., Marttila, H., Welker, J. M., Mustonen, K-R., Klöve, B., & Ala-aho, P. (2023). Snow sampling strategy can bias estimation of meltwater fractions in isotope hydrograph separation. *Journal of Hydrology, 627*(Part B), 130429. https://doi.org/10.1016/j.jhydrol.2023.130429

Contributions by Kashif Noor to Publications I–III:

I Planned and conducted the fieldwork and collected the data at the Pallas research site. Contributed to the interpretation of data. Wrote and edited the manuscript in collaboration with the leading author and other co-authors.

II Conceptualized and designed the study with Hannu Marttila, Björn Klöve and Pertti Ala-aho. Conducted fieldwork and collected data. Performed laboratory analysis. Analyzed the results and wrote the manuscript. Received critical comments from all co-authors and edited the manuscript together with co-authors before it was published.

III Conceptualized and designed the study with Hannu Marttila and Pertti Ala-aho. Conducted fieldwork and collected data. Performed laboratory analysis. Analyzed the results and wrote the manuscript. Received critical comments from all co-authors and edited the manuscript together with co-authors before it was published.

Contents

1 Introduction

Snow plays a pivotal role in the Arctic water cycle, contributing significantly to the surface energy balance, and serving as both storage and a crucial freshwater source (Biskaborn et al., 2019; Bring et al., 2016; Pulliainen et al., 2020). Similarly, snowmelt water is critical in northern and alpine ecosystems (Liu et al., 2004; Penna et al., 2016; Tetzlaff et al., 2015; Winnick et al., 2017), particularly in high-latitude areas (Laudon et al., 2004). It not only replenishes soil water storage (Muhic et al., 2023; Tokunaga et al., 2022) and significantly contributes to groundwater recharge (Carroll et al., 2019; Earman et al., 2006; Flerchinger et al., 1992; Mohammed et al., 2019), but also exports solutes and nutrients. Therefore, it is integral to catchment biogeochemical and eco-hydrological processes (Buckeridge et al., 2010; Buckeridge & Grogan, 2010; Jespersen et al., 2018; Rindt et al., 2022). Climate change is projected to significantly affect snowmelt patterns in terms of their timings, magnitude, and duration in multiple regions (Bintanja & Andry, 2017; Ren et al., 2023). Rising temperatures have affected precipitation patterns (Meriö et al., 2019; Prein & Heymsfield, 2020), and caused earlier snowmelt and more frequent rain-on-snow events, e.g., in the Arctic region, specifically across the North Atlantic and the Barents Sea (Bintanja & Andry, 2017; Hale et al., 2023; Serreze et al., 2021). Globally, there is a transition from snowmelt-dominant to rainfall-dominant systems (Berghuijs et al., 2014; Bintanja & Andry, 2017). It has been documented that Arctic surface air temperatures have warmed at twice the global average since the mid-1990s (Overland et al., 2019). This shift has varied impacts at the catchment scale (Meriö et al., 2019; Pi et al., 2021). These modifications hold the potential to significantly affect stream and terrestrial ecosystems by influencing streamflow generation processes and flow regimes (Alstad et al., 1999; Gu et al., 2023; Jones et al., 2023; Mustonen et al., 2018). Hence, a comprehensive understanding of changes in snowmelt processes is essential for the study of biogeochemical and eco-hydrological processes.

The total amount of water in the hydrological cycle remains constant; however, the water amount in different compartments of the cycle, such as atmosphere (water molecule in clouds), surface storage (snowpack, lakes, ponds etc.), and subsurface storage (vadose zone, groundwater), may vary. The previous brief introduction indicated that a change in temperature may not only be responsible for the variation in the relative contribution of the amount of water in different elements of the hydrological cycle on a global scale, but it may also have consequences on a local scale. Although this study does not evaluate the impacts of climate change on the

hydrological cycle in general, this brief discussion lays the foundation motivating us to conduct this study – *The spatiotemporal evaluation of snowmelt water and snowpack isotopes (^{18}O and ^{2}H) and their application in subarctic catchment hydrology*.

1.1 Stable isotopes of ^{18}O and ^{2}H

Hydrogen and oxygen in water molecules are comprised of ^{1}H, ^{2}H and ^{3}H and ^{16}O, ^{17}O and ^{18}O isotopes, respectively. ^{3}H (Tritium) is a radioactive and unstable isotope. The number, as a superscript to the left of the symbol of hydrogen and oxygen, represents the number of neutrons in their respective atoms. Thus, isotopes are defined as atoms of the same element that have the same number of protons but a different number of neutrons. The use of these isotopes in hydrological studies is ubiquitous. There also exist other radioactive isotopes of oxygen, such as ^{14}O, ^{15}O, ^{19}O and ^{20}O, but these have an extremely short half-life, i.e., seconds, and thus, have no use in hydrological studies (Gat, 2010). The lighter isotopes of hydrogen (^{1}H with 99.985%) and oxygen (^{16}O with 99.762%) are available more abundantly in nature compared to the heavier isotopes (^{2}H, also known as deuterium with 0.015%, and ^{18}O with 0.200%). In water molecules, these isotopes occur in different configurations, such as $^{1}H_2{}^{16}O$, $^{1}H^{2}H\,^{16}O$, $^{2}H_2{}^{16}O$, $^{1}H_2{}^{18}O$, $^{1}H^{2}H\,^{18}O$ and $^{2}H_2{}^{18}O$, and, of course, in some other configurations, including radioactive isotopes. For convenience, here, we limit the discussion to only ^{1}H, ^{2}H, ^{16}O and ^{18}O isotopes because of their wider use in hydrological applications.

Water isotopologues with lighter configurations, e.g., $^{1}H_2{}^{16}O$, exhibit higher surface vapor pressure and molecular kinetic energy. This makes them evaporate or sublimate more quickly than their heavier counterparts, such as $^{2}H_2{}^{18}O$. When snow or liquid surfaces are exposed to the atmosphere, these lighter isotopologues tend to vaporize more readily. As a result, the vaporized water molecules are primarily composed of lighter water isotopologues depleted in heavier isotopes, leaving the residual surface enriched in heavier isotopes (DeWalle & Rango, 2008).

Although the abundance of heavier isotopes is smaller in nature, their relative abundance can be reliably measured with a traditional mass spectrometer and laser-based Cavity Ring Down Spectrometer (CRDS) analyzers (Kendall & McDonnell, 2012). Since heavier isotopes are rare, this makes them even more useful in tracer-based hydrological applications because they can detect small-scale variations of hydrological processes in catchment studies, in contrast to other types of hydrometric point measurements in integrated catchment applications, such as

ground-level monitoring, rainfall amount, stream gauging, etc., which often require extrapolation and/or additional assumptions (Kendall & McDonnell, 2012).

Isotope values are represented as ratios, i.e., the concentration ratio between heavier and lighter isotopes (e.g., $^{2}H/^{1}H$ or $^{18}O/^{16}O$). On their own, these ratios are not especially meaningful. They are standardized against known reference isotope values, like Vienna Standard Mean Ocean Water 2 (VSMOW2) standard isotope values, as suggested by the International Atomic Energy Agency (IAEA) (Gonfiantini, 1978). This isotope ratio of ratios is represented using δ and is measured in 'per mil' or (‰) units. The isotopic composition of a sample can be determined as

$$\delta^{2}H \text{ or } \delta^{18}O = \left(\frac{R_{sample}}{R_{VSMOW2}} - 1\right) \times 1000, \quad (1)$$

where R_{sample} and R_{VSMOW2} denote the concentration ratios of the heavier to lighter isotopes for the examined sample ($^{2}H/^{1}H$ or $^{18}O/^{16}O$) and the standard VSMOW2, respectively.

When analyzing isotope values for samples, a dual isotope plot with $\delta^{2}H$ on the y-axis and $\delta^{18}O$ on the x-axis offers the first plot for assessing their relationship. Globally, precipitation samples manifest a linear relationship between $\delta^{2}H$ and $\delta^{18}O$ values, represented with the equation $\delta^{2}H = 8\times\delta^{18}O + 10$. This equation defines the Global Meteoric Water Line (GMWL) (Craig, 1961). The GMWL's intercept is known as the deuterium excess (d-excess). Depending on factors such as moisture source, transport mechanisms, and local recycling of water molecules, precipitation samples at specific locations might deviate from the GMWL. This deviation results in a linear relationship between $\delta^{2}H$ and $\delta^{18}O$ but with different slope and intercept, known as the Local Meteoric Water Line (LMWL). In studies focusing on local water cycles using $\delta^{2}H$ and $\delta^{18}O$ stable isotopes, the LMWL is most predominantly utilized and is preferred over the GMWL. On a dual isotope plot, lines connecting evaporated and sublimated samples are termed the Local Evaporation Line (LEL) and Local Sublimation Line (LSL), respectively. Another secondary parameter, akin to d-excess, is the line conditioned excess (lc-excess), derived from the LMWL's equation (Landwehr & Coplen, 2004)

$$lc - excess = \delta^{2}H - a \times \delta^{18}O - b, \quad (2)$$

where, 'a' represents the LMWL's slope and 'b' as its intercept.

Any deviation from the LMWL shows nonequilibrium processes like evaporation or sublimation, a phenomenon termed non-equilibrium kinetic fractionation. If a sample aligns with the LMWL, its lc-excess approximates 0‰.

Positive values indicate the sample's position above the LMWL, while negative values indicate a position below it (Landwehr & Coplen, 2004). Snowfall samples are presumed to align with the LMWL and exhibit a larger standard deviation in their isotopic ratios compared to snowpack samples. In turn, snowpack samples show a greater standard deviation than snowmelt water samples (Beria et al., 2018). In other words, the hierarchy of the standard deviation of isotope variability is as follows: snowfall isotope ratios > snowpack isotope ratios > snowmelt water isotope ratios.

Isotope fractionation is the process in which the relative partitioning of heavier and lighter isotopes of the same compound or molecule (in our case, a water molecule) changes in two co-existing phases due to the different nature of their chemical and physical properties, such as differences in their relative weights, inter-molecular vibration energy, strength of chemical bonds, etc. (Gat, 2010; Kendall & McDonnell, 2012). The most common types of isotope fractionation are equilibrium, kinetic, and transport fractionation, which are also commonly known as mass-dependent fractionation because the processes that cause these fractionation effects involve changes in the mass of two co-existing phases. There also exist mass-independent fractionation processes that are less common and depend on factors causing changes in the relative abundance of isotopes other than their mass difference, such as nuclear interactions, photochemical reactions, etc. (Gat, 2010; Kendall & McDonnell, 2012; Mook, 2000). In tracer-based hydrological applications, the investigation of mass-dependent fractionation processes is common (Gat, 2010; Kendall & McDonnell, 2012).

Equilibrium isotope fractionation processes are those processes in which the redistribution of isotopes occurs between two co-existing phases in the equilibrium state. In equilibrium fractionation, the exchange of isotopes can occur in both directions due to forward and backward chemical reactions. The most common example of equilibrium fractionation is the change from vapor condensation to rain in clouds, which is commonly understood as occurring in the equilibrium state (Kendall & McDonnell, 2012). On the other hand, kinetic fractionation occurs at a non-equilibrium state in which the relative abundance of isotopes changes between two co-existing states in one direction due to irreversible, unidirectional kinetic reactions. The evaporation of water bodies is commonly viewed as a kinetic fractionation process. More comprehensive details about both equilibrium and kinetic isotope fractionation can be found in Gat (2010) and Kendall & McDonnel (2012).

1.2 Importance and application of ^{18}O and ^{2}H isotopes in hydrological studies

In any hydrological study, information about the quantity and quality of water, flow-generation mechanisms, and source water partitioning is essential. For several decades, stable isotopes of water (^{18}O and ^{2}H) and radioactive (^{3}H) isotopes have played an important role in this regard. As highlighted by Klaus and McDonnell (2013), the use of stable water isotopes has significantly shifted our understanding of how event and pre-event waters partition since the late 1960s (Crouzet et al., 1970; Dinçer et al., 1970; Hubert et al., 1969). Thus, these isotopes play a fundamental role in advancing hydrological science. The ^{18}O and ^{2}H isotopes have been widely employed in surface water and groundwater hydrological studies, plant water uptake studies, and atmospheric moisture transport studies (Kendall & McDonnell, 2012). For example, these isotopes have been used to estimate the seasonality of precipitation contribution, the snowmelt water contribution to streamflow, lakes, rivers or seas, groundwater recharge estimation, the age of water estimation, the quantification of spring water exfiltration, moisture source estimation in the atmosphere, and in the analysis of their transport processes (Gat, 2010; Kendall & McDonnell, 2012; Mook, 2000). They are instrumental in providing insights into various hydrological processes across different spatial and temporal scales (Bowen et al., 2019). They serve as invaluable tracers, offering insights into phenomena ranging from broad atmospheric moisture transport patterns (Akers et al., 2017; Sjostrom & Welker, 2009; Vachon et al., 2010) to the micro-scale movements of water within soil pores and plants (Penna et al., 2018; Sprenger et al., 2016; Welker et al., 2005). In the context of the water cycle (Penna et al., 2018; Terzer-Wassmuth et al., 2021) and snow hydrology (Beria et al., 2018; Taylor et al., 2001), the utility of these isotopes is profound. For instance, the isotopic composition of snowmelt water (^{18}O and ^{2}H) can exhibit different ranges compared to precipitation isotopes (Beria et al., 2018; Gat, 1996; Hooper & Shoemaker, 1986; McNamara et al., 1997; Rodhe, 1981, 1998), highlighting diverse water cycle processes.

One of the fundamental applications of ^{18}O and ^{2}H isotopes in hydrology is the estimation of the partitioning of source waters (Klaus & McDonnell, 2013), where they are commonly employed as endmembers in Isotope Hydrograph Separation (IHS). The IHS is based on the principle of mass conservation (Klaus & McDonnell, 2013) and is a reliable approach for estimating source water partitioning in the mix (Hooper & Shoemaker, 1986; Rodhe, 1981; Sklash & Farvolden, 1979). A simpler

approach of IHS uses two endmembers in an Endmember Mixing Model Analysis (EMMA). In recent years, more complex methods, like the Bayesian Endmember Mixing Model Analysis (BEMMA) (Beria et al., 2020; Birkel et al., 2020, 2021; Cable et al., 2011; Fang et al., 2022; He et al., 2020; Marx et al., 2021; Popp et al., 2019, 2021) and Ensemble Hydrograph Separation (EHS) (Kirchner, 2019; Kirchner & Knapp, 2020; Knapp et al., 2019), have also been developed and utilized in numerous studies.

To better understand hydrological processes on local, regional, and global scales, hydrological modeling is at the core of any hydrological investigation, particularly for estimating and predicting the quantity of water in different forms present in the hydrosphere. Tracer-aided hydrological and ecohydrological models, such as the Spatially Distributed Tracer-Aided Rainfall-Runoff (STARR) model (Ala-Aho et al., 2017), the tracer-based Ecohydrological (EcH2O-iso) model (Kuppel et al., 2018), the isoWATFLOOD (Stadnyk, 2008; Stadnyk et al., 2007), and the University of Manitoba Stable Water Isotope Model (UMSWIM) (Smith et al., 2016), have increasingly gained popularity for better constraining model parameters, reliably estimating and simulating water ages, source water partitioning, evapotranspiration rates and the rate of plant water uptake.

1.3 Challenges in the application of ^{18}O and ^{2}H isotopes

Exploring seasonal snowpack is vital in hydrological studies of cold regions. The seasonal snowpack is often assumed to sequentially preserve the isotopic information of the atmospheric moisture and moisture transport processes, corresponding to individual snowfall events in snowpack profiles (Helsen et al., 2006; Sinclair & Marshall, 2008). However, post depositional and other isotope fractionation processes (Dietermann & Weiler, 2013; Hürkamp et al., 2019; Ohlanders et al., 2013; Siegenthaler & Oeschger, 1980; Sinclair & Marshall, 2008) can modify the snowpack isotope composition from individual precipitation events. These processes include isotope exchange caused by vapor diffusion (Friedman et al., 1991; Neumann et al., 2008; Sturm & Benson, 1997), freeze-thawing and condensation-sublimation processes (Ala-aho et al., 2017; Earman et al., 2006; Lechler & Niemi, 2012), all of which lead to frequent phase changes of water (solid-liquid-vapor), and thus, contribute to isotope fractionation in the snowpack (Evans et al., 2016; Lee et al., 2010; O'Neil, 1968; Stichler, 1987; Stichler et al., 1981; Zhou et al., 2008). Snow cover redistribution through wind drift and interception also impacts the snowpack $\delta^{18}O$ and $\delta^{2}H$ values, especially in forested

areas where snow falls from the canopy and alters the original isotope composition (Koeniger et al., 2008; von Freyberg et al., 2020; Vystavna et al., 2021).

The influence of site-specific controls on local precipitation isotopes has been extensively examined (Akers et al., 2017; Puntsag et al., 2016; Vachon et al., 2010), but the way the snowpack may distort the original vapor and snowfall isotope signal (Grootes & Stuiver, 1997; Steen-Larsen et al., 2011) remains less explored. Furthermore, the cumulative impact of isotope fractionation processes on snowpack isotope stratigraphy throughout winter is not well understood (Beria et al., 2018; Evans et al., 2016; Stichler, 1987; Stichler et al., 1981; Unnikrishna et al., 2002).

As accumulated snow begins to melt, a gradual increase in the isotopic enrichment of snowmelt ^{18}O and ^{2}H isotopes is typically observed (Laudon et al., 2002; Taylor et al., 2001), adding complexity to the temporal variability of meltwater. It is vital to investigate the temporal variability of snowpack and meltwater ^{18}O and ^{2}H isotopes, as it informs the assessment of liquid-ice fractionation processes (Ham et al., 2019; Lee et al., 2009, 2010). This, in turn, leads to a progressive enrichment of meltwater, affecting isotopic-based hydrological analyses such as the estimation of young water fractions and event and pre-event water contributions (Ceperley et al., 2020).

In cold and high-latitude regions, the lack of availability of high-resolution spatiotemporal hydrological datasets often poses an obstacle for modeling studies, especially in the wake of climate changes that have enhanced the unpredictability of hydrological predictions and future projections. Characterizing the spatial and temporal variations of meltwater ^{18}O and ^{2}H isotopic composition for applications in snow-influenced regions is challenging (Beria et al., 2018; Penna et al., 2018). The scarcity of studies addressing these variations on a catchment scale (Marttila et al., 2021) can be attributed to the difficulty of obtaining snow and meltwater samples in high latitude and altitude regions (Pu et al., 2020; Tetzlaff et al., 2018). Thus, with a limited number of samples for isotopic analysis, the accurate representation of progressive ^{18}O and ^{2}H enrichment in melting snowpacks and meltwater may be compromised (Taylor et al., 2001; Taylor, Feng, Williams, et al., 2002). Interestingly, the isotopic fractionation of early meltwater may vary from that during peak and post-peak meltwater (Schmieder et al., 2016) due to low sublimation at the beginning of the melting phase caused by relatively low ambient temperatures (Evans et al., 2016; Gustafson et al., 2010) and varying rates of liquid-ice isotopic fractionation (Feng et al., 2002; Lee et al., 2010; Taylor, Feng, Williams,

et al., 2002). Therefore, understanding these dynamics presents a gap in our knowledge.

Despite advancements in IHS and tracer-aided modeling, the lack of snowmelt isotope data in snow-influenced regions has a particularly negative impact on the reliability of model estimations and predictions. To accommodate the snowmelt component in tracer-aided models, empirical equations are often used (Ala-Aho et al., 2017; Kuppel et al., 2018). However, ideally, the isotope values of snowmelt water should be based on actual snowmelt isotope data, which is often unavailable.

Moreover, a globally unified approach to snowmelt sampling remains ambiguous in the literature. This adds complexity to the identification of the reliable event water endmember in the application of IHS in a seasonally snow influenced catchments. Researchers have used various methods for meltwater sampling, including a precipitation collector (Earman et al., 2006; Gui et al., 2019; Lucianetti et al., 2020), a snow corer for depth-integrated snowpack (Dinçer et al., 1970; Moore, 1989; Rodhe, 1981; Sueker et al., 2000), and a snowmelt lysimeter for snowmelt water (Laudon et al., 2002, 2004, 2007; McNamara et al., 1997; Rücker, Zappa, et al., 2019). Yet, a unified mathematical approach for defining a snowmelt event water endmember in the IHS model remains unclear (Klaus & McDonnell, 2013).

Field studies to date have either focused on the high-resolution temporal evolution of snowmelt water ^{18}O and ^{2}H isotopes based on a limited number of snowmelt lysimeters (Pu et al., 2020; Rücker, Zappa, et al., 2019), neglecting broad spatial isotopic variation, or they have investigated numerous lysimeters across the landscape (Laudon et al., 2002; Rücker, Boss, et al., 2019), while overlooking high-resolution temporal variability. Ala-Aho et al. (2017) have attempted to simulate these spatial and temporal variations, but validation of such simulations remains challenging due to inadequate high-resolution field data on concurrent snowpack and snowmelt water ^{18}O and ^{2}H isotopes. As a result, our understanding of the simultaneous isotope changes and fractionation processes of the snowpack and meltwater in field conditions is still limited (Carroll, Deems, Maxwell, et al., 2022; Carroll, Deems, Sprenger, et al., 2022; Lee et al., 2010). Furthermore, the sensitivity of estimating snowmelt contribution to stream water, based on different methods of approximating snowmelt ^{18}O and ^{2}H isotopes, has not been extensively investigated. The potential bias introduced by using snowfall or depth-integrated snowpack isotope-based event water endmember as a surrogate for the snowmelt water endmember remains largely unexplored.

1.4 Research questions and objectives

The overarching objective of this thesis was to enhance our understanding of snow hydrological processes through the lens of stable water isotopes ^{18}O and ^{2}H. The research was mostly carried out in the Pallas catchment in Northern Finland, with intensive fieldwork in 2019 and 2020. This involved the sampling of snowfall, depth-integrated snowpack, stratigraphy of fixed 5-cm vertical snowpack, and subsequent snowmelt water. The collected samples were later analyzed for their isotopic composition using an advanced laser-based stable water isotopic analyzer at the University of Oulu's laboratory.

The aim was to decipher the hydrological processes, particularly the snowmelt processes, by leveraging the isotopes of ^{18}O and ^{2}H. The thesis also aimed to contrast the isotopic composition of snowpack and snowmelt water and investigate the underlying causes of any discrepancies. The final goal was to understand the spring streamflow generation process and perform a more reliable estimation of snowmelt water's contribution to the outlet stream in the Pallas catchment by analyzing potential biases resulting from differences in methodology for approximating snowmelt isotopes.

This thesis sought to answer the following central research questions:

1. How do the snowpack isotope values change, as reflected by the vertical isotopic stratigraphy in the accumulated snowpack in Arctic conditions? [Publication I and Publication II]
2. How do snowpack and snowmelt water isotope values evolve over time across different landscape conditions/features? [Publication II]
3. How do we quantify the potential bias in the estimation of snowmelt water's contribution to streamflow, based on the characterization of meltwater endmember isotopes, through different sampling methods and mathematical approximations? [Publication III]

To address the first question, we sampled numerous snow pits across two contrasting Arctic snow regimes: (i) the taiga snowpack in Pallas and the tundra snowpack in Alaska, and (ii). The obtained isotope data were used to evaluate the isotopic stratigraphy within the snowpack [Publication I]. Additionally, we assessed the spatiotemporal evolution of vertical isotope profiles within the Pallas snowpack from late winter to spring, until the complete melting of the snow [Publication II].

In order to address the second question, we collected meltwater samples for isotopic composition analysis using several snowmelt lysimeters. These were deployed for three distinct landscape features in Pallas: (i) forest hillslope, (ii) mixed forest, and (iii) open mires. We examined the meltwater isotope data to evaluate the spatiotemporal evolution of meltwater isotopes. The meltwater isotopes were then compared to the depth-integrated snowpack isotopes from the pre-peak melt to post-peak melt periods [Publication II].

In literature, different methods are used to characterize snow meltwater isotopes, for instance, melting the snowfall and depth-integrated snowpack samples and directly obtaining the meltwater samples, e.g., using a snowmelt lysimeter. To answer the third question, we utilized isotope data from snowfall events, depth-integrated snowpack, and meltwater using an isotope hydrograph separation approach. This method was used to analyze the potential bias in the contribution of meltwater to streamflow, where the meltwater isotopes were characterized through different sampling methods and mathematical approximations [Publication III].

2 Study area, methodology and analysis

2.1 Study area

The Pallas research catchment situated within the Arctic Circle in Northern Finland, as depicted in Fig. 1, is located at coordinates 67.99°N and 24.24°E. The catchment, with an area of 4.42 km^2, has an elevation varying between 268 m and 364 m above sea level. Its landscape is characterized by spruce tree hillslopes, mixed woodland forests with spruce, birch, and pine trees, shrubs, and open mires and peatlands. The soil consists of mineral deposits on hillslopes, covered by a 5–10 cm layer of organic soil. Peat soil, however, extends up to 3 m deep in the open mires, which are dominated by mosses and low sedges. The site has four eddy covariance flux stations, two of which are within the catchment boundaries: the Kenttärova weather station (Finnish Meteorological Institute's Station ID: 101987) and the Lompolojänkkä wetland weather station (Station ID: 778135), which became operational in 2002 and 2013, respectively.

The climate of the site is subarctic, with a consistent snow blanket during winter only. Despite its high latitude, the Pallas site is not influenced by permafrost and experiences complete thaw soon after snowmelt. Meteorological variables have been monitored in this region for over eight decades, owing to a well-established network of hydrological and eco-hydrological instruments (Marttila et al., 2021). The catchment's research activities have seen a particular surge since 2014, when ecohydrological investigations were initiated.

In this study, we relied on meteorological data from the Kenttärova weather station. Data from 2003 to 2019 reveals a mean annual air temperature of 0.4 °C, while the period from 2008 to 2019 experienced an average precipitation of 639 mm annually. Snowfall accounts for around 42% of this precipitation, with snow usually melting entirely by June. Notably, in 2020, snowfall constituted 48% of the total precipitation and the snow depth peaked at 130 cm, which was 30 cm more than the previous year [Publication II]. More comprehensive details on the Pallas catchment's characteristics can be found in the work of Marttila et al. (2021).

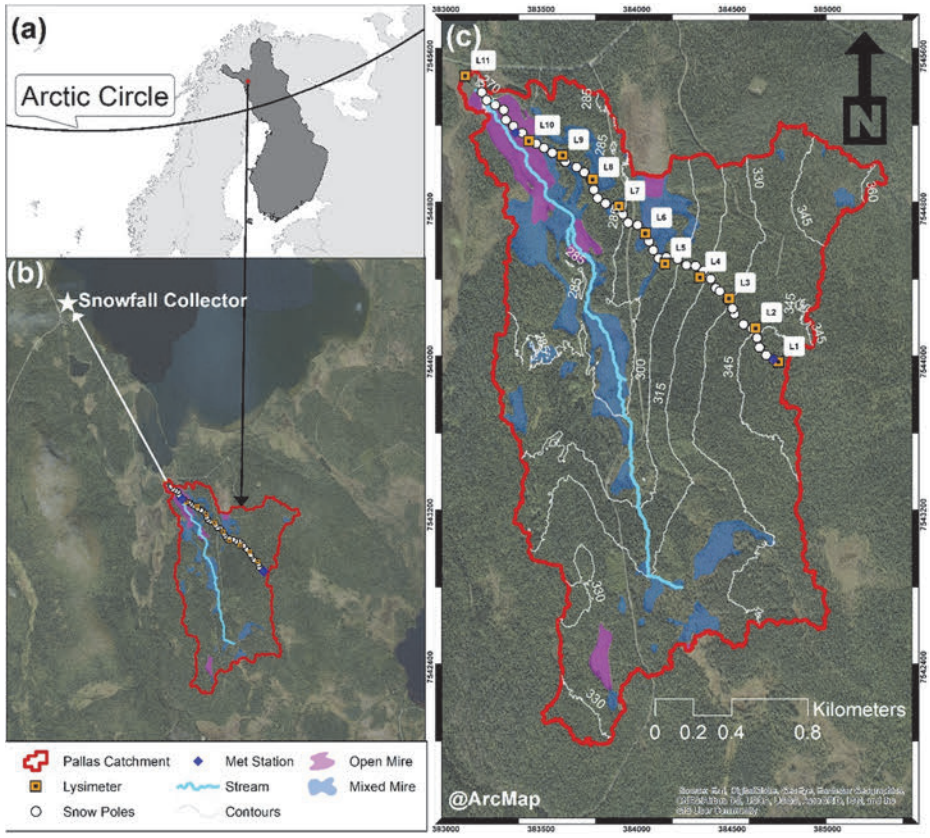

Fig. 1. (a) Displays the position of the Pallas catchment, situated within the Arctic Circle in Northern Finland (67.99°N and 24.24°E); (b) illustrates the placement of the snowfall collector, installed approximately 3.5 km to the northwest of the catchment's outlet stream; and (c) indicates the positions of the snowmelt lysimeters and snow poles within the Pallas catchment (Reprinted under CC BY 4.0 license from Publication III © 2023 Authors).

We excavated ten snowpits along the snow monitoring transect, collected and analyzed a number of snow samples based on the vertical snow stratigraphy, identified by a hand hardness test from the Imnavait research location (68.6°N, 149.3°W). This site is located in the northern foothills of the Alaskan Brooks Range, U.S.A., with an elevation ranging from 844–960 m a.s.l. It lies in a continuous permafrost region, with the soil is characterized by glacial till clay covered with an organic layer at the top. Treeless tundra vegetation consists primarily of tussock sedge and dwarf shrub tundra. As a long-standing observation point for permafrost

hydrology and tundra snowpack, it offers more than three decades' worth of data on snow depth and snow water equivalent. The area experiences an average annual surface air temperature of -7.7 °C and receives a total of 334 mm of precipitation annually, based on records from 1985–2017. The snow-covered period usually spans from October to May, with the long-term averages for end-of-winter snow-water equivalent and snow depth at 124 mm and 50 cm, respectively. We sourced climate data for our study from the SNOTEL snow telemetry and snow course data network meteorological station (Station ID 968). Further details and a map of the Imnavait research site can be found in Publication I.

2.2 Data, methodology and laboratory analysis

2.2.1 Meteorological, hydrological and hydrometric data

The data sets employed in this study were collected from 2018 to 2020. Daily meteorological parameters were obtained from the Finnish Meteorological Institute's database (FMI) for the Kenttärova station (ID: 101987). Additionally, hydrometric data were sourced from the Finnish Environment Institute's (SYKE) database for the catchment's outlet stream gauging station.

A 2.2 km snow survey track was set up in the Pallas catchment, starting from a hillslope at the Kenttärova station, traversing open mires downstream, and ending at the catchment's outlet stream at the v-notch weir station (Fig. 1). Snow Depth (S_h) and Snow Density (S_d) were recorded at 46 and 11 locations, respectively, along the survey transect. Snow depth was recorded every 50 m, while snow density was measured approximately every 200 m, near snowmelt lysimeter locations specifically (Fig. 1).

Snow density was primarily measured using a graduated plastic snow tube, with a diameter of 10.3 cm and weighing 1.65 kg. However, tubes of varying lengths (but the same diameter) were occasionally used in accordance with the snowpack depth. The snow tube's weight was recorded using a hanging weighing scale. Subsequently, the Snow Water Equivalent (SWE) was calculated from the recorded and measured S_h and S_d values.

2.2.2 ^{18}O and ^{2}H isotope data

To sample snowmelt, we used snowmelt lysimeters (Fig. 2a). We established a snowmelt lysimeter system across diverse landscape features within the Pallas catchment at 11 locations (Fig. 1); on a forest hillslope containing predominantly evergreen spruce trees along the 2.2 km transect of the catchment (L1, L2, L3, L4, and L5); in a mixed forest area consisting of both evergreen and deciduous trees (L7, L8, L9, and L11); and in open mires (L6 and L10). Each lysimeter setup incorporated a square metal collector with an area of 50 cm x 50 cm, although lysimeter No. 11 consisted of a larger 100 cm x 100 cm collector. Each collector was structured with 5 cm raised rims and an outlet corner extended by a roughly 1 m pipe (less than 0.5 m at L10), which was designed to enable meltwater outflow. A claw-coupling (Fig. 2a) was fixed at the pipe's end to facilitate the convenient attachment and detachment of a plastic bag for water collection, and finally the sampling mechanism was safeguarded within a plastic box. The setup was constructed in accordance with the ground's natural slope and insulated against freezing using Styrofoam. We collected snowmelt water samples daily in plastic bags as outflows from these lysimeters at 200 m intervals along the catchment's transect. The snowmelt efflux (mm/d) was determined from the meltwater sample weight, divided by the water density and cross-sectional area of the snowmelt lysimeter over the elapsed time between two consecutive sampling rounds. Isotopic compositions of the collected samples were analyzed later in the laboratory at the University of Oulu.

In 2019, during the late snow season, snow isotope stratigraphy (Fig. 2b) was sampled in snowpits around the time of maximum snow depth, specifically from 3rd to 4th April. We followed a 5 cm fixed-depth sampling approach for the Pallas catchment. Nine snowpits were sampled and analyzed for isotope analysis; these were located approximately 200 m apart along the snow-survey monitoring transect, spanning the elevation gradient in the study catchment. The sampling procedure involved extracting incremental 5 cm snow layer samples with a cubic-shaped 5 cm metal snow sampler. In 2019, the entire profile was normalized to cumulative snowfall, allowing for the relative depth estimation of each snowfall event [0–100%] relative to accumulated snowfall before sampling [Publication I].

The starting and ending plotting position of each precipitation sample on the y-axis were computed using the following 2 equations

$$Pl_{start}(i) = \frac{\sum_{i=1}^{i-1} P(i)}{\sum_{i=1}^{n} P(i)} \times 100 \quad (3)$$

and

$$Pl_{\mathrm{end}}(i) = \frac{\sum_{i=1}^{i} P(i)}{\sum_{i=1}^{n} P(i)} \times 100, \quad (4)$$

where Pl_{start} is the start of the y-axis plotting position for sample i. Pl_{end} is the end of the y-axis plotting position for sample i, P is the precipitation amount in sample i [mm], and n is the number of precipitation events.

In 2020, eleven snowpits (Fig. 2b) were excavated before the snowmelt period, from the 2nd to 6th April, at locations along the snow survey transect, adjacent to the lysimeter locations (Fig. 1). Additional spatiotemporal snowpit samplings were performed at three locations during different phases of the snowmelt period (22nd–23rd April 2020 - before peak melt, 23rd May 2020 - during peak melt, and 28th May 2020 - post peak melt). At each of these stages, snow samples were extracted from the snowpits at fixed vertical 5 cm intervals for isotopic composition analysis. The sampling depth was normalized to a scale of 0–1 in 2020 by dividing by the total snow depth monitored at each snowpit location for the layered-snowpack isotope stratigraphy. This was achieved by dividing the sampling depth by the total snow depth measured at each snowpit location, thus presenting a normalized scale ranging from 0–1. This process facilitated the comparability of the snowpit isotope data [Publication II]. The cumulative precipitation amounts were similarly normalized against the total precipitation recorded during the snow accumulation phase, up to the day of peak snow depth observation, to provide the normalized depth for a given amount of precipitation.

Depth-integrated bulk snow samples (Fig. 2c) were collected biweekly during the winters of 2019 and 2020 for water isotope analysis. Sampling was performed using a 3.5 cm diameter plastic tube at each lysimeter location, set at 200 m intervals. These samples were occasionally gathered during the 2019 snowmelt period and every two to three days in 2020. The snow density and snow water equivalent were calculated from snow depths and weights for each lysimeter location.

Event-based snowfall samples (Fig. 2d) were gathered for their isotopic composition using a 25 cm^3 open container. This was positioned approximately 3.5 km northwest of the outlet stream (68.257°N, 24.1602°E) (Fig. 1). Isotope data for snowfall, snowpack and meltwater are available through the link: https://doi.org/10.23729/c2d0ade1-cb3d-4dea-a48b-dbb5654bb662.

Stream water samples (Fig. 2e) were systematically collected using an ISCO automatic sampler (Model 6712, Teledyne ISCO, NE), encapsulated in 50 ml

plastic tubes. The sampling frequency varied seasonally, twice daily during winter and four times daily during spring in 2020. Occasionally, grab samples were also gathered and analyzed for isotope analysis. The stream water isotopes are available through the link: https://doi.org/10.23729/8369b18e-939b-4f8f-b07b-6a8e9ba7030e.

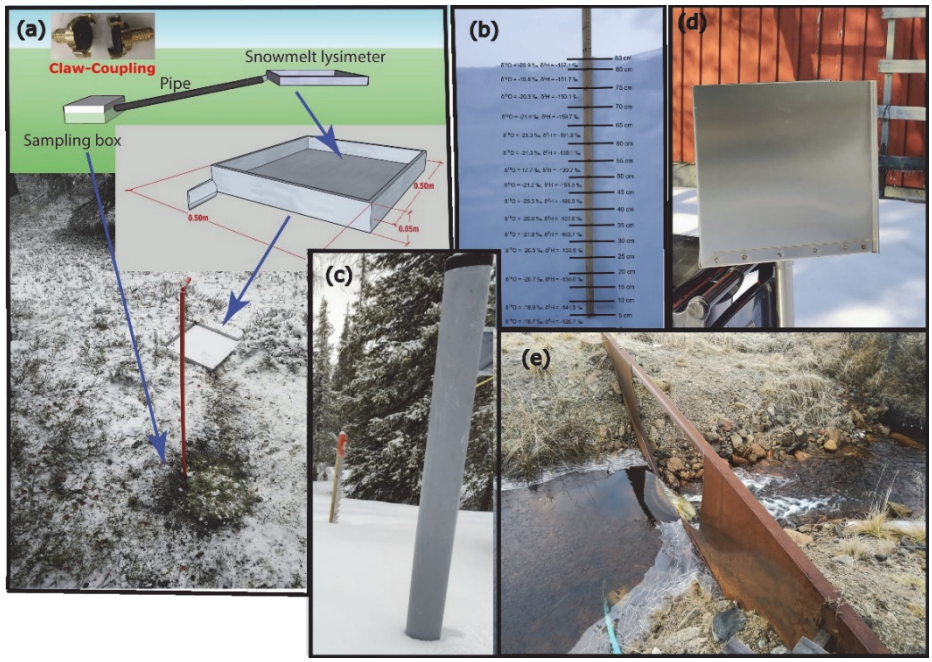

Fig. 2. Sampling design of (a) meltwater isotopes using snowmelt lysimeter, (b) vertical isotope stratigraphy in snowpit, (c) depth-integrated snowpack isotopes using snow corer, (d) snowfall isotopes using snowfall sampler, and (e) stream water isotopes from the catchment's outlet stream.

2.2.3 Isotope hydrograph separation: streamflow generation analysis

In Publication III, we focused on understanding the origins of streamflow during the peak melt period, specifically from May 21 to June 6, 2020. We achieved this by applying a two-component Isotope Hydrograph Separation (IHS) technique to distinguish between contributions from snowmelt water and pre-event water.

During the winter at Pallas, streamflow is largely maintained through baseflow, taken as a combined indicator of integrated soil and groundwater. Conversely, snowmelt water is categorized as event water. Utilizing the two mass balance

equations outlined below, we estimated the proportions of snowmelt water and baseflow present in the stream water

$$Q_{\mathrm{st}} = Q_{\mathrm{bf}} + Q_{\mathrm{sm}}, \tag{5}$$

where Q_{st}(mm/hr) is the stream water specific discharge, Q_{bf}(mm/hr) represents the baseflow specific discharge, and Q_{sm}(mm/hr) is the snowmelt flux.

$$Q_{\mathrm{st}}\delta_{\mathrm{st}} = Q_{\mathrm{bf}}\delta_{\mathrm{bf}} + Q_{\mathrm{sm}}\delta_{\mathrm{sm}}, \tag{6}$$

where δ_{st}, δ_{sm}, and δ_{bf} are the isotopic values for stream water, snowmelt water, and baseflow, respectively, expressed per mil (‰).

Upon solving these equations, we obtained the relative contributions of baseflow and snowmelt water to the stream, denoted as f_{sm} and f_{bf}, respectively

$$f_{\mathrm{sm}} = \frac{\delta_{\mathrm{bf}} - \delta_{\mathrm{st}}}{\delta_{\mathrm{bf}} - \delta_{\mathrm{sm}}} \tag{7}$$

and

$$f_{\mathrm{bf}} = \frac{\delta_{\mathrm{st}} - \delta_{\mathrm{sm}}}{\delta_{\mathrm{bf}} - \delta_{\mathrm{sm}}}. \tag{8}$$

In order to ensure consistent time intervals for our analysis, we interpolated the isotope data to accommodate hourly time steps because of the lack of availability of hourly data and variation in frequency for different water sources. We used the specific discharge-weighted averages of both stream water isotopes $\overline{\delta_{\mathrm{st}}}$ ^{18}O and baseflow isotopes $\overline{\delta_{\mathrm{bf}}}$ ^{18}O, with weights determined by hourly specific discharge values.

Furthermore, we computed the weighted averages of snowfall isotopes $\overline{\delta_{\mathrm{sf}}}$ ^{18}O,, snowmelt water isotopes $\overline{\delta_{\mathrm{sm}}}$ ^{18}O and snowpack isotopes $\overline{\delta_{\mathrm{sp}}}$ ^{18}O, based on the associated variables, such as the precipitation amount, melt flux and snow water equivalent (SWE). This weighted average can be calculated by using the formula

$$\bar{\delta} = \frac{\sum_{i=1}^{n} V_i \times \delta_i}{\sum_{i=1}^{n} V_i}, \tag{9}$$

where $\overline{\delta}$ represents the weighted average isotope value, V_i represents the specific discharge, melt flux, SWE, or precipitation amount corresponding to the isotope value at time step i, and δ_i denotes the isotope value of ^{18}O or ^{2}H at time step i.

To estimate the snowmelt water fractions during peak streamflow generation, we applied ten unique scenarios (as shown in Table 1). Each scenario utilized a fixed pre-event water endmember but varied in the utilized event water endmember.

Scenarios (VII) RCVWSP and (VIII) RCVWSM utilize a methodology proposed by Laudon et al. (2002). This approach incorporates the influence of all snowmelt episodes, including those temporarily held within the catchment that have not yet contributed to streamflow during the IHS calculations. The method takes into account the volume and timing of meltwater infiltrating the soil and entering surface water reservoirs from previous melt events, it assumes that snowmelt water stored within the catchment is uniformly mixed at any given time. The formula suggested by Laudon et al. (2002) is used to estimate the snowmelt fractions in these scenarios

$$\delta_{e_t} = \frac{(\sum_{i=1}^{t} M_i \times \delta_{\mathrm{sm}_i} - \sum_{i=1}^{t-1} E_i \times \delta_{e_i})}{(\sum_{i=1}^{t} M_i - \sum_{i=1}^{t-1} E_i)}, \quad (10)$$

where δ_{et} represents the corrected incremental SWE or melt flux-weighted average snowpack or snowmelt isotope value ($\delta^{18}O$ or $\delta^{2}H$) at time step t, M_i and E_i are the meltwater depth and event water discharge, respectively, at time step i, while $\delta_{\mathrm{sm}i}$ and δ_{ei} are the corresponding snowmelt water and event water isotope values.

The calculation of $\delta_e{}^{18}O$ at the initial time step is based on the SWE or melt flux-weighted average of the snowpack or snowmelt water isotope value from the onset of the melt period to the day before peak melt. At the first time step, E is based on $\delta_e{}^{18}O$ obtained using Eq. 7.

Scenarios (IX) Roll-RCVWSP and (X) Roll-RCVWSM are introduced as improved versions of scenarios (VII) RCVWSP and (VIII) RCVWSM. These versions utilize a combined incremental and rolling weighted average of the corrected snowpack or snowmelt isotope value. The first five days involve the use of an incremental weighted average isotope value (Eq. 10) and, subsequently, a five-day rolling weighted average isotope value is used for the days that follow. Unlike scenarios (VII) RCVWSP and (VIII) RCVWSM, these improved scenarios do not include all melt episodes in their snowmelt water fraction estimations. Nonetheless, they offer a relatively better estimation of the tail end of the snowmelt water isotopic evolution in the IHS process by assuming that the meltwater episode does not stay in the catchment for more than the 5 days of snowmelting and adheres to the principles of the runoff-correction method.

Table 1. Scenarios (ten in total) or approaches used in the IHS method to estimate snowmelt water fractions during spring peak streamflow generation. The volume weighted average term is used for the amount weighted average snowfall, specific discharge weighted average baseflow, melt flux weighted average snowmelt, and SWE weighted average snowpack.

Scenario	Event water Endmember	Assumptions
(I) Time-invariant Volume Weighted Average Snowfall (VWSF)	Volume Weighted Average Snowfall	The meltwater isotopic signal, approximated using the volume-weighted average snowfall isotopic signal, remains constant in space and time.
(II) Time-invariant Volume Weighted Average Snow Meltwater (VWSM)	Volume Weighted Average Meltwater	The meltwater isotopic signal remains constant in space and time.
(III) Time-invariant Volume Weighted Average SnowPack Before melt period (VWSPB)	Volume Weighted Average Snowpack before melt period	The meltwater isotopic signal, approximated using the volume weighted average snowpack isotopic signal before the melt period, remains constant in space and time.
(IV) Time-invariant Volume Weighted Average SnowPack During melt period (VWSPD)	Volume Weighted Average Snowpack during melt period	The meltwater isotopic signal, approximated using the volume weighted average snowpack isotopic signal during the melt period, remains constant in space and time.
(V) Time-variant SnowPack (SP)	Snowpack time series during melt period	The meltwater isotopic signal is approximated using the snowpack isotopic signal during melt period. No meltwater is stored temporally in the catchment, and all hourly meltwater contributes to streamflow at each time step of the IHS.
(VI) Time-variant Snow Meltwater (SM)	Meltwater time series	The meltwater isotopic signal is determined for the sample obtained using snowmelt lysimeter. No meltwater is stored temporally in the catchment, and all hourly meltwater contributes to streamflow at each time step of the IHS.

Scenario	Event water Endmember	Assumptions
(VII) Time-variant Incremental Runoff-Corrected Volume Weighted Average SnowPack (RCVWSP)	Incremental Runoff-Corrected Volume Weighted Average Snowpack	Equation 10 for Runoff-Correction takes into account the meltwater that is temporally stored in the catchment, where meltwater isotopic signal is approximated using the incremental volume weighted average snowpack during the melt period and this signal of all melt episodes is required for the IHS.
(VIII) Time-variant Incremental Runoff-Corrected Volume Weighted Average Snow Meltwater (RCVWSM)	Incremental Runoff-Corrected Volume Weighted Average Meltwater	Equation 10 for Runoff-Correction takes into account the meltwater that is temporally stored in the catchment, where meltwater isotopic signal is approximated using the incremental volume weighted average meltwater and this signal of all melt episodes is required for the IHS.
(IX) Time-variant Rolling Runoff-Corrected Volume Weighted Average SnowPack (Roll-RCVWSP)	Incremental Runoff-Corrected Volume Weighted Average for the first 5 days and a 5-day Rolling Runoff-Corrected Volume Weighted Average Snowpack for the following days	Equation 10 for Runoff-Correction takes into account the meltwater that is temporally stored in the catchment, where meltwater isotopic signal is approximated using the incremental volume weighted average snowpack for the first 5 days and a 5-day Rolling Runoff-Corrected volume weighted average snowpack isotopic signal for the following days.
(X) Time-variant Rolling Runoff-Corrected Volume Weighted Average Snow Meltwater (Roll-RCVWSM)	Incremental Runoff-Corrected Volume Weighted Average for the first 5 days and a 5-day Rolling Runoff-Corrected Volume Weighted Average Meltwater for the following days	Equation 10 for Runoff-Correction takes into account the meltwater that is temporally stored in the catchment, where meltwater isotopic signal is approximated using the incremental volume weighted average meltwater for the first 5 days and a 5-day Rolling Runoff-Corrected volume weighted average meltwater isotopic signal for the following days.

Note: three other assumptions which are same for all scenarios:

- The baseflow isotopic signal (Volume Weighted Average Baseflow) remains constant in space and time.
- Streamflow is generated from baseflow and meltwater only.
- The isotopic signal of the considered scenario and the volume-weighted average baseflow isotopic signal are significantly different from each other.

2.2.4 Estimation of uncertainty

The uncertainty associated with the contribution of event snowmelt water to stream outlet is estimated using a general or Guassian Uncertainty Propagation technique, as presented by Genereux (1998). The formula is expressed as follows

$$W_{f_{\mathrm{sm}}} = \sqrt{\left(\frac{\partial f_{\mathrm{sm}}}{\partial \delta_{\mathrm{sm}}} W_{\delta_{\mathrm{sm}}}\right)^2 + \left(\frac{\partial f_{\mathrm{sm}}}{\partial \delta_{\mathrm{bf}}} W_{\delta_{\mathrm{bf}}}\right)^2 + \left(\frac{\partial f_{\mathrm{sm}}}{\partial \delta_{\mathrm{st}}} W_{\delta_{\mathrm{st}}}\right)^2}, \qquad (11)$$

where $W_{f\mathrm{sm}}$ represents the uncertainty of the snowmelt water fraction (f_{sm}), $W_{\delta\mathrm{sm}}$ is the uncertainty of the snowmelt isotopes (δ_{sm}) or the uncertainty of the input isotope values if different endmembers are used, $W_{\delta\mathrm{bf}}$ is the uncertainty of the baseflow isotopes (δ_{bf}), and $W_{\delta\mathrm{st}}$ is the uncertainty in the stream water isotopes (δ_{st}).

By implementing Eq. 10 at each time step, we derive

$$W_{f_{\mathrm{sm}\,t}} = \sqrt{\left[\frac{(\delta_{\mathrm{bf}t} - \delta_{\mathrm{st}t})}{(\delta_{\mathrm{bf}t} - \delta_{\mathrm{sm}t})^2} W_{\delta_{\mathrm{sm}\,t}}\right]^2 + \left[\frac{(\delta_{\mathrm{st}t} - \delta_{\mathrm{sm}t})}{(\delta_{\mathrm{bf}t} - \delta_{\mathrm{sm}t})^2} W_{\delta_{bf\,t}}\right]^2 + \left[\frac{(-1)}{(\delta_{\mathrm{bf}t} - \delta_{\mathrm{sm}t})} W_{\delta_{\mathrm{st}}}\right]^2}, \qquad (12)$$

where the subscript *t* indicates the time step at which the corresponding variable is computed. The fixed value in Eq. 12, i.e., $W_{\delta\mathrm{st}}$, is based on 5% of the measuring instrument's analytical uncertainty.

Note that Eqs. 10 and 11 do not include covariance terms, as they represent simplified versions of a more comprehensive error propagation equation. These equations presume no covariance among the measurands, considering them as independent entities. The analytical uncertainty of the instrument, assumed to be 5%, is applied to the uncertainty in stream water at each time step (Genereux, 1998) because stream water is the mix, where calculations are made at each time-step. The uncertainties in stream water, pre-event, and event water endmembers (i.e., W_{δ} values), outlined in Table 2, are used to estimate the uncertainty of the final snowmelt water fraction.

Table 2. Spatial and temporal uncertainties in pre-event and event water endmembers and stream water using 95% confidence levels. The term 'W_δ' is estimated as the product of standard error and the student's t-value (95% confidence level).

Scenario	Uncertainty in Pre-Event Water Endmember			Uncertainty in Event Water Endmember			Uncertainty in Streamwater (Mix)		
	Symbol	Temporal Uncertainty	Spatial Uncertainty	Symbol	Temporal Uncertainty	Spatial Uncertainty	Symbol	Temporal Uncertainty	Spatial Uncertainty
I VWSF	$W_{\delta bf}$	0.020	-	$W_{\delta VWSF}$	1.020	-	$W_{\delta st}$	5%	-
II VWSM	$W_{\delta bf}$	0.020	0.020	$W_{\delta VWSM}$	0.584	*	$W_{\delta st}$	5%	5%
III VWSPB	$W_{\delta bf}$	0.020	0.020	$W_{\delta VWSPB}$	0.267	*	$W_{\delta st}$	5%	5%
IV VWSPD	$W_{\delta bf}$	0.020	0.020	$W_{\delta VWSPD}$	0.188	*	$W_{\delta st}$	5%	5%
V SP	$W_{\delta bf}$	-	0.020	$W_{\delta SP}$	-	*	$W_{\delta st}$	-	5%
VI SM	$W_{\delta bf}$	-	0.020	$W_{\delta SM}$	-	*	$W_{\delta st}$	-	5%
VII RCVWSP	$W_{\delta bf}$	0.020	-	$W_{\delta RCVWSP}$	**	-	$W_{\delta st}$	5%	-
VIII RCVWSM	$W_{\delta bf}$	0.020	-	$W_{\delta RCVWSM}$	**	-	$W_{\delta st}$	5%	-
IX Roll-RCVWSP	$W_{\delta bf}$	0.020	-	$W_{\delta Roll\text{-}RCVWSP}$	***	-	$W_{\delta st}$	5%	-
X Roll-RCVWSM	$W_{\delta bf}$	0.020	-	$W_{\delta Roll\text{-}RCVWSM}$	***	-	$W_{\delta st}$	5%	-

- no estimation.

* Variable W values for spatial uncertainty, computed at each time step.

** time series of incremental W values.

*** time series of incremental W values for the first 5 days, and time series of a 5-day rolling W values for the subsequent days.

We used Standard Error (SE) instead of Standard Deviation (SD); where the latter is thought of as the dispersion of the data that is spread around the mean value, the former is the dispersion of the sample mean around the true population mean. Although the sampling does not cover an extensive number of years, the quantity of samples taken within each year can be substantial. The formula for computing SE is given by Eq. 13

$$SE = \frac{SD}{\sqrt{n}}, \tag{13}$$

where n is the sample size.

Since we have 11 snowmelt lysimeters at Pallas, we were able to estimate spatial and temporal uncertainties. The spatial uncertainty was based on the spatial variability of the analyzed meltwater isotope values at each melting day, while the temporal uncertainty was based on the temporal variability of the estimated weighted mean values over the course of the melt period. This was achieved by first estimating weighted means from meltwater isotope values at all locations for each day, and then computing the SE of these temporal weighted means. The same procedure was followed for the Depth-integrated (DI) snowpack isotope values, which were also sampled spatiotemporally. For snowfall sampling, we had only one sampler; thus, we were only able to estimate the temporal uncertainty.

2.2.5 Laboratory isotope analysis

After collection, the snowpack samples were securely stored in sealed plastic bags on-site before being transferred to the Ecology and Geotechnical laboratories at the University of Oulu. These samples were allowed to fully melt at room temperature and were then stored in 15 ml or 50 ml plastic tubes. Prior to their isotopic analysis, all samples, including snowmelt water, were refrigerated at a temperature of 4 °C. Before the analysis, samples were transferred from the 15 ml plastic tubes to 2 ml glass vials, which were sealed with septa-capped screws. The isotopic composition of the samples was analyzed following standard Picarro guidelines. Each sample underwent seven analyses, with the initial four injections disregarded due to their higher isotope value variability. The average of the final three injections was used to obtain the raw isotope values for each sample.

The snowfall and stream snow samples were analyzed using a laser-based Cavity Ring-Down Spectroscopy (CRDS) Picarro analyzer, L2130-i, at the Ecology and Genetics Research Unit Lab, University of Oulu. Concurrently,

snowpack and snowmelt water samples were analyzed using the CRDS Picarro analyzer, L2140-i, at the Geotechnical Lab, University of Oulu. The Ecology Lab utilized the USGS 45 and USGS 46 standards for calibration, whereas the Geotechnical Lab employed three in-house standards: (i) Hawaii, (ii) Tap, and (iii) Viro. The isotopic values were determined relative to the Vienna Standard Mean Ocean Water (VSMOW) international standard and are expressed in per mil (‰).

3 Results

3.1 Snowpack ^{18}O isotopes [Publication I and Publication II]

3.1.1 Comparison of snowpack ^{18}O isotopes in two different Arctic regions [Publication I]

As there is a strong correlation between ^{18}O and ^{2}H isotopes, only one of these isotopes is needed to investigate the objectives of this research work, avoiding redundancy. We primarily focused on ^{18}O isotopes but used both to calculate the lc-excess. This study compared the snowpack ^{18}O profiles from two different research sites within the Arctic circle: Imnavait and Pallas. We utilized the isotope data derived from snowpack samples obtained during the 2019 winter sampling campaign, which was closer to the period of maximum snow depth. Notably, there were significant differences in $\delta^{18}O$ values at both research sites.

The snow depth at Imnavait was less consistent and lower overall compared to Pallas. However, each research site displayed nearly identical ranges of $\delta^{18}O$ values at different snowpit sampling locations. Therefore, it is visually difficult to discern clear distinctions in isotope profiles (see Fig. 3). Snowpit isotope profiles at Pallas are represented by different colors, while at Imnavait, different colors show the density profiles of snowpits (Fig. 3). At Imnavait, the bottom quarter (0–25% relative snow depth) consistently displayed higher $\delta^{18}O$ values compared to the snowpack's top but with greater variability in $\delta^{18}O$ values, i.e., variability ranging from ~ -25‰ to -21‰ at the base as compared to -33‰ to -30‰ at the surface (Fig. 3). A similar higher $\delta^{18}O$ value trend was recorded at the snowpack base (below 10% relative snow depth) at Pallas, as illustrated in Fig. 3b. At Pallas, there was no clear difference in $\delta^{18}O$ values between the top and base of the snowpack, and the $\delta^{18}O$ variability spanned approximately ~5‰ across all depths, with the greatest variability observed closer to the surface snow (above 60% relative snow depth). We have not found any evident correlation between the variability of isotope values and snow depth. Overall, snowpack isotope profiles at Pallas demonstrated greater variability in isotope values than Imnavait.

At Imnavait, most of the $\delta^{18}O$ values at the upper section of the snowpack (75–100% of the total depth) were found to be less than -30‰ and the section was characterized by low-density snow, ~100 kg/m^3 (Fig. 3). The $\delta^{18}O$ values at the central segment of the snowpack (25–75% of the total depth) varied between -25‰

and -30‰, and the density was higher at this segment, i.e., within a range of ~300–400 kg/m^3. The bottom section of the snowpack (0–25% of the total depth) comprised a moderately dense layer (~200 kg/m^3), and $\delta^{18}O$ values at this section were higher than those in the layers above, i.e., within the range of -20‰ to -25‰. While this discussion only compares the $\delta^{18}O$ snowpack isotope profiles at Imnavait and Pallas, readers seeking additional details are referred to Publication I.

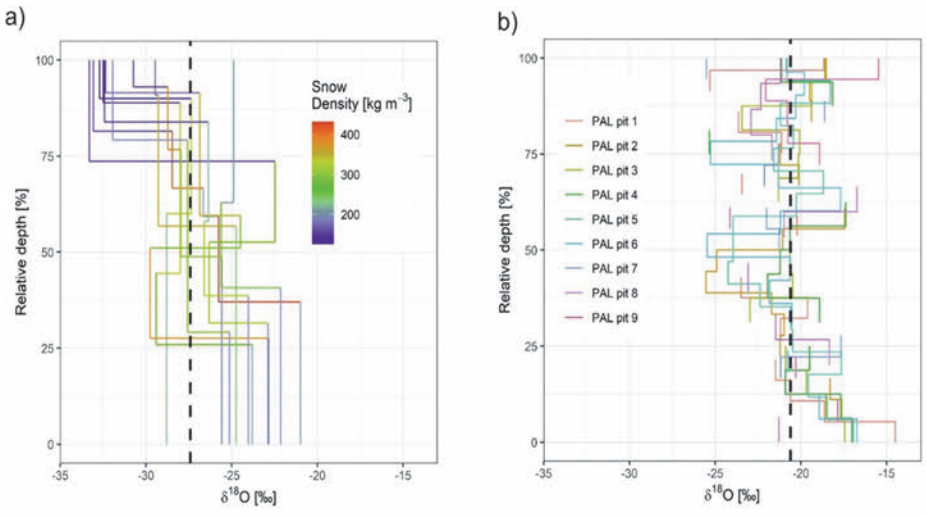

Fig. 3. Representation of snowpack $\delta^{18}O$ values with respect to the depth normalized to the total depth at each snowpit for a) Imnavait and b) Pallas. For Imnavait, the variation in snow density in each layer is illustrated through different colors. The dashed line indicates the average $\delta^{18}O$ value across all samples (Reprinted under CC BY 4.0 license from Publication I © 2021 Authors).

3.1.2 In-depth analysis of snowpack ^{18}O isotopes and their evolution [Publication II]

For in-depth analysis of snowpack $\delta^{18}O$ isotope evolution, we used spatial and temporal snowpack $\delta^{18}O$ isotope stratigraphy data for late winter and spring 2020 in the Pallas catchment (Figs. 4 and 5). During the late stages of the winter season before melt, i.e., in early April, the patterns of isotope values and densities were consistent across all 11 snowpit locations in the catchment (as shown in Fig. 4a). The base of the snowpack, comprised of moderate snow density, was enriched in heavy ^{18}O isotopes. The highest densities were recorded as being from 0.2 to 0.4

(20 to 40%) of the normalized snow depth from the snowpack's base, where the snow layers exhibited a depletion of ^{18}O isotopes. The surface layers demonstrated low snow densities, which might be indicative of recent snowfall events and the non-compaction of surface layers. Most profiles had more negative $\delta^{18}O$ values at the surface, pointing to a recent snowfall event with a depleted ^{18}O isotope composition.

Over the course of the snowmelt period, there was a gradual homogenization of both snow isotope values and densities in the vertical snow profiles, as shown by snowpit samples that were taken at different melting stages (Fig. 4b). In general, a relatively constant density (~ 400–450 kg/m^3) was achieved across different snow profiles at varying depths at the peak melt period (Fig. 4b). At the beginning of peak melting, the $\delta^{18}O$ values became increasingly uniform, indicating a reduction in the variability of isotope values in vertical snow profiles. The average $\delta^{18}O$ value (denoted by the dotted line in Fig. 4) became higher (i.e., from less than -19‰ in all snow profiles to more than -18.5‰ in Fig. 4b), signifying an enrichment of the snowpack in ^{18}O isotopes over the snowmelt period. It is also clearly evident that the ^{18}O isotope-depleted surface layer, present in pits 1 and 11 prior to snowmelt (as seen in Fig. 4a), had largely vanished during the melting process.

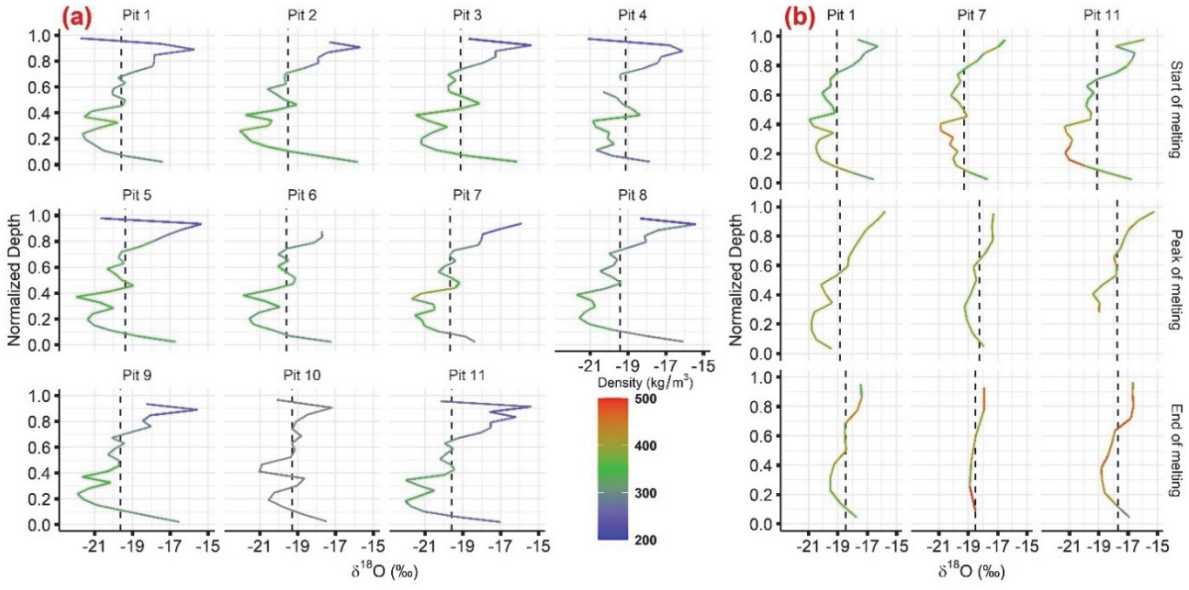

Fig. 4. The illustration of the spatiotemporal evolution of vertical isotope profiles in the snowpack along the snow survey transect. (a) depicts the vertical isotope profiles at 11 diverse locations from 2–6 April 2020, while (b) shows these isotope profiles at three locations on 22–23 April, 23 May, and 28 May 2020. These dates respectively correspond to the period before peak melt, during peak melt, and after the peak melt period. Varying snow densities are represented with different colors, and the snowpack weighted average $\delta^{18}O$ values are represented with vertical dotted lines (Reprinted, with permission, from Publication II © 2023 American Geophysical Union).

In Fig. 5, step lines illustrate the isotope values from snowfall events with respect to the normalized cumulative precipitation amounts on a 0 to 1 scale. The $\delta^{18}O$ values ranged from -30.62‰ to -7.72‰. At the base of the snowpack (Fig. 5), early season snowfall events that are enriched with high $\delta^{18}O$ values are evident. Between normalized depths of 0.1–0.4 (10 to 40%), the most depleted snowfall isotopes are observed, characterized by low $\delta^{18}O$ values. A gradual enrichment of snowfall isotopes is generally observed between normalized depths of 0.5–0.9 (50 to 90%). As compared to the base of the snowpack, relatively depleted snowfall isotope values are found corresponding to the top of the snowpack isotope profiles, i.e., at 0.9–1.0 (90 to 100%). Between the two snowpit sampling periods (22–23 April 2020 to 23 May 2020), several rainfall events took place. Yet, these events did not seem to significantly influence the evolution of the vertical isotope profiles of the snowpack.

Throughout the snowmelt period, the snowpack isotope profiles generally exhibit similar patterns at the top of the hillslope (pit 1), the middle of the catchment's transect (pit 7), and near the location of the outlet stream (pit 11), indicating the spatial coherence of vertical snowpack isotope profiles. During early April and the peak snow accumulation period, the vertical isotope profiles demonstrate maximum vertical isotopic variation. However, less variation and greater consistency in the vertical isotope profiles is observed during the post-peak melt period. The ranges of layered-snowpack isotope stratigraphy, densities, and SWEs at different times can be found in supplementary Tables S6 and S7 of Publication II.

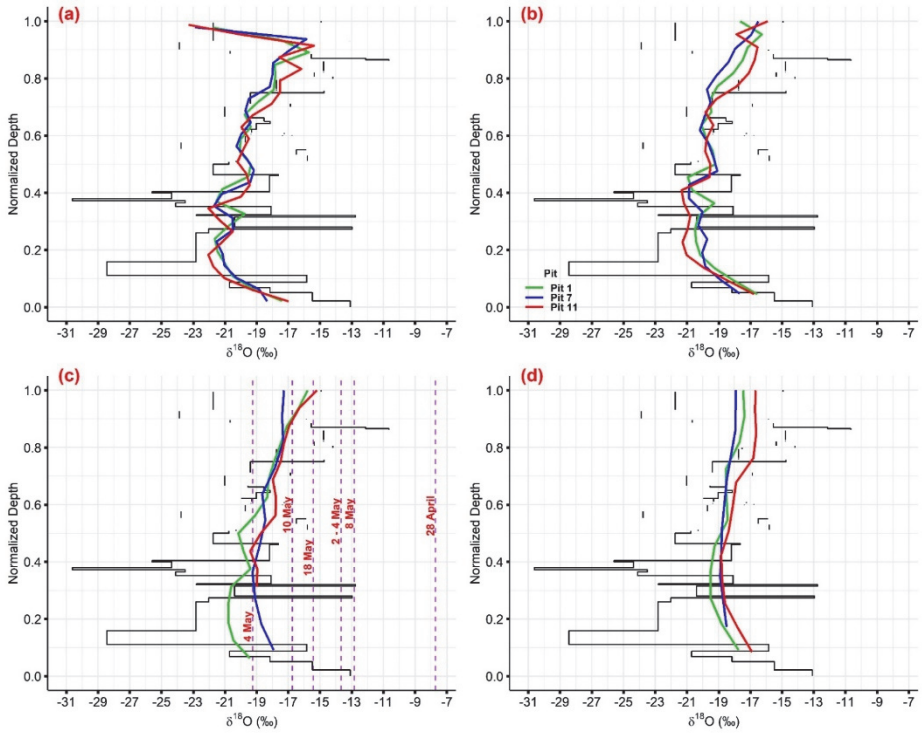

Fig. 5. The illustration of a comparison between layered snowpack and snowfall isotope values at three distinct locations, labeled as: (a) from 2–6 April 2020, (b) from 22–23 April 2020 (before the peak melt period), (c) on 23 May 2020 (during the peak melt period), and (d) on 28th May (after the peak melt period). Green, blue, and red lines illustrate the vertical isotope profiles at snowpit locations 1, 7, and 11, respectively. Black lines show snowfall isotope values during the snow accumulation phase. The dotted purple vertical lines represent the isotope values of rainfall events which took place after the maximum snow accumulation period and on specific dates: 28 April (1.4 mm), 2–4 May (11.1 mm), 4 May (2.8 mm), 8 May (0.3 mm), 10 May (6.6 mm), and 18 May (0.2 mm) (Reprinted, with permission, from Publication II © 2023 American Geophysical Union).

3.2 Snowmelt ^{18}O isotopes [Publication II]

3.2.1 Spatiotemporal evolution of snowmelt ^{18}O isotopes

Factors such as landscape features, and weather conditions have the greatest influence on snowmelt rate (Fig. 6). From mid-May, the snowmelt rate began to

rise; a notable step-change in melt rate was observed around 22nd May 2020. Starting from 22nd May, the daily average air temperature consistently stayed above freezing (Fig. 6a). This rapid melting is further evident from the swiftly decreasing snow depth (Fig. 6b). In 2020, the peak snowmelt efflux reached approximately 59 mm/day (Fig. 6c). Day-to-day variations in snowmelt efflux were relatively more evident even within identical landscape features (Fig. 6c). Conversely, the spatial variation of snowmelt water $\delta^{18}O$ values was relatively less notable within the same landscape features (Fig. 7).

The time-series snowmelt water $\delta^{18}O$ isotope plots across three spatial locations, (i) the forest hillslope, (ii) mixed forest, and (iii) open mires, reveal a noticeable correlation between isotope values and snowmelt efflux magnitude (Fig. 7). Specifically, lower snowmelt water $\delta^{18}O$ values are generally associated with the snowmelt of lower magnitude effluxes and higher efflux magnitudes correspond to relatively higher $\delta^{18}O$ values. Our meltwater $\delta^{18}O$ isotope data show an intriguing pattern, i.e., the initial isotope values did not represent the minimum isotope values. However, the lowest isotope values were recorded a few days following the onset of the snowmelt period, as can be seen from 5 May to 11 May in Fig. 7.

Throughout the early snowmelt season, the meltwater $\delta^{18}O$ values remained comparatively consistent. This demonstrates the co-variability of meltwater isotopes, a pattern which could hold true for any region with similar landscape characteristics. However, an evident shift from more negative to less negative $\delta^{18}O$ values (depletion to enrichment) was observed from 22 May 2020. This shows that the $\delta^{18}O$ values became higher with the rapid increase in snowmelt efflux from 22 May 2020 and onwards. What is interesting is the way in which this temporal covariance in isotope values extended across different landscape features (Fig. 7). At the post-peak melting period, the range of variation in isotope values narrowed across landscape features, with some exceptions (as depicted in Fig. 7, post 22 May 2020). This shows that the spatial covariation of isotope values can become stronger during the late melting period.

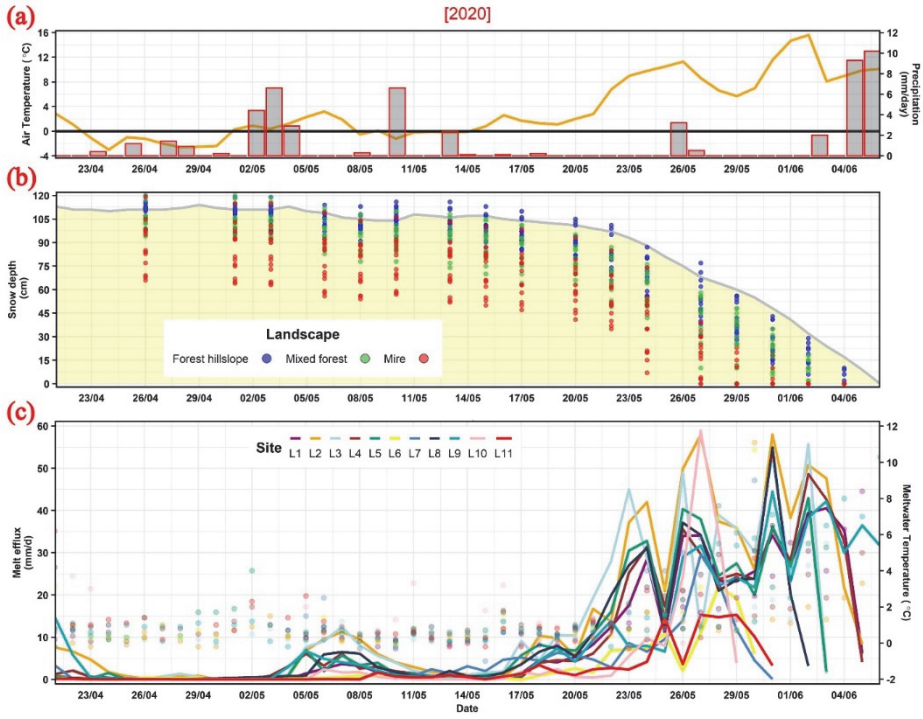

Fig. 6. Various hydrometeorological variables for 2020 are presented. (a) illustrates air temperature (represented with an orange line) alongside precipitation data (displayed as bars/columns), (b) illustrates snow depth at the Kenttärova station (area highlighted in yellow) and snow depth measurements across different landscape features along the snow survey transect (displayed as points), and (c) illustrates both the snowmelt efflux and its corresponding temperature for all lysimeters (Reprinted, with permission, from Publication II © 2023 American Geophysical Union).

The lc-excess values for snowmelt water for 2020 were positive, as illustrated in the lower panel of Fig. 7, during the early melt period and became negative only during the post-peak melt period. These lc-excess values show similar spatial correlation as was evident in the meltwater $\delta^{18}O$ values. Notably, the largest positive lc-excess values (~ 10‰) were recorded before the onset of the peak melt period (i.e., from 9 May to 11 May 2020) in Fig. 7.

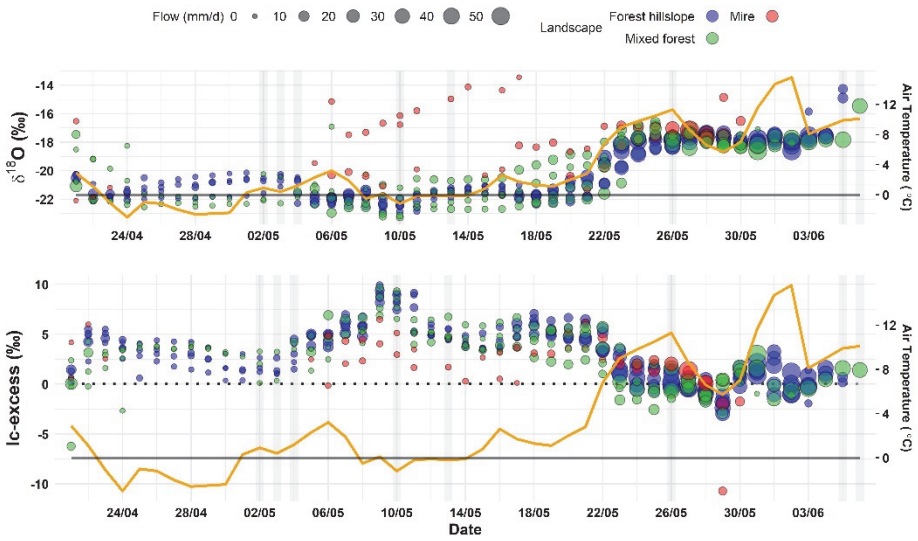

Fig. 7. The time-series plots of snowmelt for 2020. The $\delta^{18}O$ and lc-excess values for various locations are illustrated, namely the forest hillslope (L1, L2, L3, L4, L5), the mixed forest (L7, L8, L9, L11), and the open mires (L6, L10). The magnitude of the effluxes is represented through circle size. The solid orange line indicates air temperature, while the solid black line shows the 0 °C air temperature. In the lower panel, the dotted black line represents the lc-excess value of 0. Furthermore, precipitation events of more than 2 mm are illustrated with grey vertical bars (Reprinted, with permission, from Publication II © 2023 American Geophysical Union).

3.2.2 Comparison of snowmelt and snowpack ^{18}O and ^{2}H isotopes

We also compared the $\delta^{18}O$ and $\delta^{2}H$ values in snowmelt water with those in the DI snowpack at a catchment scale (Fig. 8). The flow-weighted mean of snowmelt water $\delta^{18}O$ and $\delta^{2}H$ values is consistently higher than the density-weighted mean of DI snowpack $\delta^{18}O$ and $\delta^{2}H$ values across both study years. This is illustrated by the weighted mean, symbolized by a yellow circle, and the standard error, represented as red error bars in the boxplots of Fig. 8. For instance, the weighted mean of snowmelt water $\delta^{18}O$ values exceeded the corresponding DI snowpack isotope values by 1.98 ± 0.06 and 0.46 ± 0.24‰ $\delta^{18}O$ in the forest hillslope, and by 2.33 ± 0.22 and 0.77 ± 0.27‰ $\delta^{18}O$ in the mixed forest in 2019 and 2020, respectively. The most substantial variation was identified in open mires, where the weighted mean of snowmelt water $\delta^{18}O$ values was higher by 6.19 ± 1.64 and 1.51

± 0.21‰ $\delta^{18}O$ in comparison to the DI snowpack $\delta^{18}O$ values. The consistency of the weighted mean and the variation in the ranges of DI snowpack $\delta^{18}O$ and $\delta^{2}H$ values was more pronounced than that of the snowmelt water $\delta^{18}O$ and $\delta^{2}H$ values, except in open mires. It is also worth mentioning that meltwater sampling at open mire locations posed a challenge. Firstly, installing snowmelt lysimeters in these locations was more complicated due to water ubiquity. Secondly, these locations are the initial hotspot for snowmelt, becoming flooded while a snow blanket still covers the surrounding forests. The meltwater flood lingers over the frozen wetlands for some time before it makes its way to nearby ditches and streams to be flushed away. Consequently, the presence of flooded meltwater in open mires created challenges for snowmelt sampling.

The Local Meteoric Water Line (LMWL: $\delta^{2}H = 7.68\delta^{18}O + 2.49$) was derived only from the snowfall $\delta^{18}O$ and $\delta^{2}H$ values spanning 2019 through to winter 2020, i.e., excluding the rainfall isotopes for better comparison. Dual-isotope plots from both 2019 (see supplementary Fig. S2 of Publication II) and 2020 (Fig. 8) indicate that most of the recorded values for snowmelt water and snowpack $\delta^{18}O$ and $\delta^{2}H$ isotopes fall closely on the LMWL. A minor exception is noted in open mires, which may demonstrate the enrichment of open standing water in heavier isotopes.

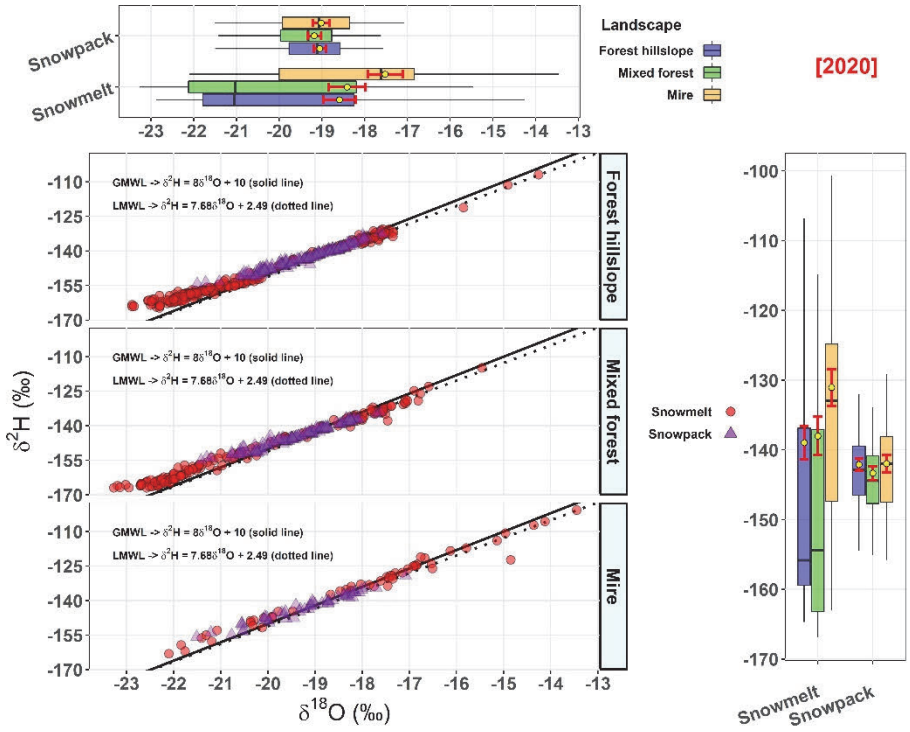

Fig. 8. Dual isotope plots for snowmelt water and DI snowpack for the year 2020, represented by circles and triangles, respectively. The $\delta^{18}O$ and $\delta^{2}H$ values are shown for three distinct landscape features: (i) the forest hillslope, (ii) the mixed forest, and (iii) the mire. Accompanying boxplots present weighted mean values as yellow circles, and error bars, designated by red lines. The solid and dotted black lines represent the Global Meteoric Water Line (GMWL) and the Local Meteoric Water Line (LMWL), respectively (Reprinted, with permission, from Publication II © 2023 American Geophysical Union).

3.2.3 Coevolution of snowmelt and snowpack ^{18}O isotopes

The snowmelt water $\delta^{18}O$ values reveal greater temporal variability in the $\delta^{18}O$ as compared to those of the DI snowpack (Fig. 9). Similarly, the comparison between the two suggests that the $\delta^{18}O$ values of snowmelt water exhibited more spatial variability within the same landscape feature than those of the DI snowpack on most occasions, as indicated by the error bars in Fig. 9. Between 21 April and 21 May 2020, the ^{18}O isotopes of snowmelt water are significantly depleted relative to the DI snowpack ^{18}O isotopes, with a difference closer to the equilibrium

fractionation difference of 3.1‰ $\delta^{18}O$ between ice and liquid water (O'Neil, 1968). However, during the peak melt period, the snowmelt water $\delta^{18}O$ values became closer to, and during the post-peak melt period, slightly surpassed, the DI snowpack $\delta^{18}O$ values from 22 May to 6 June 2020 (Fig. 9). On 21 May 2020, an increase of 3.64 ± 0.01‰ $\delta^{18}O$, 3.09 ± 0.08‰ $\delta^{18}O$, and 1.29 ± 0.33‰ $\delta^{18}O$ was observed in the snowmelt water $\delta^{18}O$ values in the forest hillslope, mixed forest, and open mires, respectively. Fig. 9b indicates how the lc-excess values for the DI snowpack approximated 0 in all three landscape features, while those for snowmelt water exhibited relatively greater variability.

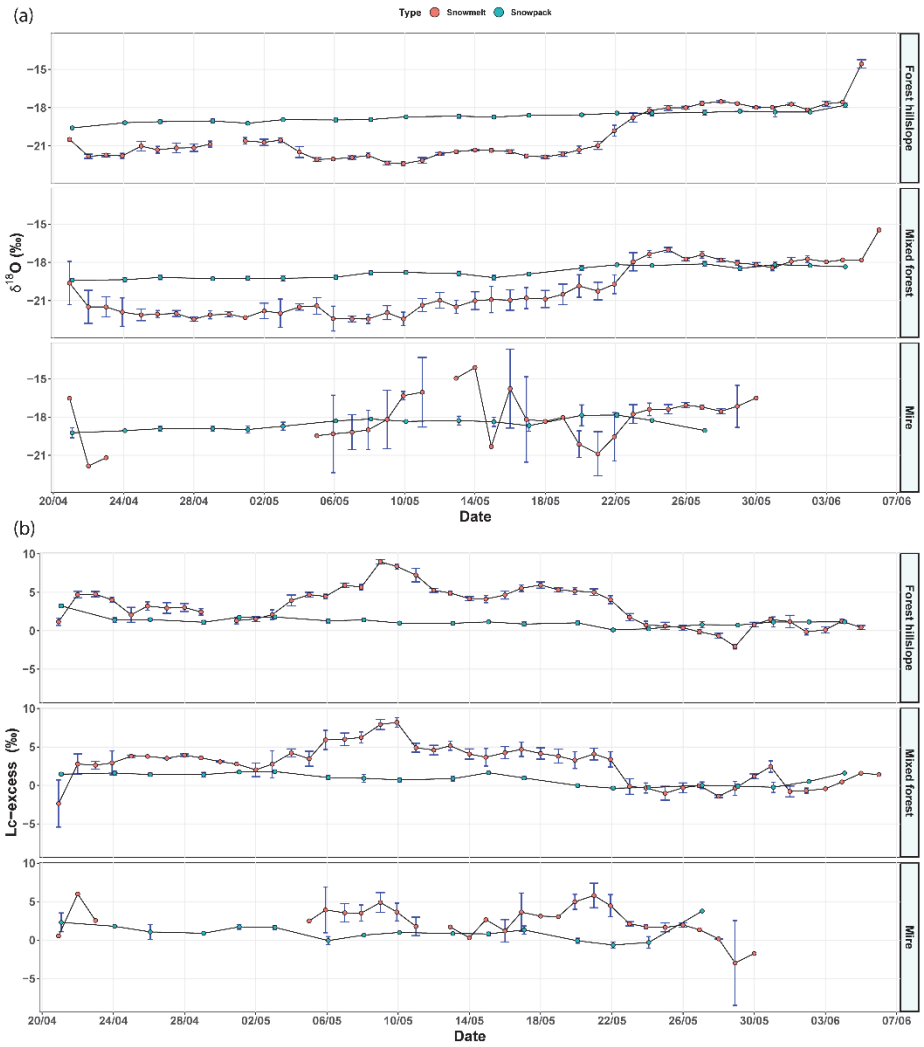

Fig. 9. The illustration of the comparison of weighted means and standard error bars between snowmelt water and DI snowpack isotope values for the year 2020 across three landscape features: (i) forest hillslope, (ii) mixed forest, and (iii) mires. (a) depicts the temporal evolution of $\delta^{18}O$ values, while (b) provides the corresponding evolution of lc-excess values (Reprinted, with permission, from Publication II © 2023 American Geophysical Union).

3.3 Snowmelt isotope hydrograph separation [Publication III]

We utilized a two-component IHS and applied it to 10 different scenarios, as outlined in Table 1. The IHS was employed to analyze spring peak streamflow generation processes during the peak melt period from May 21st to June 4th, 2020. During this period, the total observed streamflow discharge was 117.21 mm. Hourly $\delta^{18}O$ values for both endmembers and stream water were used in the IHS.

We set the pre-event water endmember as constant across all scenarios because the discharge-weighted average baseflow $\delta_{bf}{}^{18}O$ value (ranging from -14.78‰ to -14.03‰) was -14.38‰ (± 0.01‰) and was fairly stable during the winter period. In contrast, the $\delta_{event}{}^{18}O$ value of the event water endmember varied across all 10 scenarios. These scenarios are based on diverse sampling strategies for collecting meltwater, which include the use of a snowfall collector, DI snowpack and a snowmelt lysimeter. They also incorporate different mathematical approaches to approximate meltwater isotopic signal as an event water endmember in IHS. Table 1 provides further details on these scenarios.

3.3.1 Combined ^{18}O isotopic evolution: stream water, snowfall, snowpack and snowmelt

By analyzing all isotope datasets, we find a consistent $\delta^{18}O$ value range (-14.78‰ to -14.03‰) in stream water during winter, as shown in Fig. 10. However, a notable decline in the streamflow isotope values occurred during the melt period, and the most significant drop in values can be observed from 21 May 2020. This period coincides with the peak melt phase, and during this peak period, we observed stream $\delta^{18}O$ values reaching a minimum and maximum of -16.8 and -15.56 ‰, respectively. After this spring freshet, the stream water $\delta^{18}O$ values returned to the pre-melt levels.

Furthermore, Fig. 10 also highlights the distinct $\delta^{18}O$ values in snowfall, snowpack, and snowmelt. The snowfall $\delta^{18}O$ values during winter 2020 exhibited the greatest temporal variation, ranging from -30.62‰ to -7.72‰. The amount-weighted average for these values was -19.43‰ (± 0.52‰). In the winter of 2020, the DI snowpack $\delta^{18}O$ values varied between -20.94‰ and -19.46‰, with a SWE-weighted average of -20.09‰ (± 0.12‰). The lowest of these values were observed at the end of March 2020, as can be seen in Fig. 10. In the spring season, the snowpack isotope values presented a linearly increasing trend, moving from -19.47‰ to -18.05‰. Their SWE-weighted average value was -18.82‰ (± 0.09‰).

Throughout the melt period, the snowmelt $\delta^{18}O$ values exhibited a range of -22.21‰ to -15.46‰. The flux-weighted average during this period was -18.2‰ (± 0.29‰). At the beginning of the melt period, these snowmelt water $\delta^{18}O$ values were lower than the DI snowpack $\delta^{18}O$ values which had been measured during the entire winter and spring of 2020. However, a shift in snowmelt $\delta^{18}O$ values occurred during the peak and post-peak melt periods, starting from 21 May 2020, as shown by the orange shaded area in Fig. 10. In these periods, the lysimeter snowmelt water $\delta^{18}O$ values exceeded those of the DI snowpack. Fig. 11 presents the $\delta^{18}O$ values for distinct event water endmember scenarios, along with a relatively consistent pre-event water endmember and stream water.

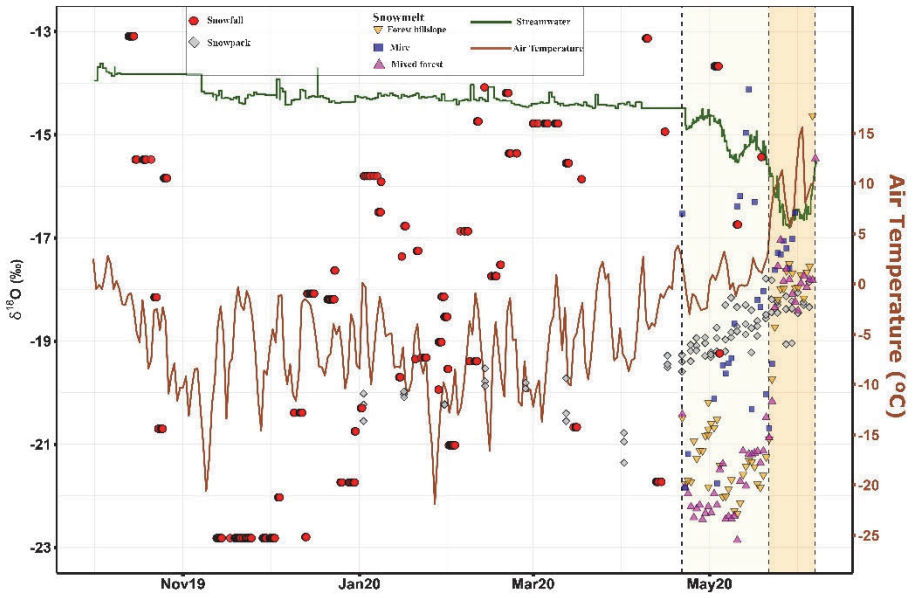

Fig. 10. The illustration of the $\delta^{18}O$ values from different sources, i.e., snowfall, snowpack, snowmelt, and stream water across distinct landscape features. The yellow shaded area marks the time from the onset of the melt period up to the end of the pre-peak melt period. The orange shaded area highlights the start of the peak melt period to the end of the melt season. The brown line represents air temperature (Reprinted under CC BY 4.0 license from Publication III © 2023 Authors).

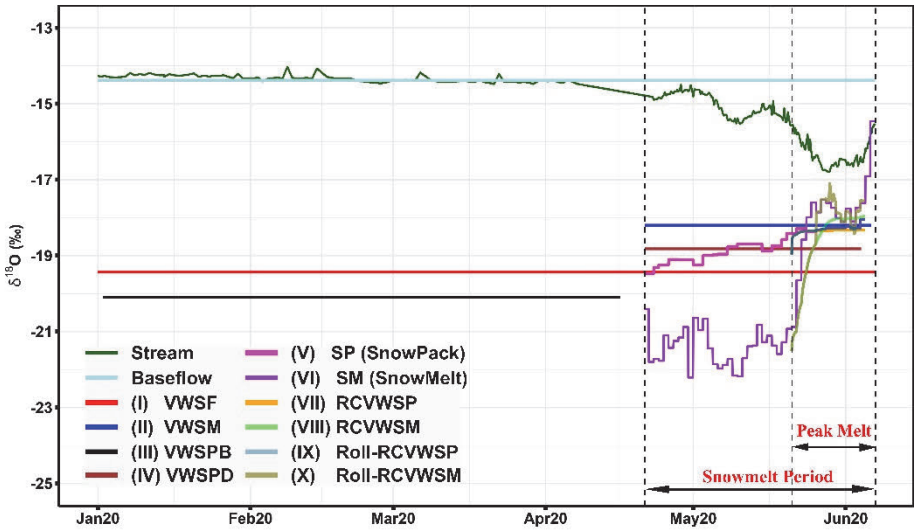

Fig. 11. The illustration of the $\delta^{18}O$ values for a fixed pre-event water endmember (namely, baseflow), event water endmembers, and stream water. The horizontal lines display amount, melt flux, or SWE-weighted $\delta^{18}O$ (represented by volume weighted, VW) values for scenarios (I) VWSF, (II) VWSM, (III) VWSPB, and (IV) VWSPD. The lines for scenarios (V) SP and (VI) SM represent the instantaneous $\delta^{18}O$ values, which have varying slopes. Scenarios (VII) RCVWSP and (VIII) RCVWSM are represented with lines with slopes that vary in a single direction only. For scenarios (IX) Roll-RCVWSP and (X) Roll-RCVWSM, the lines show the cumulative incremental weighted $\delta^{18}O$ values for the initial 5 days, as well as a rolling weighted average for the days following (Reprinted under CC BY 4.0 license from Publication III © 2023 Authors).

3.3.2 Estimation of meltwater contribution using IHS

Fig. 12. displays the hydrographs of snowmelt water contribution, calculated using several event water scenarios (Table 1). We selected scenario (X) Roll-RCVWSM (i.e., Rolling Runoff-Corrected Volume Weighted SnowMelt) as the optimal scenario for a number of reasons: (i) its basis on snowmelt $\delta^{18}O$ values, (ii) its consideration of the time delay and contribution from previously melted water and temporal subsurface storage in the catchment, as detailed in Laudon et al. (2002), and (iii) its prevention of oversimplification of post-peak melt isotope values sampled with snowmelt lysimeters. For quantitative and visual comparisons, other scenarios are plotted as line hydrographs against scenario (X) Roll-RCVWSM

(indicated by grey area), which serves as a reference and baseline case (Fig. 12). The pattern of snowmelt water hydrographs mirrors that of the total hydrograph (Fig. 12a). The contribution of snowmelt water to streamflow varies with stream water discharge values, i.e., it is lower at low discharge values and higher at elevated values (Fig. 12b). Compared to scenario (X) Roll-RCVWSM, all scenarios underestimate the contribution of snowmelt water with the exception of scenario (VI) SM, which overestimates it by 1.5% (Fig. 12).

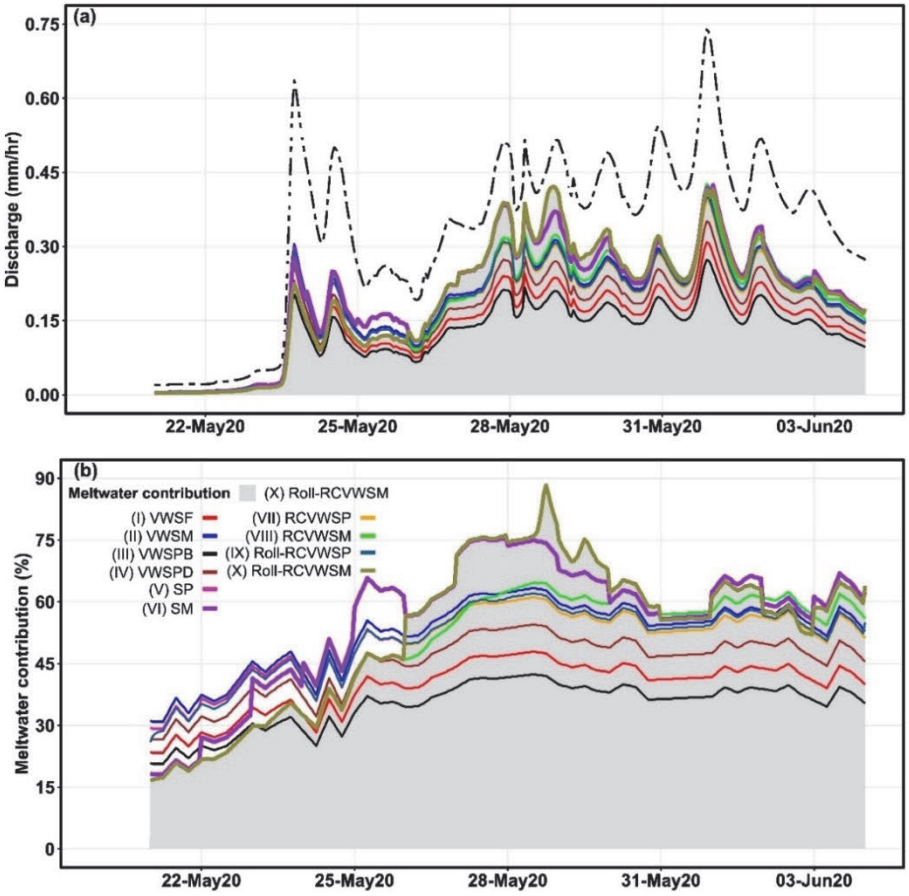

Fig. 12. The representation of (a) the total hydrograph (represented as a dotted and dashed black line) alongside the snowmelt water hydrographs derived from the 10 different scenarios, and (b) the calculated percentage values of the snowmelt water contribution at each time step. The grey shaded area in the figure corresponds to scenario (X) Roll-RCVWSM, which is used as a benchmark for comparison with the other scenarios (Reprinted under CC BY 4.0 license from Publication III © 2023 Authors).

For the base scenario (X) Roll-RCVWSM, the snowmelt contribution constitutes 69.9 mm (± 2.3 mm with 95% confidence level), or 59.6% (± 2% with 95% confidence level) of the total discharge during spring freshet (Fig. 13). Most scenarios tend to underestimate snowmelt contribution, with the smallest underestimations shown by scenarios (V) SP and (IX) Roll-RCVWSP, 5.4% and 5.4%, respectively. Both of these are based on snowpack isotope data rather than snowmelt isotope data. Scenarios (I) VWSF and (III) VWSPB drastically underestimate the snowmelt contribution, by 17.8% and 22.6%, respectively. Scenario (VI) SM indicates the highest snowmelt contribution, i.e., 71.7 mm or 61.1% (± 7% with a 95% confidence level) of the total discharge. In contrast, scenario (III) VWSPB displays the smallest total snowmelt contribution, i.e., 43.4 mm (37% with ± 2% and 3% temporal and spatial uncertainty, respectively).

The error bars in Fig. 13 signify how uncertainties in the estimated values vary across different scenarios. The largest uncertainties are observed in scenarios (I) VWSF and (II) VWSM (8%), whereas the smallest are demonstrated by scenarios (VII) RCVWSP and (IX) Roll-RCVWSP (1%).

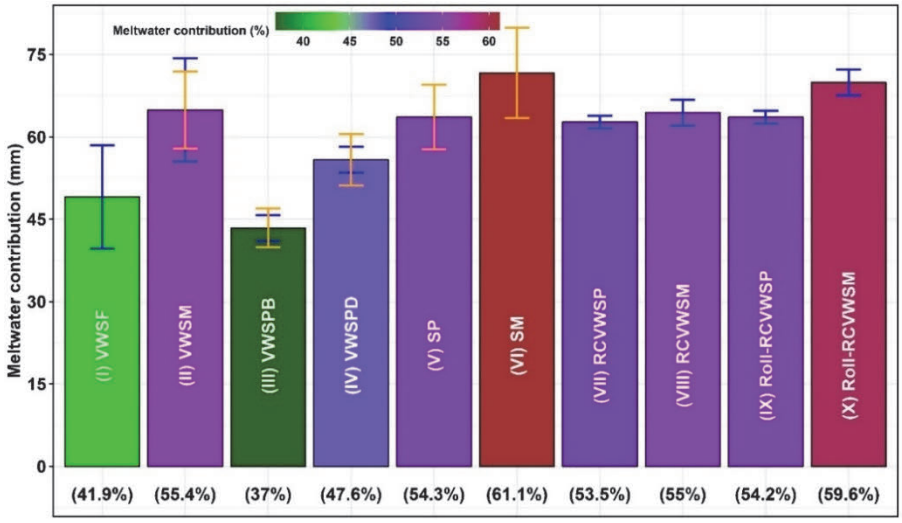

Fig. 13. The illustration of the estimated total meltwater contribution during the peak streamflow generation period using multiple scenarios for the IHS. Panel (a) presents the total snowmelt contribution in mm, along with the associated uncertainty (95% confidence level). The orange error bars show spatial uncertainty, while the blue ones represent temporal uncertainty. Panel (b) displays the snowmelt contribution expressed as a percentage for all 10 scenarios (Reprinted under CC BY 4.0 license from Publication III © 2023 Authors).

3.3.3 Sensitivity analysis and uncertainty estimation

We performed a sensitivity analysis for the $\delta^{18}O$ values of both stream and event water at hourly intervals across nine scenarios with reference to the (X) Roll-RCVWSM base scenario (Fig. 14). When $\delta^{18}O$ values in stream water become more negative (depleted) and converge with the isotopic values of event water (at -16.5‰ $\delta^{18}O$ or lower), a bias arises in the different scenarios, leading to an underestimation of snowmelt water contribution (Fig. 14a), observed as positive biases. Scenarios (III) VWSPB and (I) VWSF produce the highest underestimations in this case, while scenario (VI) SM results in the smallest underestimation when stream water isotope values are more negative. Conversely, when stream water $\delta^{18}O$ values are less negative (enriched) and converge towards the baseflow weighted average isotope value (pre-event water -14.38‰ (± 0.01‰) $\delta^{18}O$), most scenarios overestimate snowmelt contribution, with the exception of scenario (III) VWSPB. The most pronounced overestimations are caused by scenarios (VI) SM and (II) VWSM, while scenario (VIII) RCVWSM produces a negligible bias.

When the event water isotopes are more depleted (i.e., -20 ‰ $\delta^{18}O$ or lower, as shown in Fig. 14b), the bias from different scenarios overestimates the contribution of snowmelt water, observed as negative biases. Conversely, less negative (enriched) $\delta^{18}O$ values lead to an underestimation of the snowmelt water contribution. Scenario (III) VWSPB shows the most significant underestimation of snowmelt water contributions at higher $\delta^{18}O$ values. All nine scenarios significantly underestimate snowmelt contribution at -18‰ or higher $\delta^{18}O$ values.

Upon evaluating all nine scenarios using average BIAS and RMSE metrics, scenarios (V) SP and (IX) Roll-RCVWSP stand out as the most reliable for estimating snowmelt water contributions in the absence of snowmelt water isotopes. Both show RMSE of 0.1 and an average BIAS of 0.02 (Fig. 14c).

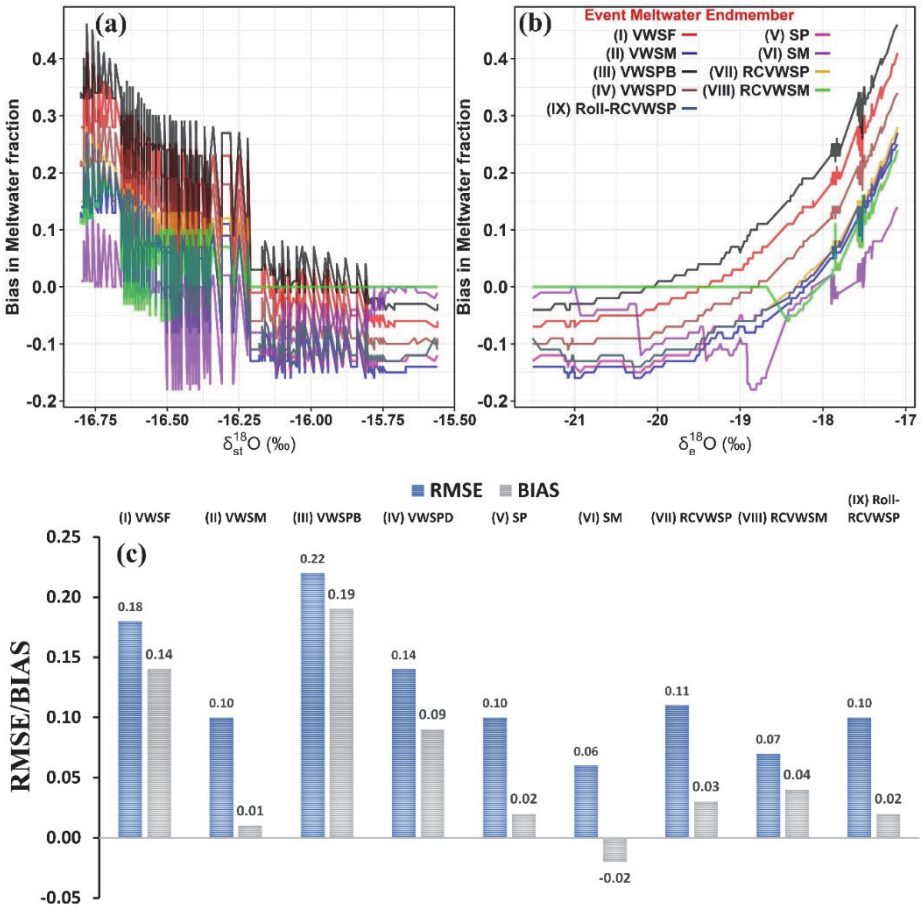

Fig. 14. The representation of uncertainty estimation and performance. Panel (a) shows the relationship between the time-series of BIAS estimates for different scenarios and the $\delta^{18}O$ values of stream water. Panel (b) illustrates the relationship between these BIAS estimates and the $\delta^{18}O$ values of event water, with reference to the $\delta^{18}O$ values in the (X) Roll-RCVWSM scenario. Panel (c) illustrates the Root Mean Squared Error (RMSE) and the overall BIAS metrics for all scenarios (Reprinted under CC BY 4.0 license from Publication III © 2023 Authors).

4 Discussion

4.1 Snowpack ^{18}O isotopes [Publication I and Publication II]

4.1.1 Snowpack ^{18}O isotopes in the Arctic: ^{18}O isotopic comparison based on two Arctic research sites [Publication I]

This study aims to enrich our understanding of the ^{18}O isotopic composition of snowpack, focusing on the 2018–2019 snowy season in two research locations: Pallas and Imnavait. We observed a common pattern at both sites, i.e., the base of the snowpack consistently exhibited higher $\delta^{18}O$ values than the surface snow (Figs. 3 and 4). The prevailing theory attributes such observations to the seasonality effect. Snowfall $\delta^{18}O$ isotopes corresponding to the relatively warmer temperatures, i.e., October and November being characterized as having relatively higher values (enriched isotopes). On the other hand, snowfall $\delta^{18}O$ isotopes corresponding to the mid-to-late winter (i.e., December through March) season exhibit lower values (depleted isotopes, see Fig. 2 of Publication I). This seasonal effect is confirmed by a positive correlation between air temperature and $\delta^{18}O$ values, evident in precipitation samples from the two sites (see supplementary Fig. A6 of Publication I). As winter progresses, both the snowpack and vapor isotope composition gradually transition from higher to lower $\delta^{18}O$ values.

We utilized early season precipitation samples at Imnavait for $\delta^{18}O$ values to directly compare against the snowpack's base $\delta^{18}O$ values (see Fig. 9a of Publication I). This comparison revealed that the base of the snowpack exhibited higher $\delta^{18}O$ values than the corresponding precipitation events. This implies that the earlier precipitation ^{18}O isotope signal was not preserved within the snowpack. This may happen due to the post-depositional enrichment of heavy isotopes over winter. Several previous studies have attributed this heavy ^{18}O isotope enrichment in the basal snow layers to soil water diffusion into the snowpack over winter, as well as to the molecular diffusion due to vapor transport through the snowpack (Friedman et al., 1991; Sinclair & Marshall, 2008; von Freyberg et al., 2020). In our study, the shallow tundra snowpack at Imnavait showed significant temperature gradients between the soil and air (see Fig. 2 of Publication I). Therefore, we may conclude that the vapor movement from the soil-snow interface through the snowpack might have occurred (Sturm & Benson, 1997), as indicated by the depth hoar layers (Fig. 3). Thus, it is highly likely that the higher $\delta^{18}O$ values at the

Imnavait snowpack base cannot be solely attributed to seasonality but is also caused by isotope modification through the soil vapor movement over winter.

As compared to Pallas (see Fig. 3 of Publication I), the snowpack $\delta^{18}O$ values at Imnavait are relatively higher compared to the snowfall $\delta^{18}O$ values. These disparities between snowfall and snowpack $\delta^{18}O$ values may suggest potential isotope fractionation due to sublimation and evaporation, in addition to the previously discussed soil water-snowpack interactions in the tundra snowpack (Imnavait). Sublimation processes are more favorable, with higher wind speeds, lower relative humidity, and greater solar insolation (Gustafson et al., 2010). According to modeling studies, the sublimation process is favorable for open tundra sites like the Imnavait research site because simulations yield larger snow accumulations than measured accumulations when sublimation is not introduced into the model (Essery et al., 1999; Liston & Sturm, 1998; Pomeroy et al., 1997; Sturm & Wagner, 2010). From an isotopic perspective, snowpack samples from both sites closely align with the GMWL, displaying a $\delta^{2}H$-$\delta^{18}O$ slope nearly equal to 8 (see Fig. 3 of Publication I). Pallas' snowpit samples, however, display a slope below the GMWL, suggesting the possibility of kinetic fractionation. This kinetic fractionation signal was not clearly evident in Imnavait's tundra snowpack in the dual isotope plot, as the isotope samples did not deviate from the GWML. This either implies that wind-transported sublimation hadn't occurred significantly at the time of sampling, or it was accounted for by the whole-grain ice-vapor transport in blowing snow (Friedman et al., 1991). This process leaves no residual higher $\delta^{18}O$ isotopes in the remaining snowpack, allowing the entire snow grain to sublimate. It can, therefore, be concluded that sublimation effects are more pronounced in open tundra and taiga sites, but less so in subarctic forested sites. The absence of clear sublimation signals in the dual isotope plot could suggest that the surface snow layers either had not experienced wind transport at the time of sampling, or the entire snow grains had been wind-transported.

4.1.2 Spatiotemporal evolution of snowpack ^{18}O isotopes [Publication II]

In our analysis of the snowpack $\delta^{18}O$ isotopes at Pallas during the 2019–2020 winter, we found consistency in the vertical isotope profiles across various landscape features: (i) forest hillslope, (ii) mixed forest, and (iii) open mires. These profiles exhibited identical patterns, particularly in late winter before the onset of snowmelt, (early April 2020), as illustrated in Fig. 4a. This period, extending from

early to mid-April, typically marks peak snow accumulation, and the maximum snow depth reached was 130 cm in 2020. Pit 10 displayed a smaller range of $\delta^{18}O$ isotopic variation (~-17.5 to -21‰) compared to other snow pit locations. Positioned in the middle of open mires (Fig. 1), Pit 10 typically has a lower snow depth than forest sites and is more significantly affected by wind and solar insolation. These meteorological and environmental factors influence isotopic fractionation in the snowpack at this location. Thus, relatively higher isotopic consistency and homogenization existed, likely due to the relatively smaller snow depth at the Pit 10 location and/or isotopic fractionation leading to an increase in the $\delta^{18}O$ values. This in turn reduced the variability in the vertical isotope profiles caused by more negative values. The basal snowpack was similarly enriched in ^{18}O isotopes as was the case in the previous year (Figs. 3b and 4a). Coinciding with these findings, we noticed that, at Pallas, the highest snow densities occurred from 20 to 40% of the relative snow depth during the same period. On the other hand, lowest snow densities were detected at the snowpack's surface and base. Depths of maximum densities corresponded to the lowest $\delta^{18}O$ isotope levels (Fig. 4a). This implies a positive correlation between $\delta^{18}O$ isotopes and snow density.

From late October to December, the beginning of the winter season, the snowfall ^{18}O isotopes at Pallas were enriched and exhibited higher values (Fig. 5a). This could explain the enriched basal layers of the snowpack. This was not the case at Imnavait, where early snowfall events were depleted and the upward transport of vapor flux might have caused the isotopic enrichment of the basal layers at Imnavait (Beria et al., 2018; Friedman et al., 1991; Unnikrishna et al., 2002). Despite this, it does not confirm vapor transport at the soil-snow interface as negligible at Pallas. This shows that the upward transport of vapor flux at soil-interface may explain the formation of depth hoars in some regions (Friedman et al., 1991; Unnikrishna et al., 2002) but may not solely explain the isotopic enrichment of basal layers.

During the peak melt period, both the $\delta^{18}O$ values and the density profiles became consistent and homogenized, with the density peaking at approximately 400–450 kg/m^3 (Fig. 4b). This homogenization in the snowpack's isotopic composition at various depths during the post peak melt period may indicate the diffusive movement of meltwater within the snowpack caused by the mass movement of percolated meltwater (Evans et al., 2016; Moran & Marshall, 2009; Taylor et al., 2001). Furthermore, the $\delta^{18}O$ isotope-depleted surface layer, initially present in pits 1 and 11 before snowmelt (as observed in Fig. 4a), largely disappeared or became enriched during the melting process (Fig. 4b). Isotopic

homogenization can also occur due to isotopic redistribution, when the snowpack becomes isothermal, as has been shown by previous research (Carroll, Deems, Maxwell, et al., 2022; Evans et al., 2016; Moran & Marshall, 2009; Papina et al., 2022; Taylor et al., 2001; Unnikrishna et al., 2002). However, our results also showed the degree of gradual isotopic homogenization of vertical snow profiles that were sampled during different periods (early April near to maximum snowpack accumulation, the start of the melt period, peak melt period and post-peak melt period), as shown in Figs. 4 and 5.

Several rainfall events were observed from the onset to the peak melt period (Fig. 5c). However, there was not an immediately discernible shift in the isotopic evolution of the snowpack's vertical profiles due to these rainfall events. This observation might be attributed to two factors:

I Each rainfall event had distinct isotope values, which mostly lie within those of the existing snowpack. If these events had consistently higher isotope values, then a noticeable shift from lower to higher isotope values in the snowpack might have occurred.

II The volume of each rainfall event was not sufficiently large compared to the snowpack's volume, so it could not profoundly saturate the snowpack's isotope values with those from rainfall.

For example, Rücker, Boss, et al. (2019) established criteria for rain-on-snow events: rainfall rates should exceed 0.1 mm h^{-1}, total rainfall should be at least 20 mm within a 12-hour span, air temperatures should be above 0 °C, and an initial snowpack depth should be a minimum of 10 cm. In our study, the total rainfall volume did not meet these criteria (details in Appendix 1). This might have been the reason for the rainfall events not significantly altering the isotopic values in the snowpack's vertical profiles.

4.2 Snowmelt ^{18}O isotopes [Publication II]

4.2.1 Inter-annual difference between snowmelt ^{18}O isotopes and spatiotemporal evolution of snowmelt ^{18}O isotopes

The temporal variation of snowmelt water $\delta^{18}O$ values was evident during the melt periods of 2019 and 2020 across different landscape features. In the forest hillslope, the change in isotope values from the onset of melting to the final melt events was

7.25‰ and 4.17‰ $\delta^{18}O$ in 2019 and 2020. The mixed forest sites exhibited a transition of 6.03‰ and 5.91‰ $\delta^{18}O$ from the first to the last melt episodes (see Fig. 7). This increase in $\delta^{18}O$ value trend over the course of the melt period aligns with the snowmelt water ^{18}O and ^{2}H enrichment observed in prior laboratory and field studies (Feng et al., 2002; Laudon et al., 2002; Lee et al., 2010; Taylor et al., 2001; Taylor, Feng, Renshaw, et al., 2002). Interestingly, the forest regions demonstrated temporal covariation of snowmelt water $\delta^{18}O$ values at several sites (as depicted with green and blue bubbles in Fig. 7). However, this covariation did not exist between the forest and open mires. Furthermore, distinct dynamics of snowmelt water $\delta^{18}O$ values were found between the periods before and after peak melt (Fig. 7). Notably, the pattern of snowmelt water $\delta^{18}O$ values displayed higher spatiotemporal consistency in $\delta^{18}O$ values in 2020 compared to 2019 (denoted by various colors representing different landscape features in Fig. 7 of this thesis and Fig. S5 of Publication II). The variations may temporally influence the evolution of snowmelt $\delta^{18}O$ values, and spatial evolution might remain consistent at any given specific time under identical climate conditions across various landscape features (i.e., forest hillslope, mixed forest). This indicates that meteorological variables, such as temperature, wind speed, input energy fluxes, and relative humidity, play a more pronounced role in shaping the evolution of snowmelt water $\delta^{18}O$ values than changes in the physical features of the catchment. Thus, special considerations should be made for the seasonality of hydrometeorological variables when assessing the evolution of snowmelt water $\delta^{18}O$ values.

4.2.2 Comparison of snowmelt and snowpack ^{18}O isotopes

We investigated the spatiotemporal variations in DI snowpack and snowmelt water $\delta^{18}O$ and $\delta^{2}H$ values across different landscape features: forests and adjacent mires. We observed that the volume-weighted total snowmelt efflux across the Pallas catchment in Northern Finland was isotopically heavier than the DI snowpack. The $\delta^{18}O$ and $\delta^{2}H$ values in the snowmelt water exhibited more significant variability compared to the corresponding DI snowpack values within these diverse landscapes, as illustrated in Fig. 8 (see Table S1 of Publication II for ranges).

In 2019, the weighted mean of the DI snowpack isotopic values was higher on the forest hillslope sampling sites than in open mires, showing a difference of 1.84 ± 0.23‰ $\delta^{18}O$ and 11.28 ± 0.86‰ $\delta^{2}H$ (see supplementary Fig. S2 of Publication II). However, in 2020, the difference was slightly lower at -0.03 ± 0.05‰ $\delta^{18}O$ and -0.14 ± 0.34‰ $\delta^{2}H$ (Fig. 8). Our 2020 results contrast with those presented by

Koeniger et al. (2008), who suggested that dense and partially cut forests exhibited isotopically heavier snow and streamflow than clear-cut forests. However, it should be noted that their conclusion was primarily inferred from streamflow isotopes, whereas our study directly analyzed snowmelt water $\delta^{18}O$ and $\delta^{2}H$ values. It is also worth mentioning that our research setting included open mires (wetlands), while Koeniger et al. (2008) made conclusions for dense and partially cut forests compared to clear-cut forests.

The isotopic lapse rate is defined as the change in isotope value alongside the change in altitude. This occurs when the air mass rises under adiabatic conditions due to an increase in altitude, as both the temperature and the pressure fall. Then, when the air mass condenses under saturated conditions to form precipitation, the falling precipitation will be relatively depleted in heavier isotopes (Friedman et al., 1964). The isotopic lapse rate can differ across regions (Beria et al., 2018) and mainly depends on local hydrometeorological conditions, such as the ambient air temperature, moisture source in the atmosphere, relative humidity, wind speed, topography, and time of precipitation (e.g., fall, winter, spring, or summer). For example:

- The range of isotopic lapse rates (for $\delta^{18}O$) of snowpack samples for mountain regions in the South American Andes, the Hindu Kush, the Himalayas, and Mount Kenya in Africa was -0.6‰ to -1‰ per 100 m of altitude (Niewodnizański et al., 1981).
- The range of isotopic lapse rates (for $\delta^{18}O$) of precipitation for Global Network of Isotopes in Precipitation (GNIP) stations in Switzerland was 0.27‰ per 100 m of altitude (Beria et al., 2018), where snow precipitation is typically observed for stations located above ~800 m in winter (Marty, 2008).
- The isotopic lapse rate of precipitation and fresh snow samples for the Canadian Rocky Mountains exhibited both positive and negative values; the range (for $\delta^{18}O$) was -0.3‰ to +1.8‰ per 100 m of altitude. The relationship depends on the direction of the slope; for the leeward slope, the relationship was inverse (increasing enrichment with increasing altitude), and vice versa for the windward slope (T. A. Moran et al., 2007).

We found no elevation effects on the isotope values in the DI snowpack and snowmelt water at the Pallas catchment for two main reasons: (i) Ideally, the measurement should be taken immediately after the snowfall events when determining the isotopic lapse rate. Otherwise, because of several processes such as sublimation, melting-freezing, snow metamorphism, vapor diffusion due to

temperature gradient, etc., the snowpack can become enriched and the original isotopic lapse rate can be obscured and compromised (Beria et al., 2018; Carroll, Deems, Maxwell, et al., 2022; Hürkamp et al., 2019; Niewodnizański et al., 1981; Unnikrishna et al., 2002). In our case, we measured the DI snowpack and snowmelt isotopes in spring when substantial isotopic fractionations were expected from the initial winter snowfall precipitation. (ii) The Pallas catchment has an elevation range of less than 100 meters (see supplementary Table S8 of Publication II); thus, the elevation range is not substantial for exerting any isotopic lapse rate.

Our findings reveal significant temporal variability in snowmelt water $\delta^{18}O$ values which considerably outweighed the spatial isotopic variability across the 2.2 km transect of the catchment (Fig. 7). This aligns with the study by Laudon et al. (2007), which also found temporal isotopic variability to be more pronounced than spatial variability in closed canopy, open canopy, and open field sites. A clear indication of the lighter water molecules melting out of the snowpack was seen in the depleted $\delta^{18}O$ values found in earlier snowmelt water (Feng et al., 2002; Taylor et al., 2001; Taylor, Feng, Renshaw, et al., 2002). Although the DI snowpack samples generally exhibited consistent isotope values compared to snowmelt water $\delta^{18}O$ values, gradual isotopic enrichment over the melt season was also observed (Fig. 9a). Statistical analysis demonstrated the temporal trend of snowmelt water $\delta^{18}O$ values to be non-linear, contrasting with the relatively linear trend of the DI snowpack $\delta^{18}O$ values (see supplementary Table S9 of Publication II). When examining our field data, we noticed a significant difference in the relationship between snowmelt water and DI snowpack $\delta^{18}O$ values before and during peak melting (see Fig. 6 of Publication II). To the best of our knowledge, such a comparison has not been presented in existing literature. Unnikrishna et al. (2002) demonstrated a completely opposite relationship between snowmelt and snowpack $\delta^{18}O$ values, where the initial snowmelt was isotopically heavier than the snowpack, and only during the major melt event did the snowmelt $\delta^{18}O$ values become lower than those of the snowpack. From their research, it remains unclear whether the DI snowpack $\delta^{18}O$ values were used for this comparison, or the volume-weighted average $\delta^{18}O$ value of vertical isotope profiles in the snowpack was employed. In their case, the mechanism of snow melting was different; they noted that melting initially started in the lower layers, which were enriched with heavier isotopes, and top layer melting only occurred once the snowpack became isothermal. Thus, we can infer from this analysis that the divergence between the snowpack and snowmelt $\delta^{18}O$ values is dependent on the specific melting mechanism.

4.2.3 Evaluation of earlier meltwater's depletion in ^{18}O Isotopes and its shift to enrichment during peak melt period

Previous studies have consistently shown that the initial snowmelt water pulse generally displays low $\delta^{18}O$ and $\delta^{2}H$ values, which steadily increase over the snowmelt period (Langman et al., 2022; Laudon et al., 2002; Lee et al., 2010; Stichler, 1987; Taylor et al., 2001; Taylor, Feng, Williams, et al., 2002). This trend is typically attributed to liquid-ice fractionation, which causes the early melting water to be isotopically depleted. The early depleted melted water leaves behind an enriched snowpack. This snowpack experiences further enrichment during the later stages of snowmelt due to isotopic fractionation via evaporation or sublimation (Laudon et al., 2002; Lee et al., 2010; Taylor et al., 2001; von Freyberg et al., 2020). In our study, the analysis of snowmelt water and DI snowpack $\delta^{18}O$ isotope datasets from forest hillslope and mixed forest areas highlighted three key isotopic evolution processes (Figs. 6 and 8):

The offset or clear distinction between snowmelt water and DI snowpack δ18O values during an earlier stage of snowmelt with low melt rates (Fig. 9a)

During the preliminary melt phase, or before the peak melt period, we identified a noticeable difference between the $\delta^{18}O$ values of snowmelt water and the DI snowpack. This difference aligned closely with the equilibrium offset of 3.1‰ $\delta^{18}O$ between ice and liquid water (O'Neil, 1968). The first values at the onset of the snowmelt period were slightly higher in $\delta^{18}O$ and $\delta^{2}H$ values, which is in line with the observations of Evans et al. (2016) and Lee et al. (2010). They proposed that the melting of the relatively isotopically heavier uppermost layers could directly contribute to the final observed $\delta^{18}O$ values of snowmelt water at the base of the snowpack. This indicates that percolation of meltwater may not achieve liquid-ice equilibrium due to the entire surface layer melting and reaching the snowpack's base via preferential flow paths or lateral flow (Evans et al., 2016) at the beginning of the snowmelt period. In subsequent melting episodes, the smaller volume of percolating meltwater might have interacted with the solid snowpack, potentially causing an isotopic exchange between the two states before the peak melt period. This exchange favors lighter isotopes in the liquid state (O'Neil, 1968). As Fig. 9a demonstrates, the difference between the $\delta^{18}O$ values of snowmelt water and the DI snowpack was not consistently 3.1‰ $\delta^{18}O$, as minor fluctuations were observed.

This indicates a variable liquid-ice interaction which fluctuates between equilibrium and non-equilibrium fractionation during this period.

The variability in lc-excess values during the earlier stage of the snowmelt with low melt rates (Figs. 6 and 8)

During the initial stages of snowmelt with low melt rates, the lc-excess values of snowmelt water fluctuated between 0‰ and 10‰ (Figs. 6 and 8). In the dual-isotope space (δ^2H vs. $\delta^{18}O$), this range is depicted by a slope lower than the LMWL (see supplementary Fig. S12 of Publication II). The lc-excess values close to 0 suggested that the liquid-ice fractionation had reached an equilibrium state. Conversely, higher lc-excess values pointed towards a departure from this equilibrium, wherein kinetic fractionation prevailed as a dominant process. The most significant lc-excess, i.e., a value of 10‰, was observed from May 6th to 11th, prior to the peak melt period. During this phase, characterized by low melt efflux (Fig. 7), the isotopic stratigraphy within the snowpack had not yet achieved significant consistency or homogeneity when compared to the stratigraphy during and after the peak melt period (plot (b) in Fig. 4 and plots (c) and (d) in Fig. 5).

The increase in lc-excess values before the peak melt period is an indication of time-variant kinetic liquid-ice fractionation, which is in line with a close difference of equilibrium isotopic exchange of 3.1‰ $\delta^{18}O$ between the DI snowpack and snowmelt. The variability in lc-excess values of snowmelt suggested the kinetic fractionation process was dominant compared to equilibrium isotopic exchange due to liquid-ice interaction, but this was not evident from the analysis of the DI snowpack samples (see supplementary Fig. S3 of Publication II).

Some literature has discussed the d-excess value, recognized as a conventional second-order isotope parameter for snowmelt water, as comparable to the lc-excess parameter for understanding equilibrium or kinetic fractionation processes (Carroll, Deems, Maxwell, et al., 2022; Feng et al., 2022; Lee et al., 2010). However, lc-excess has the added advantage of reducing the bias that may result from extreme $\delta^{18}O$ values (Landwehr & Coplen, 2004). The lc-excess value, as previously mentioned, distinctly reveals the contrast between evaporative fractionation (when lc-excess is negative) and moisture source difference (when lc-excess is positive) (Landwehr & Coplen, 2004). Lee et al. (2010) proposed that the variability in d-excess (or lc-excess in our case) values is not always significant. Their study found the d-excess values to be largely consistent for winter 1998 snowmelt samples, with only a few exceptions. In contrast, their 2001 snowmelt samples displayed

significant variability of d-excess values. This pattern aligns closely with our findings, where during the early snowmelt period, the d-excess value (lc-excess value in our case) was higher, decreasing in later stages. Carroll, Deems, Maxwell, et al. (2022) reached similar conclusions, indicating that the d-excess value diminishes as snowmelt progresses.

This suggests the importance of analyzing lc-excess values in meltwater. It appears that, often, the variability in lc-excess or d-excess value of early meltwater leans towards the positive side, while in late-stage meltwater, the value can decrease significantly. As a result of the liquid-ice interaction within the snowpack, the heavier isotopes tend to persist in the solid state, and the lighter isotopes favor the liquid state, leading to higher d-excess or lc-excess values. As significant melt-out processes occur, the remaining snowpack becomes enriched with heavier isotopes, and the depletion of lighter isotopes in the late-stage snowmelt water points to lower or negative values. The noticeable co-variability in lc-excess across different sampling locations implies that kinetic fractionation processes are influenced by ambient environmental conditions and the resulting melt rates. To our knowledge, such a spatiotemporal correlation of lc-excess values has not previously been observed in melting natural snowpacks.

Absence of a significant difference between snowmelt water and DI snowpack δ18O values in the late snowmelt stage (Fig. 9)

As the peak melt period approached, the significant difference between the $\delta^{18}O$ (i.e., 3.1‰) and lc-excess values of snowmelt water and DI snowpack began to fade (Fig. 9). The convergence of $\delta^{18}O$ and lc-excess values of snowmelt and DI snowpack occurred with the rising temperatures and increasing energy fluxes to the snowpack. These environmental factors escalated the rate of snowmelt and the velocity of meltwater percolation through the snowpack. The onset of the peak melt period resulted in homogenization of $\delta^{18}O$ values throughout the snow depth profiles (Figs. 4 and 5). This homogeneity continued through the post peak melt period and may suggest a diffuse movement of meltwater within the snowpack caused by the extensive mass movement of percolating meltwater (Evans et al., 2016). Minimal interaction between percolated meltwater and solid ice may have precluded isotopic exchange during liquid-ice equilibration or fractionation (Feng et al., 2002; Lee et al., 2009, 2010; Taylor et al., 2001; Taylor, Feng, Renshaw, et al., 2002). This limited interaction likely resulted in the similar $\delta^{18}O$ isotopic compositions of the snowmelt water and snowpack.

Early meltwater's depleted (lower) $\delta^{18}O$ values may be attributed to: (a) the melting of freshly fallen isotopically depleted snow from the surface layers which percolates down via a bypassing flow mechanism, i.e., through preferential flow path or lateral flow (Evans et al., 2016); (b) significant liquid-ice fractionation of percolating meltwater within the snowpack (Feng et al., 2002; Lee et al., 2009, 2010; Taylor et al., 2001; Taylor, Feng, Renshaw, et al., 2002); or (c) a combination of both of these factors (Pu et al., 2020).

The persistent ~3.1‰ offset between DI snowpack and snowmelt water throughout the early melt period (Fig. 9) does not suggest that individual surface layers melted from the top, bypassing the snowpack through preferential or lateral flow. Thus, the surface layer's melting may not be the main driver of the observed temporal isotopic evolution in snowmelt water (Pu et al., 2020). Based on our findings, we propose that liquid-ice fractionation during periods of low melt rates was mainly responsible for the early depleted $\delta^{18}O$ values. In contrast, as melt rates increased and vertical homogenization occurred in the snow isotope profiles, liquid-ice fractionation became weakened. This led to enriched snowmelt water, which closely matched the DI snowpack isotopically. To our knowledge, our work is the first to extensively investigate the spatial and temporal variations in snowpack and meltwater lc-excess values, providing evidence of the occurrence of kinetic isotopic fractionation caused by liquid-ice interaction within the snowpack during early melting with low rates (Feng et al., 2002; Lee et al., 2009, 2010; Taylor, Feng, Renshaw, et al., 2002). The magnitude and rate of snow melting are mainly dependent on local hydrometeorological conditions, but if similar meteorological patterns are observed in other regions, results from our findings can be extrapolated to other regions.

4.3 Snowmelt isotope hydrograph separation [Publication III]

4.3.1 Estimating meltwater contribution to streamflow during peak melt

For the application of IHS, our research focused on the peak snowmelt period, while avoiding the overlooking of prior melt episodes that have affected snowmelt isotopic evolution. To best characterize the pre-event water endmember, we considered the winter pre-melt baseflow (Buttle et al., 1995) and employed it in IHS as a consistent endmember across all scenarios. In defining the snowmelt event

water endmember, we opted for scenario (X) Roll-RCVWSM (Rolling Runoff-Corrected Volume Weighted SnowMelt) as the base scenario over scenario (VIII) RCVWSM, as proposed by Laudon et al (2002). The latter scenario exhibited a flat and steady late-melt isotopic signal which poorly reflected the actual late melt signal, as depicted in Fig. 11 (also see Fig. 7 of Publication III). Moreover, it incorporates all melt episodes into the computation (Eq. 10). In contrast, scenario (X) Roll-RCVWSM facilitates better interpretation of the snowmelt isotopic signal of the actual meltwater flowing through the landscape and contributing to peak streamflow generation.

The IHS results demonstrated how the peak melt period's total snowmelt water contribution was 69.9 mm ± 2.3 mm (59.6% ± 2%), which is based on scenario (X) Roll-RCVWSM. The IHS based meltwater estimations were similar in Krycklan catchment (i.e., over 50%) (Laudon et al., 2007). The Krycklan catchment is also located in the subarctic (approximately 465 km southwest of the Pallas catchment), Sweden. This higher percentage of meltwater contribution may be due to the presence of adjacent wetlands to the outlet stream, which are frozen, as most of the meltwater over the frozen wetland contributes to the outlet stream. Previous research has indicated that spatial variation of $\delta^{18}O$ values may lead to different estimations for snowmelt contribution (Penna & van Meerveld, 2019). Nevertheless, in our Pallas catchment and the boreal Krycklan catchment, it is evident that spatial snowmelt variability is relatively less significant than temporal variability, and there exists a potential for spatiotemporal snowmelt water isotope covariation across the catchment (Laudon et al., 2004).

Because the Pallas catchment has a limited area of 4.42 km^2 and an elevation range from 268 m to 364 m a.s.l., We did not observe an isotope lapse rate with elevation, and significant spatial homogeneity may be responsible for the spatial $\delta^{18}O$ isotopic covariation [Publication II]. Therefore, our analysis employed an integrated snowmelt signal for the entire catchment, comprised of forest hillslope, mixed forest, and open mires. However, for higher elevation catchments, the significantly differing snowpack melt rates could cause spatial variations in snowmelt isotopes (Beaulieu et al., 2012; Carroll, Deems, Maxwell, et al., 2022). Consequently, the integrated snowmelt isotopic signal may not be suitable for IHS application in such regions.

Our findings suggest a 17.8% underestimation of the snowmelt water contribution when using time-invariant snowfall isotopes as a substitute for the time-variant snowmelt water isotopic composition. Buttle et al. (1995) proposed that pre-melt snowpack $\delta^{18}O$ values can serve as event water endmember

characterization, but this approach doesn't hold true for suburban areas with thin snow cover. Our investigation showed that utilizing isotopic measurements of the DI snowpack from the pre-peak melt period in the IHS application resulted in an even more substantial underestimation, i.e., 22.6%. Further quantitative comparisons between various scenarios are presented in Fig. 13. Besides the snowmelt isotopes, scenarios (V) SP and (IX) Roll-RCWSP provided estimations closest to those of scenario (X) Roll-RCVWSM (Fig. 13b). It is worth noting, however, that our calculations did not consider rain-on-snow events because they were not significant during the 2020 melt period. These events could significantly impact the selection of the event water endmember, particularly in regions with thin snow cover (Buttle et al., 1995). Previous research focusing on snowfall or snowpack isotopes may have introduced biases when evaluating the role of snowmelt water and winter precipitation in isotope studies (Boumaiza et al., 2020; Chesnaux & Stumpp, 2018; Earman et al., 2006; Jasechko et al., 2017; Kirchner & Allen, 2020). The potential biases that we have discussed highlight the significance of snowmelt isotopes in IHS research.

4.3.2 Sensitivity and performance analysis of multiple event water endmember ^{18}O isotopes

The application of a mass-balance isotope hydrograph separation method simplifies the estimation of the final snowmelt water fractions in stream water which leads to significant uncertainties (Klaus & McDonnell, 2013; Uhlenbrook et al., 2002). These uncertainties can stem from the mixing model utilized, water sampling procedures, and the extensive spatial and temporal variations of isotope tracers (He et al., 2020). Despite the basic assumptions which may cause uncertainties to some extent (Genereux, 1998), the traditional EMMA approach remains effective for estimating the total snowmelt fraction in stream water because of its adherence to the mass conservation principle. The recently applied BEMMA approach may be more useful for studies that are based on multiple sources and fewer tracers. However, estimating several sources concurrently using BEMMA may be associated with greater uncertainties (Phillips & Gregg, 2001). A more recently used EHS approach is based on a statistical linear regression model, which can be useful in estimating mean event water fractions and transit times yet lacks the mass conservation principle (Kirchner, 2018).

In our investigation, we determined that the traditional EMMA approach yielded a 2% uncertainty in the final meltwater fractions when employing scenario

(X) Roll-RCVWSM. In comparison, we noted that the largest uncertainties, around 8%, stemmed from the amount-weighted average snowfall (VWSF) and the melt flux-weighted average snowmelt isotope values (VWSM). Conversely, the smallest uncertainty, around 1%, came from the incremental and rolling runoff-corrected SWE-weighted average snowpack isotope values (RCVWSP and Roll-RCVWSP). The discrepancy in uncertainties across different scenarios can be ascribed to the type of input $\delta^{18}O$ values used as an event water endmember in IHS (see Fig. 7 of Publication III). Our data indicated that snowpack isotope values displayed less variability than snowfall and snowmelt isotope values, hence, exhibiting smaller uncertainty when quantified based on the standard error.

The event water isotopic signal, employed in IHS, is an integrated signal across the entire catchment, thus it exhibits both temporal and spatial uncertainties (Genereux, 1998; Laudon et al., 2002). Nevertheless, numerous IHS investigations overlooked spatial uncertainties due to the lack of availability of spatiotemporal isotope datasets. In contrast, our extensive spatiotemporal datasets allowed us to calculate both temporal and spatial uncertainties, thereby facilitating a comparison of these uncertainties (Tables 1 and 2, and Fig. 13). Temporal uncertainty refers to the uncertainty which arises due to changes in the isotopes of snowmelt event water endmember over time. Spatial uncertainty, on the other hand, refers to the uncertainty which arises from isotopic differences across various locations. We also estimated bias and detailed the performance of each scenario (Fig. 14). Our results highlight how when the $\delta^{18}O$ values of stream water during peak discharge align closely with the event water endmember values, it results in the underestimation of snowmelt water contribution for the different event water scenarios. This is because the isotope data used to define the snowmelt event water endmember yield more negative values (such as for snowfall or pre-melt snowpack) compared to the true snowmelt. However, if these values mirror those of the pre-event water endmember, it will likely overestimate snowmelt water contribution (Fig. 14a). Similarly, if the event water endmember isotope values lean towards the negative side, the IHS will underestimate snowmelt water estimations, and the opposite is true if the values are less negative (Fig. 14b).

Existing literature does not present a standardized method for meltwater sampling. Some studies have used snowfall collectors to characterize meltwater samples (Earman et al., 2006; Gui et al., 2019; Lucianetti et al., 2020), while others have relied on DI snowpack samples to represent meltwater (Dinçer et al., 1970; Moore, 1989; Rodhe, 1981; Sueker et al., 2000; Wang et al., 2015). Nevertheless, the most reliable in-situ meltwater can often be obtained using specialized

equipment, such as a snowmelt lysimeter (Laudon et al., 2002, 2004, 2007; McNamara et al., 1997; Rücker, Boss, et al., 2019; Rücker, Zappa, et al., 2019). Different sampling methods may lead to meltwater exhibiting distinct isotopic compositions that poses a challenge for accurately determining meltwater isotopes.

Our analysis, as illustrated in Fig. 14c, indicates a potential bias in meltwater fraction estimates when samples obtained through snowmelt lysimeters are not used in IHS applications. While DI snowpack sampling is more convenient than installing equipment like a snowmelt lysimeter, using snowpack isotopes sampled during the melt period provides better estimates for snowmelt water contributions compared to using snowfall or pre-melt snowpack isotopes, with a 0.1 RMSE and 0.02 average bias (Fig. 14c). However, it is important to remember that these findings are based on a small catchment with an elevation range of less than 100 meters, as shown in Fig. 14c. Therefore, these results may not be applicable to high-elevation mountainous catchments without the careful evaluation of the average biases caused by different sampling methods. Overall, it highlights the importance of considering snowpack isotopes during the peak melt period in IHS studies, in the absences of meltwater isotopes of in-situ samples, obtained through snowmelt lysimeters.

5 Conclusions

Snowmelt water ^{18}O and ^{2}H isotopes are important tools in ecohydrological and other tracer-based hydrological investigations in seasonal snow-influenced regions. Having a thorough understanding of water ^{18}O and ^{2}H isotopes' journey—from snowfall to snowpack accumulation, and finally to snow melting—is pivotal to the reliability of meltwater isotope applications in hydrological studies. It is also important to consider variations in landscape features to account for the temporal and spatial variability of meltwater ^{18}O and ^{2}H isotopes.

This study extensively characterized the water $\delta^{18}O$ and $\delta^{2}H$ isotope values in a seasonal snowpack, exploring their variabilities from snowfall to snowpack to snowmelt. First, we focused on the Arctic research sites of Pallas, Finland, and Imnavait, USA, which allowed a comprehensive comparison of vertical isotope profiles within the snowpack in Arctic taiga and tundra snow regimes. This comparison sought to broaden our understanding of ^{18}O isotopic modification from initial snowfall to spring snowmelt, a field where current knowledge is limited but which carries significant implications for isotope-based hydrological investigations in cold climate regions.

A thorough in-situ snowpit sampling was conducted across both sites, which provided insights into the complex interplay of isotope values with vertical depths, specifically at soil-snow and snow-air interfaces. The meteorological conditions differed at each site, with the Pallas location exhibiting more substantial seasonality in temperature and other meteorological variables. However, the post-depositional isotopic modification was more noticeable at Imnavait, especially when the basal snow layers were compared to the isotope values of the earliest snowfall events. Our comparative study unambiguously demonstrated that the isotope values at the soil-snow interface were higher than those in the middle portion of the snowpack at both research sites. The lightest isotopes were found between 20 and 40% of the relative snow depth, correlating with consistently higher snow densities. This means that the isotope values in the middle of the snowpack were relatively closer to the snowfall isotope values. Thus, the middle layers of the snowpack can better preserve the snowfall isotopes and are less prone to post-depositional isotopic modification. From this, we conclude that in those cold regions where post-depositional isotopic modification is experienced less, the isotope values corresponding to the middle layers of the snowpack can be used as a proxy for snowfall isotope values. Such proxies can be useful in regions where event-based snowfall samples are unavailable. On the other hand, the modification in isotope

values at the snow-air interface depends on several factors, including the isotope values of snowfall throughout the season and the hydrometeorological and topographic conditions which may influence snow sublimation and condensation processes.

We performed a comprehensive investigation into the spatiotemporal evolution of water ^{18}O isotopes at the Pallas catchment, focusing on three key elements: (i) vertical isotope profiles across snowpack depths, (ii) depth-integrated (DI) snowpack ^{18}O isotopes, and (iii) meltwater ^{18}O isotopes, for three distinct landscape features. We utilized eleven snowmelt lysimeters for snowmelt isotope sampling and the quantifying of snowmelt effluxes, installed at 200 m intervals along the catchment's transect. Our analysis revealed that earlier snowmelt water presented isotopically lighter values than the DI snowpack, while peak snowmelt water was isotopically heavier in comparison. Notably, the $\delta^{18}O$ values of early-season snowmelt water were found to be even lower in some locations than those in the vertical isotope profiles of snowpack stratigraphy, clearly indicating the isotopic fractionation effects caused by the phase change from solid to liquid, differential in bond strengths and activation energies of solid and liquid molecules during the slow early melt period, and isotopic exchange between solid-liquid water interaction. Over the snowmelt period in 2020, the DI snowpack isotope values exhibited a relatively linear temporal trend, transitioning from low (depleted) to high (enriched) values over the course of the snowmelt. However, the meltwater $\delta^{18}O$ values showed a highly non-linear temporal trend. These findings highlight that without a detailed understanding of the liquid-ice isotope fractionation process, the spatiotemporal evolution of snowmelt water $\delta^{18}O$ values based on snowpack $\delta^{18}O$ values alone cannot be predicted. Our data further suggest that liquid-ice fractionation processes, both kinetic and equilibrium, governed the isotopic composition of the subsequent snowmelt water. These processes, occurring within the snowpack, were heavily influenced by the snowmelt rate. The liquid-ice isotopic fractionation became noticeable during periods of low melt but were less evident during high melt rates. This necessitates detailed input of liquid-ice fractionation information in the modeling of snowmelt water isotopes, along with their uncertainties, for reliable prediction.

For the application of water ^{18}O isotopes in cold climate catchment hydrology, we used an extensive dataset of snow (comprising snowmelt, snowpack, and snowfall) and stream water ^{18}O isotopes to delve into the sensitivity analysis when defining snowmelt event water endmember in Isotope Hydrograph Separation (IHS). We aimed to quantify the snowmelt water fractions and explore the potential

bias that may arise from different sampling strategies of snowmelt endmember. We selected the snowmelt event water endmember based on the incremental and rolling runoff-corrected weighted average snowmelt isotope value caused by its relatively better assumptions for mass conservation based mixing analysis of IHS. During peak streamflow, our analysis showed that a significant portion of the stream water, roughly 59.6% ± 2%, originated from snowmelt water. Nevertheless, the usage of snowfall or depth-integrated snowpack isotope values, sampled before the onset of the snowmelt season, resulted in the underestimation of this fraction. When the snowpack-based event water endmember which was sampled during the peak melt period was used, the resulting snowmelt water fractions were closer to the reliable values but still indicated a 5–6% underestimation.

Thus, we conclude that utilizing snowpack sampling during melting periods with high snowmelt rates as a proxy for snowmelt water isotopes can be a valuable strategy, particularly when direct sampling of snowmelt water isotopes is unavailable or logistically impractical. Determining an accurate estimation of snowmelt water partitioning is essential for understanding its role in catchment hydrology and avoiding misinterpretations of snowmelt-dependent hydrological, ecohydrological, and biogeochemical processes in stream water or terrestrial ecosystems. The detailed analysis of extensive datasets of snowpack and meltwater ^{18}O and ^{2}H isotopes has provided novel insights and foundational knowledge for future isotope hydrology studies in cold regions. Furthermore, our openly available isotope data for snowfall, snow layers, and snowmelt can be used for benchmark testing of tracer-based hydrological models, bayesian endmember mixing analysis, endmember mixing and splitting analysis, ensemble hydrograph separation, young water fraction analysis, and in comparisons of any novel tracer-based application with the existing methods.

5.1 Recommendations for future studies and suggestions

The ^{18}O and ^{2}H isotope tools are increasingly being used in cold climate hydrological studies, and their usage is expected to further increase in the future. Therefore, it is fundamentally important to evaluate and quantify these isotopes in snowfall, snow layers, and snowmelt through field studies, and to discuss the importance of their proper characterization in hydrological research. It is also crucial to discuss the importance of correct flux input for flow propagation in the catchment, and the connectivity of hydrological processes occurring in different storages of the catchment and compartments of the water cycle.

In our study, we observed spatially consistent isotope variability in snow stratigraphy across both the Pallas catchment in Finland and the Imnavait research site in the U.S.A. This concordance aligns with several studies conducted in other regions. We deduce that spatial isotope variability in vertical snow layers primarily hinges on the synoptic scale isotope variability in precipitation. Fractionation processes occurring during winter, such as sublimation, condensation, and vapor diffusion within the snowpack, are spatially correlated. As a result, conducting vertical snow profiling at a limited number of locations during the same time frame might suffice. However, it is essential to note that isotopic discrepancies in snow stratigraphy do manifest between forested and open areas. Canopy coverage should thus be a significant consideration when selecting sampling locations. This is because the interception of snow by the canopy and its temporary storage can influence isotope values on the snow's surface. Given that our catchment has an elevation of less than 100 m, spatial discrepancies may become more pronounced in areas with pronounced elevation differences, such as mountainous regions. Other studies have indicated that the isotopic lapse rate is particularly noticeable in high-altitude regions. Factors like wind scouring and melting at elevated sites can further complicate isotope dynamics within snow stratigraphy.

Homogenization in isotope values within snow stratigraphy during the late melt period aligns with findings from other studies. However, the exact timing of when these isotope values become homogenized is influenced by local meteorological and hydrological processes. A pronounced vapor diffusion process at the soil-snow interface can lead to depth hoar formation, resulting in basal layers that are enriched with heavier isotopes. While sublimation tends to enrich surface layers with these isotopes, the condensation process does the opposite. Such processes are largely contingent upon local energy fluxes, humidity, wind speed, temperature and existing antecedent moisture conditions. Therefore, to gain insights into the homogenization of isotope values in snow stratigraphy, it is crucial to thoroughly examine these local processes, along with snow isotopic composition. We further advocate that future technology based on in-situ snow isotope analysis would be the most suitable approach when observing the temporal homogenization of isotope values within snow stratigraphy in greater detail.

Sublimation and condensation fronts, which induce isotopic fractionation, are limited to snow surface layers. Vapor diffusion is influenced by the temperature gradient, which is more pronounced at the soil-snow interface. Therefore, middle layers of the snowpack might better preserve the isotopic composition of corresponding winter precipitation events. As a result, the isotope values from these

layers can serve as isotope proxies for winter precipitation, especially if these layers are substantial in vertical depth, shielded from extended exposure to ambient temperatures, and located in shaded areas. However, it is essential to recognize that surface sublimation, condensation, and pronounced diffusion at the snowpack's base can impact the isotopic composition of these middle layers, resulting in the redistribution of snow isotopic composition.

Emerging technologies which facilitate in-situ, high-resolution snow isotopic analyses may help in deciphering these effects. Grasping the spatiotemporal isotopic evolution of snow stratigraphy is vital for comprehending the subsequent isotopic evolution of snowmelt water. Understanding the latter is crucial for catchment scale isotope-based hydrological research, such as in tracer-based modeling studies evaluating water flow paths, water fluxes, water ages and water fractions in different sources. This is because, hydrologically, the dynamic meltwater, which either infiltrates or becomes overland flow before finding its way to streams, ditches, lakes, rivers, and oceans, is more important than the static solid snow residing in the snowpack. Therefore, we thoroughly investigated the importance of snowmelt isotopes and their application in hydrological analysis. We observed a shift in the variability of lc-excess values in early meltwater, as opposed to the relatively stable meltwater isotope values. Future studies should also prioritize examining meltwater lc-excess values. Such scrutiny may shed light on fractionation processes occurring within the snowpack.

Our findings suggest that snowpack isotopes can act as a suitable alternative for snowmelt isotopes, but only if sampled during the peak melt period. When using DI snowpack isotopes sampled during snowmelt for analysis, the bias was significantly smaller (with a 5–6% underestimation) compared to when using snowpack isotopes sampled before the melt period (which resulted in a 22.6% underestimation), or snowfall isotopes (which led to a 17.8% underestimation) as the snowmelt event water endmember in IHS. This is because during the peak melt period, the isotopic composition of the meltwater becomes more homogenous with that of the DI snowpack due to the harmonization of vertical isotope stratigraphy within the snowpack. This isotopic harmonization causing enrichment of snowpack in heavier isotopes occurs primarily because of an accelerated snowmelt rate, a melt-out process of heavier isotopes from the snowpack, and isotope fractionation processes, such as sublimation/evaporation and vapor diffusion. Consequently, the isotopic values of the DI snowpack align more closely with those of the snowmelt during periods of peak runoff generation. This implies that prior studies which have relied on snowfall or snowpack isotopes prior to melt season might have

encountered similar biases when assessing the influence of snowmelt water in isotope studies.

Though snowmelt isotopes are particularly beneficial for studies estimating snowmelt during peak runoff generation using isotope-based investigations, practical limitations might favor the use of DI snowpack sampling. DI snowpack isotopes prove particularly valuable at lower elevations or flatter areas, where accessing snowmelt water isotope data directly may not be possible due to the absence of specialized equipment like snowmelt lysimeters. In our case, we experienced challenges while attempting to collect meltwater in waterlogged, flat peatland areas using snowmelt lysimeters. However, in remote or mountainous areas, or when a high spatiotemporal resolution is required, the meltwater contribution estimates based on DI snowpack isotopes may not be reliable. Further research in mountainous and permafrost catchments is needed to formulate effective sampling strategies. These strategies should consider factors like lapse rates in isotope values influenced by elevation, and varying snowmelt rates and timings. To minimize uncertainty in final fraction estimations, increasing the sampling frequency, where possible, would be advantageous. This would lead to a more reliable estimation of the sample mean in relation to the population mean.

It is important to point out that the Pallas catchment demonstrated a limited spatial variation of snow isotopes [Publication II]. As a result, the applicability of a straightforward two-component endmember IHS method may not extend to larger or mountainous catchments, where substantial spatial discrepancies in isotope values may be expected. In such cases, intensive sampling of endmembers across the catchment becomes essential, and uncertainties linked with the method must be rigorously evaluated.

The spatial coherence of snow isotope values in flat regions, where the elevation range is less than 100 m (e.g., in the Pallas catchment), indicates that the calibration of tracer-aided spatially distributed hydrological models such as STARR, EcH2O-iso, and iso-WATFLOOD based on the snow isotopes available at a few spatial locations should be sufficient and can be generalized to other locations due to the spatial coherence of the snow isotopes. Furthermore, tracer-based hydrological models use empirical equations to estimate spatiotemporal snowmelt isotopes, e.g., STARR, EcH2O-iso. Our extensive, high-resolution spatiotemporal snowmelt data can be used to improve and update these empirical equations in tracer-based hydrological models.

List of references

Akers, P. D., Welker, J. M., & Brook, G. A. (2017). Reassessing the role of temperature in precipitation oxygen isotopes across the eastern and central United States through weekly precipitation-day data. *Water Resources Research*, *53*(9), 7644–7661. https://doi.org/10.1002/2017WR020569

Ala-aho, P., Tetzlaff, D., McNamara, J. P., Laudon, H., Kormos, P., & Soulsby, C. (2017). Modeling the isotopic evolution of snowpack and snowmelt: Testing a spatially distributed parsimonious approach. *Water Resources Research*. https://doi.org/10.1002/2017WR020650

Ala-Aho, P., Tetzlaff, D., McNamara, J. P., Laudon, H., & Soulsby, C. (2017). Using isotopes to constrain water flux and age estimates in snow-influenced catchments using the STARR (Spatially distributed Tracer-Aided Rainfall-Runoff) model. *Hydrology and Earth System Sciences*, *21*(10), 5089–5110. https://doi.org/10.5194/hess-21-5089-2017

Alstad, K. P., Welker, J. M., Williams, S. A., & Trlica, M. J. (1999). Carbon and water relations of Salix monticola in response to winter browsing and changes in surface water hydrology: an isotopic study using δ13C and δ18O. *Oecologia 1999 120:3*, *120*(3), 375–385. https://doi.org/10.1007/S004420050870

Beaulieu, M., Schreier, H., & Jost, G. (2012). A shifting hydrological regime: a field investigation of snowmelt runoff processes and their connection to summer base flow, Sunshine Coast, British Columbia. *Hydrological Processes*, *26*(17), 2672–2682. https://doi.org/10.1002/HYP.9404

Berghuijs, W. R., Woods, R. A., & Hrachowitz, M. (2014). A precipitation shift from snow towards rain leads to a decrease in streamflow. *Nature Climate Change 2014 4:7*, *4*(7), 583–586. https://doi.org/10.1038/nclimate2246

Beria, H., Larsen, J. R., Ceperley, N. C., Michelon, A., Vennemann, T., & Schaefli, B. (2018). Understanding snow hydrological processes through the lens of stable water isotopes. *Wiley Interdisciplinary Reviews: Water*, *5*(6), e1311. https://doi.org/10.1002/WAT2.1311

Beria, H., Larsen, J. R., Michelon, A., Ceperley, N. C., & Schaefli, B. (2020). HydroMix v1.0: A new Bayesian mixing framework for attributing uncertain hydrological sources. *Geoscientific Model Development*, *13*(5), 2433–2450. https://doi.org/10.5194/GMD-13-2433-2020

Bintanja, R., & Andry, O. (2017). Towards a rain-dominated Arctic. *Nature Climate Change 2017 7:4*, *7*(4), 263–267. https://doi.org/10.1038/nclimate3240

Birkel, C., Correa Barahona, A., Duvert, C., Granados Bolaños, S., Chavarría Palma, A., Durán Quesada, A. M., Sánchez Murillo, R., & Biester, H. (2021). End member and Bayesian mixing models consistently indicate near-surface flowpath dominance in a pristine humid tropical rainforest. *Hydrological Processes*, *35*(4), e14153. https://doi.org/10.1002/HYP.14153

Birkel, C., Correa-Barahona, A., Martinez-Martinez, M., Granados-Bolaños, S., Venegas-Cordero, N., Gutiérrez-García, K., Blanco-Ramírez, S., Quesada-Mora, R., Solano-Rivera, V., Mussio-Mora, J., Chavarría-Palma, A., Vargas-Arias, K., Moore, G. W., Durán-Quesada, A. M., Vasquez-Morera, J., Soulsby, C., Tetzlaff, D., Espinoza-Cisneros, E., & Sánchez-Murillo, R. (2020). Headwaters drive streamflow and lowland tracer export in a large-scale humid tropical catchment. *Hydrological Processes*, *34*(18), 3824–3841. https://doi.org/10.1002/HYP.13841

Boumaiza, L., Chesnaux, R., Walter, J., & Stumpp, C. (2020). Assessing groundwater recharge and transpiration in a humid northern region dominated by snowmelt using vadose-zone depth profiles. *Hydrogeology Journal*, *28*(7), 2315–2329. https://doi.org/10.1007/S10040-020-02204-Z

Bowen, G. J., Cai, Z., Fiorella, R. P., & Putman, A. L. (2019). Isotopes in the Water Cycle: Regional- to Global-Scale Patterns and Applications. *Https://Doi.Org/10.1146/Annurev-Earth-053018-060220*, *47*, 453–479. https://doi.org/10.1146/ANNUREV-EARTH-053018-060220

Buckeridge, K. M., Cen, Y. P., Layzell, D. B., & Grogan, P. (2010). Soil biogeochemistry during the early spring in low arctic mesic tundra and the impacts of deepened snow and enhanced nitrogen availability. *Biogeochemistry*, *99*(1), 127–141. https://doi.org/10.1007/S10533-009-9396-7/FIGURES/5

Buckeridge, K. M., & Grogan, P. (2010). Deepened snow increases late thaw biogeochemical pulses in mesic low arctic tundra. *Biogeochemistry*, *101*(1), 105–121. https://doi.org/10.1007/S10533-010-9426-5/FIGURES/6

Buttle, J. M., Vonk, A. M., & Taylor, C. H. (1995). Applicability of isotopic hydrograph separation in a suburban basin during snowmelt. *Hydrological Processes*, *9*(2), 197–211. https://doi.org/10.1002/HYP.3360090206

Cable, J., Ogle, K., & Williams, D. (2011). Contribution of glacier meltwater to streamflow in the Wind River Range, Wyoming, inferred via a Bayesian mixing model applied to isotopic measurements. *Hydrological Processes*, *25*(14), 2228–2236. https://doi.org/10.1002/HYP.7982

Carroll, R. W. H., Deems, J., Maxwell, R., Sprenger, M., Brown, W., Newman, A., Beutler, C., Bill, M., Hubbard, S. S., & Williams, K. H. (2022). Variability in observed stable water isotopes in snowpack across a mountainous watershed in Colorado. *Hydrological Processes*, *36*(8), e14653. https://doi.org/10.1002/HYP.14653

Carroll, R. W. H., Deems, J. S., Niswonger, R., Schumer, R., & Williams, K. H. (2019). The Importance of Interflow to Groundwater Recharge in a Snowmelt-Dominated Headwater Basin. *Geophysical Research Letters*, *46*(11), 5899–5908. https://doi.org/10.1029/2019GL082447

Carroll, R. W. H., Deems, J., Sprenger, M., Maxwell, R., Brown, W., Newman, A., Beutler, C., & Williams, K. H. (2022). Modeling Snow Dynamics and Stable Water Isotopes Across Mountain Landscapes. *Geophysical Research Letters*, *49*(20), e2022GL098780. https://doi.org/10.1029/2022GL098780

Ceperley, N., Zuecco, G., Beria, H., Carturan, L., Michelon, A., Penna, D., Larsen, J., & Schaefli, B. (2020). Seasonal snow cover decreases young water fractions in high Alpine catchments. *Hydrological Processes*, *34*(25), 4794–4813. https://doi.org/10.1002/HYP.13937

Chesnaux, R., & Stumpp, C. (2018). Advantages and challenges of using soil water isotopes to assess groundwater recharge dominated by snowmelt at a field study located in Canada. *Https://Doi.Org/10.1080/02626667.2018.1442577*, *63*(5), 679–695. https://doi.org/10.1080/02626667.2018.1442577

Craig, H. (1961). Isotopic Variations in Meteoric Waters. *Science*, *133*(3465), 1702–1703. https://doi.org/10.1126/SCIENCE.133.3465.1702

Crouzet, E., Hubert, P., Olive, P., Siwertz, E., & Marce, A. (1970). Le tritium dans les mesures d'hydrologie de surface. Determination experimentale du coefficient de ruissellement. *Journal of Hydrology*, *11*(3), 217–229. https://doi.org/10.1016/0022-1694(70)90063-6

DeWalle, D. R., & Rango, A. (2008). Principles of snow hydrology. *Principles of Snow Hydrology*, *9780521823623*, 1–418. https://doi.org/10.1017/CBO9780511535673

Dietermann, N., & Weiler, M. (2013). Spatial distribution of stable water isotopes in alpine snow cover. *Hydrology and Earth System Sciences*, *17*(7), 2657–2668. https://doi.org/10.5194/HESS-17-2657-2013

Dinçer, T., Payne, B. R., Florkowski, T., Martinec, J., & Tongiorgi, E. (1970). Snowmelt runoff from measurements of tritium and oxygen-18. *Water Resources Research*, *6*(1), 110–124. https://doi.org/10.1029/WR006I001P00110

Earman, S., Campbell, A. R., Phillips, F. M., & Newman, B. D. (2006). Isotopic exchange between snow and atmospheric water vapor: Estimation of the snowmelt component of groundwater recharge in the southwestern United States. *Journal of Geophysical Research: Atmospheres*, *111*(D9), 9302. https://doi.org/10.1029/2005JD006470

Essery, R., Li, L., & Pomeroy, J. (1999). A distributed model of blowing snow over complex terrain. *Hydrological Processes*, *13*(14–15), 2423–2438. https://doi.org/10.1002/(SICI)1099-1085(199910)13:14/15

Evans, S. L., Flores, A. N., Heilig, A., Kohn, M. J., Marshall, H. P., & McNamara, J. P. (2016). Isotopic evidence for lateral flow and diffusive transport, but not sublimation, in a sloped seasonal snowpack, Idaho, USA. *Geophysical Research Letters*, *43*(7), 3298–3306. https://doi.org/10.1002/2015GL067605

Fang, J., Yi, P., Stockinger, M., Xiong, L., & Shen, J. (2022). Investigation of factors controlling the runoff generation mechanism using isotope tracing in large-scale nested basins. *Journal of Hydrology*, *615*, 128728. https://doi.org/10.1016/J.JHYDROL.2022.128728

Feng, M., Zhang, W., Zhang, S., Sun, Z., Li, Y., Huang, Y., Wang, W., Qi, P., Zou, Y., & Jiang, M. (2022). The role of snowmelt discharge to runoff of an alpine watershed: Evidence from water stable isotopes. *Journal of Hydrology*, *604*, 127209. https://doi.org/10.1016/J.JHYDROL.2021.127209

Feng, X., Taylor, S., Renshaw, C. E., & Kirchner, J. W. (2002). Isotopic evolution of snowmelt 1. A physically based one-dimensional model. *Water Resources Research*, *38*(10), 35–1. https://doi.org/10.1029/2001WR000814

Flerchinger, G. N., Cooley, K. R., & Ralston, D. R. (1992). Groundwater response to snowmelt in a mountainous watershed. *Journal of Hydrology*, *133*(3–4), 293–311. https://doi.org/10.1016/0022-1694(92)90260-3

Friedman, I., Benson, C., & Gleason, J. (1991). Isotopic changes during snow metamorphism. *Stable Isotope Geochemistry: A Tribute to Samuel Epstein*, *Special Publication No. 3*, 211–221.

Friedman, I., Redfield, A. C., Schoen, B., & Harris, J. (1964). The variation of the deuterium content of natural waters in the hydrologic cycle. *Reviews of Geophysics*, *2*(1), 177–224. https://doi.org/10.1029/RG002I001P00177

Gat, J. R. (1996). Oxygen and hydrogen isotopes in the hydrologic cycle. *Annual Review of Earth and Planetary Sciences*, *24*, 225–262. https://doi.org/10.1146/ANNUREV.EARTH.24.1.225

Gat, J. R. (2010). *Isotope hydrology: a study of the water cycle* (Vol. 6). World scientific.

Genereux, D. (1998). Quantifying uncertainty in tracer-based hydrograph separations. *Water Resources Research*, *34*(4), 915–919. https://doi.org/10.1029/98WR00010

Gonfiantini, R. (1978). Standards for stable isotope measurements in natural compounds. *Nature 1978 271:5645*, *271*(5645), 534–536. https://doi.org/10.1038/271534a0

Grootes, P. M., & Stuiver, M. (1997). Oxygen 18/16 variability in Greenland snow and ice with 10−3- to 105-year time resolution. *Journal of Geophysical Research: Oceans*, *102*(C12), 26455–26470. https://doi.org/10.1029/97JC00880

Gu, L., Yin, J., Slater, L. J., Chen, J., Do, H. X., Wang, H.-M., Chen, L., Jiang, Z., & Zhao, T. (2023). Intensification of Global Hydrological Droughts Under Anthropogenic Climate Warming. *Water Resources Research*, *59*(1), e2022WR032997. https://doi.org/10.1029/2022WR032997

Gui, J., Li, Z., Yuan, R., & Xue, J. (2019). Hydrograph separation and the influence from climate warming on runoff in the north-eastern Tibetan Plateau. *Quaternary International*, *525*, 45–53. https://doi.org/10.1016/J.QUAINT.2019.09.002

Gustafson, J. R., Brooks, P. D., Molotch, N. P., & Veatch, W. C. (2010). Estimating snow sublimation using natural chemical and isotopic tracers across a gradient of solar radiation. *Water Resources Research*, *46*(12), 12511. https://doi.org/10.1029/2009WR009060

Hale, K., Kiewiet, L., Trujillo, E., Krohe, C., Hedrick, A., Marks, D., Kormos, P., Havens, S., McNamara, J., Link, T., & Godsey, S. E. (2023). Drivers of spatiotemporal patterns of surface water inputs in a catchment at the rain-snow transition zone of the water-limited western United States. *Journal of Hydrology*, *616*, 128699. https://doi.org/10.1016/J.JHYDROL.2022.128699

Ham, J.-Y., Hur, S. Do, Lee, W. S., Han, Y., Jung, H., & Lee, J. (2019). Isotopic variations of meltwater from ice by isotopic exchange between liquid water and ice. *Journal of Glaciology*, *65*(254), 1035–1043. https://doi.org/10.1017/JOG.2019.75

He, Z., Unger-Shayesteh, K., Vorogushyn, S., M. Weise, S., Duethmann, D., Kalashnikova, O., Gafurov, A., & Merz, B. (2020). Comparing Bayesian and traditional end-member mixing approaches for hydrograph separation in a glacierized basin. *Hydrology and Earth System Sciences*, *24*(6), 3289–3309. https://doi.org/10.5194/HESS-24-3289-2020

Helsen, M. M., van de Wal, R. S. W., van den Broeke, M. R., Masson-Delmotte, V., Meijer, H. A. J., Scheele, M. P., & Werner, M. (2006). Modeling the isotopic composition of Antarctic snow using backward trajectories: Simulation of snow pit records. *Journal of Geophysical Research: Atmospheres*, *111*(D15), 15109. https://doi.org/10.1029/2005JD006524

Hooper, R. P., & Shoemaker, C. A. (1986). A Comparison of Chemical and Isotopic Hydrograph Separation. *Water Resources Research*, *22*(10), 1444–1454. https://doi.org/10.1029/WR022I010P01444

Hubert, P., Marin, E., Meybeck, M., Olive, P., & Siwertz, E. (1969). Aspects hydrologique, géochimique et sédimentologique de la crue exceptionnelle de la Dranse du Chablais du 22 septembre 1968. *Archives Des Sciences*, *22*(3), 581–604. https://doi.org/http://pascal-francis.inist.fr/vibad/index.php?action=getRecordDetail&idt=GEODEBRGM7018014807

Hürkamp, K., Zentner, N., Reckerth, A., Weishaupt, S., Wetzel, K. F., Tschiersch, J., & Stumpp, C. (2019). Spatial and temporal variability of snow isotopic composition on Mt. Zugspitze, Bavarian Alps, Germany. *Journal of Hydrology and Hydromechanics*, *67*(1), 49–58. https://doi.org/10.2478/johh-2018-0019

Jasechko, S., Wassenaar, L. I., & Mayer, B. (2017). Isotopic evidence for widespread cold-season-biased groundwater recharge and young streamflow across central Canada. *Hydrological Processes*, *31*(12), 2196–2209. https://doi.org/10.1002/HYP.11175

Jespersen, R. G., Leffler, A. J., Oberbauer, S. F., & Welker, J. M. (2018). Arctic plant ecophysiology and water source utilization in response to altered snow: isotopic (δ18O and δ2H) evidence for meltwater subsidies to deciduous shrubs. *Oecologia*, *187*(4), 1009–1023. https://doi.org/10.1007/S00442-018-4196-1/FIGURES/7

Jones, M. W., Sebestyen, S. D., Dymond, S. F., Ng, G. H. C., & Feng, X. (2023). Soil frost controls streamflow generation processes in headwater catchments. *Journal of Hydrology*, *617*, 128801. https://doi.org/10.1016/J.JHYDROL.2022.128801

Kendall, C., & McDonnell, J. J. (Eds.). (2012). *Isotope tracers in catchment hydrology*. Elsevier. https://doi.org/10.1016/C2009-0-10239-8

Kirchner, J. W. (2018). Quantifying new water fractions and transit time distributions using ensemble hydrograph separation : theory and benchmark tests. August, 1–71. https://doi.org/10.5194/hess-23-303-2019

Kirchner, J. W. (2019). Quantifying new water fractions and transit time distributions using ensemble hydrograph separation: Theory and benchmark tests. *Hydrology and Earth System Sciences*, *23*(1), 303–349. https://doi.org/10.5194/HESS-23-303-2019

Kirchner, J. W., & Allen, S. T. (2020). Seasonal partitioning of precipitation between streamflow and evapotranspiration, inferred from end-member splitting analysis. *Hydrology and Earth System Sciences*, *24*(1), 17–39. https://doi.org/10.5194/HESS-24-17-2020

Kirchner, J. W., & Knapp, J. L. A. (2020). Technical note: Calculation scripts for ensemble hydrograph separation. *Hydrology and Earth System Sciences*, *24*(11), 5539–5558. https://doi.org/10.5194/HESS-24-5539-2020

Klaus, J., & McDonnell, J. J. (2013). Hydrograph separation using stable isotopes: Review and evaluation. *Journal of Hydrology*, *505*, 47–64. https://doi.org/10.1016/J.JHYDROL.2013.09.006

Knapp, J. L. A., Neal, C., Schlumpf, A., Neal, M., & Kirchner, J. W. (2019). New water fractions and transit time distributions at Plynlimon, Wales, estimated from stable water isotopes in precipitation and streamflow. *Hydrology and Earth System Sciences*, *23*(10), 4367–4388. https://doi.org/10.5194/HESS-23-4367-2019

Koeniger, P., Hubbart, J. A., Link, T., & Marshall, J. D. (2008). Isotopic variation of snow cover and streamflow in response to changes in canopy structure in a snow-dominated mountain catchment. *Hydrological Processes*, *22*(4), 557–566. https://doi.org/10.1002/HYP.6967

Kuppel, S., Tetzlaff, D., Maneta, M. P., & Soulsby, C. (2018). EcH2O-iso 1.0: Water isotopes and age tracking in a process-based, distributed ecohydrological model. *Geoscientific Model Development*, *11*(7), 3045–3069. https://doi.org/10.5194/GMD-11-3045-2018

Landwehr, J. M., & Coplen, T. B. (2004). Line-conditioned excess: A new method for characterizing stable hydrogen and oxygen isotope ratios in hydrologic systems. https://doi.org/10.8/S

Langman, J. B., Martin, J., Gaddy, E., Boll, J., & Behrens, D. (2022). Snowpack Aging, Water Isotope Evolution, and Runoff Isotope Signals, Palouse Range, Idaho, USA. *Hydrology 2022, Vol. 9, Page 94*, *9*(6), 94. https://doi.org/10.3390/HYDROLOGY9060094

Laudon, H., Hemond, H. F., Krouse, R., & Bishop, K. H. (2002). Oxygen 18 fractionation during snowmelt: Implications for spring flood hydrograph separation. *Water Resources Research*, *38*(11), 40–41. https://doi.org/10.1029/2002WR001510

Laudon, H., Seibert, J., Köhler, S., & Bishop, K. (2004). Hydrological flow paths during snowmelt: Congruence between hydrometric measurements and oxygen 18 in meltwater, soil water, and runoff. *Water Resources Research*, *40*(3), 3102. https://doi.org/10.1029/2003WR002455

Laudon, H., Sjöblom, V., Buffam, I., Seibert, J., & Mörth, M. (2007). The role of catchment scale and landscape characteristics for runoff generation of boreal streams. *Journal of Hydrology*, *344*(3–4), 198–209. https://doi.org/10.1016/J.JHYDROL.2007.07.010

Lechler, A. R., & Niemi, N. A. (2012). The influence of snow sublimation on the isotopic composition of spring and surface waters in the southwestern United States: Implications for stable isotope–based paleoaltimetry and hydrologic studies. *GSA Bulletin*, *124*(3–4), 318–334. https://doi.org/10.1130/B30467.1

Lee, J., Feng, X., Faiia, A. M., Posmentier, E. S., Kirchner, J. W., Osterhuber, R., & Taylor, S. (2010). Isotopic evolution of a seasonal snowcover and its melt by isotopic exchange between liquid water and ice. *Chemical Geology*, *270*(1–4), 126–134. https://doi.org/10.1016/J.CHEMGEO.2009.11.011

Lee, J., Feng, X., Posmentier, E. S., Faiia, A. M., & Taylor, S. (2009). Stable isotopic exchange rate constant between snow and liquid water. *Chemical Geology*, *260*(1–2), 57–62. https://doi.org/10.1016/J.CHEMGEO.2008.11.023

Liston, G. E., & Sturm, M. (1998). A snow-transport model for complex terrain. *Journal of Glaciology*, *44*(148), 498–516. https://doi.org/10.3189/S0022143000002021

Liu, F., Williams, M. W., & Caine, N. (2004). Source waters and flow paths in an alpine catchment, Colorado Front Range, United States. *Water Resources Research*, *40*(9). https://doi.org/10.1029/2004WR003076

Lucianetti, G., Penna, D., Mastrorillo, L., & Mazza, R. (2020). The Role of Snowmelt on the Spatio-Temporal Variability of Spring Recharge in a Dolomitic Mountain Group, Italian Alps. *Water 2020, Vol. 12, Page 2256*, *12*(8), 2256. https://doi.org/10.3390/W12082256

Marttila, H., Lohila, A., Ala-Aho, P., Noor, K., Welker, J. M., Croghan, D., Mustonen, K., Meriö, L. J., Autio, A., Muhic, F., Bailey, H., Aurela, M., Vuorenmaa, J., Penttilä, T., Hyöky, V., Klein, E., Kuzmin, A., Korpelainen, P., Kumpula, T., … Kløve, B. (2021). Subarctic catchment water storage and carbon cycling – Leading the way for future studies using integrated datasets at Pallas, Finland. *Hydrological Processes*, *35*(9), e14350. https://doi.org/10.1002/HYP.14350

Marty, C. (2008). Regime shift of snow days in Switzerland. *Geophysical Research Letters*, *35*(12). https://doi.org/10.1029/2008GL033998

Marx, C., Tetzlaff, D., Hinkelmann, R., & Soulsby, C. (2021). Isotope hydrology and water sources in a heavily urbanized stream. *Hydrological Processes*, *35*(10), e14377. https://doi.org/10.1002/HYP.14377

McNamara, J. P., Kane, D. L., & Hinzman, L. D. (1997). Hydrograph separations in an arctic watershed using mixing model and graphical techniques. *Water Resources Research*, *33*(7), 1707–1719. https://doi.org/10.1029/97WR01033

Meriö, L. J., Ala-aho, P., Linjama, J., Hjort, J., Kløve, B., & Marttila, H. (2019). Snow to Precipitation Ratio Controls Catchment Storage and Summer Flows in Boreal Headwater Catchments. *Water Resources Research*, *55*(5), 4096–4109. https://doi.org/10.1029/2018WR023031

Mohammed, A. A., Pavlovskii, I., Cey, E. E., & Hayashi, M. (2019). Effects of preferential flow on snowmelt partitioning and groundwater recharge in frozen soils. *Hydrology and Earth System Sciences*, *23*(12), 5017–5031. https://doi.org/10.5194/HESS-23-5017-2019

Mook, W. G. (2000). Environmental Isotopes in the Hydrological Cycle: Principles and Applications (Vol. 1). Int. At. Energy Agency.

Moore, R. D. (1989). Tracing runoff sources with deuterium and oxygen-88 during spring melt in a headwater catchment, southern Laurentians, Quebec. *Journal of Hydrology*, *112*(1–2), 135–148. https://doi.org/10.1016/0022-1694(89)90185-6

Moran, T. A., Marshall, S. J., Evans, E. C., & Sinclair, K. E. (2007). Altitudinal gradients of stable isotopes in lee-slope precipitation in the Canadian Rocky Mountains. *Arctic, Antarctic, and Alpine Research*, *39*(3), 455–467. https://doi.org/10.1657/1523-0430(06-022)

Moran, T., & Marshall, S. (2009). The effects of meltwater percolation on the seasonal isotopic signals in an Arctic snowpack. *Journal of Glaciology*, *55*(194), 1012–1024. https://doi.org/10.3189/002214309790794896

Muhic, F., Pertti Ala-Aho, |, Kashif Noor, |, Welker, J. M., Klöve, B., & Marttila, H. (2023). Flushing or mixing? Stable water isotopes reveal differences in arctic forest and peatland soil water seasonality. *Hydrological Processes*, *37*(1), e14811. https://doi.org/10.1002/HYP.14811

Mustonen, K. R., Mykrä, H., Marttila, H., Sarremejane, R., Veijalainen, N., Sippel, K., Muotka, T., & Hawkins, C. P. (2018). Thermal and hydrologic responses to climate change predict marked alterations in boreal stream invertebrate assemblages. *Global Change Biology*, *24*(6), 2434–2446. https://doi.org/10.1111/GCB.14053

Neumann, T. A., Albert, M. R., Lomonaco, R., Engel, C., Courville, Z., & Perron, F. (2008). Experimental determination of snow sublimation rate and stable-isotopic exchange. *Annals of Glaciology*, *49*, 1–6. https://doi.org/10.3189/172756408787814825

Niewodnizański, J., Grabczak, J., Barański, L., & Rzepka, J. (1981). The Altitude Effect on the Isotopic Composition of Snow in High Mountains. *Journal of Glaciology*, *27*(95), 99–111. https://doi.org/10.3189/S0022143000011266

Ohlanders, N., Rodriguez, M., & McPhee, J. (2013). Stable water isotope variation in a Central Andean watershed dominated by glacier and snowmelt. *Hydrology and Earth System Sciences*, *17*(3), 1035–1050. https://doi.org/10.5194/HESS-17-1035-2013

O'Neil, J. R. (1968). Hydrogen and oxygen isotope fractionation between ice and water. *The Journal of Physical Chemistry*, *72*(10), 3683–3684.

Overland, J. E., Hanna, E., Hanssen-Bauer, I., Kim, S. J., Walsh, J. E., Wang, M., Bhatt, U. S., Thoman, R. L., & Ballinger, T. J. (2019). Surface Air Temperature. In *Arctic report card*. https://arctic.noaa.gov/Report-Card/Report-Card-2019/ArtMID/7916/ArticleID/835/Surface-Air-Temperature

Papina, T., Eirikh, A., & Noskova, T. (2022). Factors Influencing Changes of the Initial Stable Water Isotopes Composition in the Seasonal Snowpack of the South of Western Siberia, Russia. *Applied Sciences (Switzerland)*, *12*(2), 625. https://doi.org/10.3390/APP12020625/S1

Penna, D., Hopp, L., Scandellari, F., Allen, S. T., Benettin, P., Beyer, M., Geris, J., Klaus, J., Marshall, J. D., Schwendenmann, L., Volkmann, T. H. M., von Freyberg, J., Amin, A., Ceperley, N., Engel, M., Frentress, J., Giambastiani, Y., McDonnell, J. J., Zuecco, G., … Kirchner, J. W. (2018). Ideas and perspectives: Tracing terrestrial ecosystem water fluxes using hydrogen and oxygen stable isotopes - Challenges and opportunities from an interdisciplinary perspective. *Biogeosciences*, *15*(21), 6399–6415. https://doi.org/10.5194/BG-15-6399-2018

Penna, D., & van Meerveld, H. J. (2019). Spatial variability in the isotopic composition of water in small catchments and its effect on hydrograph separation. *Wiley Interdisciplinary Reviews: Water*, *6*(5), e1367. https://doi.org/10.1002/WAT2.1367

Penna, D., van Meerveld, H. J., Zuecco, G., Dalla Fontana, G., & Borga, M. (2016). Hydrological response of an Alpine catchment to rainfall and snowmelt events. *Journal of Hydrology*, *537*, 382–397. https://doi.org/10.1016/J.JHYDROL.2016.03.040

Phillips, D. L., & Gregg, J. W. (2001). Uncertainty in Source Partitioning Using Stable Isotopes. *Oecologia*, *127*(2), 171–179. https://doi.org/http://www.jstor.org/stable/4222913

Pi, K., Bieroza, M., Brouchkov, A., Chen, W., Dufour, L. J. P., Gongalsky, K. B., Herrmann, A. M., Krab, E. J., Landesman, C., Laverman, A. M., Mazei, N., Mazei, Y., Öquist, M. G., Peichl, M., Pozdniakov, S., Rezanezhad, F., Roose-Amsaleg, C., Shatilovich, A., Shi, A., … Cappellen, P. Van. (2021). The Cold Region Critical Zone in Transition: Responses to Climate Warming and Land Use Change. *Https://Doi.Org/10.1146/Annurev-Environ-012220-125703*, *46*(1). https://doi.org/10.1146/ANNUREV-ENVIRON-012220-125703

Pomeroy, J. W., Marsh, P., & Gray, D. M. (1997). Application of a distributed blowing snow model to the Arctic. *Ltd. Hydrol. Process*, *11*, 1451–1464. https://doi.org/10.1002/(SICI)1099-1085(199709)11:11

Popp, A. L., Pardo-Álvarez, Á., Schilling, O. S., Scheidegger, A., Musy, S., Peel, M., Brunner, P., Purtschert, R., Hunkeler, D., & Kipfer, R. (2021). A Framework for Untangling Transient Groundwater Mixing and Travel Times. *Water Resources Research*, *57*(4), e2020WR028362. https://doi.org/10.1029/2020WR028362

Popp, A. L., Scheidegger, A., Moeck, C., Brennwald, M. S., & Kipfer, R. (2019). Integrating Bayesian Groundwater Mixing Modeling With On-Site Helium Analysis to Identify Unknown Water Sources. *Water Resources Research*, *55*(12), 10602–10615. https://doi.org/10.1029/2019WR025677

Prein, A. F., & Heymsfield, A. J. (2020). Increased melting level height impacts surface precipitation phase and intensity. *Nature Climate Change 2020 10:8*, *10*(8), 771–776. https://doi.org/10.1038/s41558-020-0825-x

Pu, T., Wang, K., Kong, Y., Shi, X., Kang, S., Huang, Y., He, Y., Wang, S., Lee, J., & Cuntz, M. (2020). Observing and Modeling the Isotopic Evolution of Snow Meltwater on the Southeastern Tibetan Plateau. *Water Resources Research*, *56*(9). https://doi.org/10.1029/2019WR026423

Puntsag, T., Mitchell, M. J., Campbell, J. L., Klein, E. S., Likens, G. E., & Welker, J. M. (2016). Arctic Vortex changes alter the sources and isotopic values of precipitation in northeastern US. *Scientific Reports 2016 6:1*, *6*(1), 1–9. https://doi.org/10.1038/srep22647

Ren, W., Tian, L., & Shao, L. (2023). Temperature and precipitation control the seasonal patterns of discharge and water isotopic signals of the Nyang River on the southeastern Tibetan Plateau. *Journal of Hydrology*, *617*, 129064. https://doi.org/10.1016/J.JHYDROL.2023.129064

Rindt, O., Rosinger, C., Bonkowski, M., Rixen, C., Brüggemann, N., Urich, T., & Fiore-Donno, A. M. (2022). Biogeochemical dynamics during snowmelt and in summer in the Alps. *Biogeochemistry*, *162*(2), 257–266. https://doi.org/10.1007/S10533-022-01005-8/FIGURES/5

Rodhe, A. (1981). Spring Flood Meltwater or Groundwater?Paper presented at the Nordic Hydrological Conference (Vemdalen, Sweden, August, 1980). *Hydrology Research*, *12*(1), 21–30. https://doi.org/10.2166/NH.1981.0002

Rodhe, A. (1998). Snowmelt-Dominated Systems. *Isotope Tracers in Catchment Hydrology*, 391–433. https://doi.org/10.1016/B978-0-444-81546-0.50019-7

Rücker, A., Boss, S., Kirchner, J. W., & von Freyberg, J. (2019). Monitoring snowpack outflow volumes and their isotopic composition to better understand streamflow generation during rain-on-snow events. *Hydrology and Earth System Sciences*, *23*(7), 2983–3005. https://doi.org/10.5194/HESS-23-2983-2019

Rücker, A., Zappa, M., Boss, S., & von Freyberg, J. (2019). An optimized snowmelt lysimeter system for monitoring melt rates and collecting samples for stable water isotope analysis. *Journal of Hydrology and Hydromechanics*, *67*(1), 20–31. https://doi.org/10.2478/JOHH-2018-0007

Schmieder, J., Hanzer, F., Marke, T., Garvelmann, J., Warscher, M., Kunstmann, H., & Strasser, U. (2016). The importance of snowmelt spatiotemporal variability for isotope-based hydrograph separation in a high-elevation catchment. *Hydrology and Earth System Sciences*, *20*(12), 5015–5033. https://doi.org/10.5194/HESS-20-5015-2016

Serreze, M. C., Gustafson, J., Barrett, A. P., Druckenmiller, M. L., Fox, S., Voveris, J., Stroeve, J., Sheffield, B., Forbes, B. C., Rasmus, S., Laptander, R., Brook, M., Brubaker, M., Temte, J., McCrystall, M. R., & Bartsch, A. (2021). Arctic rain on snow events: bridging observations to understand environmental and livelihood impacts. *Environmental Research Letters*, *16*(10), 105009. https://doi.org/10.1088/1748-9326/AC269B

Siegenthaler, U., & Oeschger, H. (1980). Correlation of 18O in precipitation with temperature and altitude. *Nature 1980 285:5763*, *285*(5763), 314–317. https://doi.org/10.1038/285314a0

Sinclair, K. E., & Marshall, S. J. (2008). Post-depositional modification of stable water isotopes in winter snowpacks in the Canadian Rocky Mountains. *Annals of Glaciology*, *49*, 96–106. https://doi.org/10.3189/172756408787814979

Sjostrom, D. J., & Welker, J. M. (2009). The influence of air mass source on the seasonal isotopic composition of precipitation, eastern USA. *Journal of Geochemical Exploration*, *102*(3), 103–112. https://doi.org/10.1016/J.GEXPLO.2009.03.001

Sklash, M. G., & Farvolden, R. N. (1979). The role of groundwater in storm runoff. *Journal of Hydrology*, *43*(1–4), 45–65. https://doi.org/10.1016/0022-1694(79)90164-1

Smith, A., Welch, C., & Stadnyk, T. (2016). Assessment of a lumped coupled flow-isotope model in data scarce Boreal catchments. *Hydrological Processes*, *30*(21), 3871–3884. https://doi.org/10.1002/HYP.10835

Sprenger, M., Leistert, H., Gimbel, K., & Weiler, M. (2016). Illuminating hydrological processes at the soil-vegetation-atmosphere interface with water stable isotopes. *Reviews of Geophysics*, *54*(3), 674–704. https://doi.org/10.1002/2015RG000515

Stadnyk, T. (2008). Mesoscale hydrological model validation and verification using stable water isotopes: The isoWATFLOOD [PhD. Thesis]. University of Waterloo.

Stadnyk, T., Amour, N. S. T., Kouwen, N., Edwards, T. W. D., Pietroniro, A., & Gibson, J. J. (2007). A groundwater separation study in boreal wetland terrain: the WATFLOOD hydrological model compared with stable isotope tracers. *Http://Dx.Doi.Org/10.1080/10256010500053730*, *41*(1), 49–68. https://doi.org/10.1080/10256010500053730

Steen-Larsen, H. C., Masson-Delmotte, V., Sjolte, J., Johnsen, S. J., Vinther, B. M., Bréon, F. M., Clausen, H. B., Dahl-Jensen, D., Falourd, S., Fettweis, X., Gallée, H., Jouzel, J., Kageyama, M., Lerche, H., Minster, B., Picard, G., Punge, H. J., Risi, C., Salas, D., … White, J. (2011). Understanding the climatic signal in the water stable isotope records from the NEEM shallow firn/ice cores in northwest Greenland. *Journal of Geophysical Research: Atmospheres*, *116*(D6), 6108. https://doi.org/10.1029/2010JD014311

Stichler, W. (1987). Snowcover and Snowmelt Processes Studied by Means of Environmental Isotopes. *Seasonal Snowcovers: Physics, Chemistry, Hydrology*, 673–726. https://doi.org/10.1007/978-94-009-3947-9_31

Stichler, W., Rauert, W., & Martinec, J. (1981). Environmental Isotope Studies of an Alpine Snowpack. *Hydrology Research*, *12*(4–5), 297–308. https://doi.org/10.2166/NH.1981.0024

Sturm, M., & Benson, C. S. (1997). Vapor transport, grain growth and depth-hoar development in the subarctic snow. *Journal of Glaciology*, *43*(143), 42–59. https://doi.org/10.3189/S0022143000002793

Sturm, M., & Wagner, A. M. (2010). Using repeated patterns in snow distribution modeling: An Arctic example. *Water Resources Research*, *46*(12), 12549. https://doi.org/10.1029/2010WR009434

Sueker, J. K., Ryan, J. N., Kendall, C., & Jarrett, R. D. (2000). Determination of hydrologic pathways during snowmelt for alpine/subalpine basins, Rocky Mountain National Park, Colorado. *Water Resources Research*, *36*(1), 63–75. https://doi.org/10.1029/1999WR900296

Taylor, S., Feng, X., Kirchner, J. W., Osterhuber, R., Klaue, B., & Renshaw, C. E. (2001). Isotopic evolution of a seasonal snowpack and its melt. *Water Resources Research*, *37*(3), 759–769. https://doi.org/10.1029/2000WR900341

Taylor, S., Feng, X., Renshaw, C. E., & Kirchner, J. W. (2002). Isotopic evolution of snowmelt 2. Verification and parameterization of a one-dimensional model using laboratory experiments. *Water Resources Research*, *38*(10), 36–1. https://doi.org/10.1029/2001WR000815

Taylor, S., Feng, X., Williams, M., & McNamara, J. (2002). How isotopic fractionation of snowmelt affects hydrograph separation. *Hydrological Processes*, *16*(18), 3683–3690. https://doi.org/10.1002/HYP.1232

Terzer-Wassmuth, S., Wassenaar, L. I., Welker, J. M., & Araguás-Araguás, L. J. (2021). Improved high-resolution global and regionalized isoscapes of δ18O, δ2H and d-excess in precipitation. *Hydrological Processes*, *35*(6), e14254. https://doi.org/10.1002/HYP.14254

Tetzlaff, D., Buttle, J., Carey, S. K., van Huijgevoort, M. H. J., Laudon, H., Mcnamara, J. P., Mitchell, C. P. J., Spence, C., Gabor, R. S., & Soulsby, C. (2015). A preliminary assessment of water partitioning and ecohydrological coupling in northern headwaters using stable isotopes and conceptual runoff models. *Hydrological Processes*, *29*(25), 5153–5173. https://doi.org/10.1002/HYP.10515

Tetzlaff, D., Piovano, T., Ala-Aho, P., Smith, A., Carey, S. K., Marsh, P., Wookey, P. A., Street, L. E., & Soulsby, C. (2018). Using stable isotopes to estimate travel times in a data-sparse Arctic catchment: Challenges and possible solutions. *Hydrological Processes*, *32*(12), 1936–1952. https://doi.org/10.1002/HYP.13146

Tokunaga, T. K., Tran, A. P., Wan, J., Dong, W., Newman, A. W., Beutler, C. A., Brown, W., Henderson, A. N., & Williams, K. H. (2022). Quantifying Subsurface Flow and Solute Transport in a Snowmelt-Recharged Hillslope With Multiyear Water Balance. *Water Resources Research*, *58*(12), e2022WR032902. https://doi.org/10.1029/2022WR032902

Uhlenbrook, S., Frey, M., Leibundgut, C., & Maloszewski, P. (2002). Hydrograph separations in a mesoscale mountainous basin at event and seasonal timescales. *Water Resources Research*, *38*(6), 31–1. https://doi.org/10.1029/2001WR000938

Unnikrishna, P. V., McDonnell, J. J., & Kendall, C. (2002). Isotope variations in a Sierra Nevada snowpack and their relation to meltwater. *Journal of Hydrology*, *260*(1–4), 38–57. https://doi.org/10.1016/S0022-1694(01)00596-0

Vachon, R. W., Welker, J. M., White, J. W. C., & Vaughn, B. H. (2010). Monthly precipitation isoscapes (δ18O) of the United States: Connections with surface temperatures, moisture source conditions, and air mass trajectories. *Journal of Geophysical Research: Atmospheres*, *115*(D21), 21126. https://doi.org/10.1029/2010JD014105

von Freyberg, J., Bjarnadóttir, T. R., & Allen, S. T. (2020). Influences of forest canopy on snowpack accumulation and isotope ratios. *Hydrological Processes*, *34*(3), 679–690. https://doi.org/10.1002/HYP.13617

Vystavna, Y., Paule-Mercado, M., Juras, R., Schmidt, S. I., Kopáček, J., Hejzlar, J., & Huneau, F. (2021). Effect of snowmelt on the dynamics, isotopic and chemical composition of runoff in mature and regenerated forested catchments. *Journal of Hydrology*, *598*, 126437. https://doi.org/10.1016/J.JHYDROL.2021.126437

Wang, X., Li, Z., Ross, E., Tayier, R., & Zhou, P. (2015). Characteristics of water isotopes and hydrograph separation during the spring flood period in Yushugou River basin, Eastern Tianshans, China. *Journal of Earth System Science*, *124*(1), 115–124. https://doi.org/10.1007/S12040-014-0517-X/TABLES/5

Welker, J. M., Rayback, S., & Henry, G. H. R. (2005). Arctic and North Atlantic Oscillation phase changes are recorded in the isotopes (δ18O and δ13C) of Cassiope tetragona plants. *Global Change Biology*, *11*(7), 997–1002. https://doi.org/10.1111/J.1365-2486.2005.00961.X

Winnick, M. J., Carroll, R. W. H., Williams, K. H., Maxwell, R. M., Dong, W., & Maher, K. (2017). Snowmelt controls on concentration-discharge relationships and the balance of oxidative and acid-base weathering fluxes in an alpine catchment, East River, Colorado. *Water Resources Research*, *53*(3), 2507–2523. https://doi.org/10.1002/2016WR019724

Zhou, S., Nakawo, M., Hashimoto, S., & Sakai, A. (2008). The effect of refreezing on the isotopic composition of melting snowpack. *Hydrological Processes*, *22*(6), 873–882. https://doi.org/10.1002/HYP.6662

Appendix

Appendix 1 Table A1: The isotopic and meteorological information for rainfall events which occurred between the two snowpit sampling periods (i.e., from 22–23 April to 23 May 2020)

Table A1: The isotopic and meteorological information for rainfall events which occurred between the two snowpit sampling periods (i.e., from 22–23 April to 23 May 2020)

Date	$\delta^{18}O$ (per mil)	$\delta^{2}H$ (per mil)	Rainfall (mm)	Avg. Air Temp (^{0}C)	Total Duration (hrs)	Note
28 April 2020	-7.72	-59.94	1.4	-2.68	12	
2–4 May 2020	-13.67	-93.59	11.1	0.71	50	Until Midnight 2 AM (4 May 2020)
4 May 2020	-19.24	-142.75	2.8	1.34	22	From Midnight 2 AM (4 May 2020)
8 May 2020	-12.84	-92.31	0.3	-0.4	24	
10 May 2020	-16.74	-121.46	6.6	-1.05	24	
18 May 2020	-15.43	-114.84	0.2	1.22	24	

Original publications

I Ala-aho, P., Welker, J. M., Bailey, H., Højlund Pedersen, S., Kopec, B., Klein, E., Mellat, M., Mustonen, K-R., Noor, K., & Marttila, H. (2021). Arctic snow isotope hydrology: a comparative snow-water vapor study. *Atmosphere, 12*(2), 150. https://doi.org/10.3390/atmos12020150

II Noor, K., Marttila, H., Klöve, B., Welker, J. M., & Ala-aho, P. (2023). The spatiotemporal variability of snowpack and snowmelt water ^{18}O and ^{2}H isotopes in a subarctic catchment. *Water Resources Research*, *59*(1), e2022WR033101. https://doi.org/10.1029/2022WR033101

III Noor, K., Marttila, H., Welker, J. M., Mustonen, K-R., Klöve, B., & Ala-aho, P. (2023). Snow sampling strategy can bias estimation of meltwater fractions in isotope hydrograph separation. *Journal of Hydrology, 627*(Part B), 130429. https://doi.org/10.1016/j.jhydrol.2023.130429

Original publications are not included in the electronic version of the dissertation.

Book orders:
Virtual book store
https://verkkokauppa.omapumu.com/fi/

UNIVERSITY OF OULU P.O. Box 8000 FI-90014 UNIVERSITY OF OULU FINLAND

ACTA UNIVERSITATIS OULUENSIS

ISBN 978-952-62-3905-7 (Paperback)
ISBN 978-952-62-3906-4 (PDF)
ISSN 0355-3213 (Print)
ISSN 1796-2226 (Online)

UNIVERSITY OF OULU